TECHNICAL UNIVERSITY OF LIBEREC
Faculty of Textile Engineering

Tensile Behavior of Staple Spun Yarns

Dissertation

Study programme: P3106 – Textile Engineering
Study branch: 3106V015 – Textile Technics and Materials Engineering

Author: **Muhammad Zubair, M.Sc.**
Supervisor: prof. Ing. Bohuslav Neckář, DrSc.

Liberec 2017

TECHNICKÁ UNIVERZITA V LIBERCI
Fakulta textilní

Tahové chovaní staplových přízí

Disertační práce

Studijní program: P3106 – Textile Engineering
Studijní obor: 3106V015 – Textile Technics and Materials Engineering

Autor práce: **Muhammad Zubair, M.Sc.**
Vedoucí práce: prof. Ing. Bohuslav Neckář, DrSc.

Liberec 2017

Prohlášení

Byl jsem seznámen s tím, že na mou disertační práci se plně vztahuje zákon č. 121/2000 Sb., o právu autorském, zejména § 60 – školní dílo.

Beru na vědomí, že Technická univerzita v Liberci (TUL) nezasahuje do mých autorských práv užitím mé disertační práce pro vnitřní potřebu TUL.

Užiji-li disertační práci nebo poskytnu-li licenci k jejímu využití, jsem si vědom povinnosti informovat o této skutečnosti TUL; v tomto případě má TUL právo ode mne požadovat úhradu nákladů, které vynaložila na vytvoření díla, až do jejich skutečné výše.

Disertační práci jsem vypracoval samostatně s použitím uvedené literatury a na základě konzultací s vedoucím mé disertační práce a konzultantem.

Současně čestně prohlašuji, že tištěná verze práce se shoduje s elektronickou verzí, vloženou do IS STAG.

Datum:

Podpis:

TABLE OF CONTENTS

ACKNOWLEDGEMENT

First, I am thankful to almighty ALLAH who gave me the courage, capability and opportunity to complete my PhD thesis. I just cannot thank enough for his immense blessings on me during all my life. Completing PhD thesis is a very long journey full of hardships and many turns. At this moment, I am feeling great pleasure to thank all those peoples who helped me during this journey.

I would like to thank my wonderful family for supporting me through all these years in Liberec, Czech Republic. I would like to thank my PhD Supervisor Prof. Ing. Neckář Bohuslav for his encouragement, advices, inclusion, and confidence in my abilities, and who helped me to see it through to the end. I would also very much thankful to my PhD supervisory committee.

I would also like to acknowledge Head of Department, Ing. Brigita Kolčavová Sirková. I also appreciate all the support I have had from my colleagues including PhD students and the staff of our Department. Without the help of all these people this thesis would never have been completed. These people include Prof. Ing. Ursíny Petěr, Ing. Krupincová Gabriela, Ing. Moučková Eva, Ing. Vyšanská Monika, Ing. Spánková Jana, Ing. Jirasková Petra, Ing. Mertová Iva, Ing. Martin Krula, Šarka Řezničková, Stranská Jana, Ludmila Zdvihalová. Ing. Moaz Eldeeb and Ing. Usman Javaid.

Here, now I would not forget to thank the kind and nice staff of Dean's Office of Faculty especially Miss Bohumila Keilová, Miss Hana Musilova and Miss Monika Mošničková.

I must acknowledge my parent institution, National Textile University, Faisalabad, Pakistan (NTU) for selecting me for PhD study under its continuous faculty development program. I would also like to offer special thanks to my colleagues there in NTU whoever helped me in my career orientation and development.

I would like to thank Faculty of Textile Engineering, Technical University of Liberec for their financial assistance.

ABSTRACT

The current study starts with a description of stress-strain curves of fiber and yarn. The effect of yarn structure can be characterized by coefficient of fiber stress utilization in yarn. The four types of models, for coefficient of fiber stress utilization in yarn, are being compared and explained based on idea of helical fibers in the yarn. The Gegauff's model is the simplest of all models, which can calculate coefficient of fiber stress utilization independent of yarn axial strain, assuming linear stress-strain relationship. The solution of "single integral" equation is possible numerically and can be used to predict coefficient of fiber stress utilization as function of yarn axial strain assuming small deformation, constant packing density and contraction ratio. The "double integral" model explains the generalized helical model and it is used to predict the coefficient of fiber stress utilization in staple spun yarns considering also random character of fiber inclination in the yarn. The real fiber stress-strain function, yarn twist, yarn diameter, and fiber orientation parameter are required for solution of this model which can be determined experimentally. The numerical integration was used to solve this equation.

The different types of fibers (viscose, cotton, polyester, linen, wool and acrylic) and yarns were used for validation of proposed mathematical models for coefficient of fiber stress utilization before the breaking process of yarn. Viscose, cotton and polyester yarns were produced from both ring and rotor technologies while linen, wool and acrylic yarns were made from ring spun technology. Combed cotton ring spun yarns from long staple cotton fiber were also used for verification of the model.

It was observed that the stress-strain curve of yarn always lies under stress-strain curve of fiber. The experimental coefficient of fiber stress utilization was compared with four types of coefficients of fiber stress utilization. The well-known Gegauff's theory overestimated the coefficient of fiber stress utilization in all studied yarns. The single integral equation predicted the coefficient of fiber stress utilization at each value of strain and it was near the Gegauff's model but not linear. The empirical constant (k) times coefficient of fiber stress utilization from single integral model was observed near the experimental coefficient of fiber stress utilization but has no logical interpretation. The partial generalization of helical model by taking fiber orientation into account resulted in satisfactory agreement with the experimental results. It was evident that fiber orientation plays an important role in deciding

the fiber stress utilization in yarns. The lower is the variability of fiber direction in relation to the corresponding helical direction of fibers, the higher is the fiber stress utilization in yarn.

The experimental coefficient of fiber stress utilization in the ring yarns was observed higher as compared with the rotor yarns due to better fiber orientation in ring yarns. Polyester yarn exhibited significantly low coefficient of fiber stress utilization due to higher slippage and specific fiber structure. The combed cotton yarn revealed higher coefficient of fiber stress utilization as compared with carded cotton yarns due to better fiber orientation from combing process.

Further, the yarn specific stress-strain curves for each type of ring, rotor and combed yarns were predicted and compared with the experimental yarn specific stress-strain curves. It was revealed that, for all types of yarns, the predicted yarn specific stress-strain curves captured well the experimental yarn specific stress-strain curves before the process of yarn break.

Keywords: Average fiber stress-strain curve, average yarn stress-strain curves, coefficient of fiber stress utilization, predicted yarn specific stress-strain curves, fiber orientation.

ABSTRAKT

V úvodu práce jsou popsány tahové křivky vlákna a příze. Vliv struktury příze na její pevnost může být charakterizován koeficientem využití pevnosti vláken v přízi. V práci jsou představeny a vysvětleny čtyři modely využití pevnosti vláken v přízi odvozené na základě šroubovicového modelu příze. Gegauffův model patří k nejjednodušším modelům a je popsaný rovnicí. Koeficient využití pevnosti vláken v přízi je dle tohoto modelu vypočten nezávisle na tahové deformaci příze. "Jednointegrálový" model je možné řešit numericky a může být využita pro predikci koeficientu využití pevnosti vláken v přízi za předpokladu malých deformací, konstantního zaplnění a konstantního poměru příčné kontrakce. "Dvouintegrální" model popisuje zobecněný šroubovicový model a lze jej využít pro predikci koeficientu využití pevnosti vláken ve staplových přízích s ohledem na náhodný charakter sklonu vláken v přízi. Tento model lze řešit na základě experimentálně stanovených hodnot počtu zákrutů příze, průměru příze, úhlu sklonu vláken a tahové křivky vláken. V této práce byla k řešení rovnice použita numerická integrace.

Různé typy vláken (viskóza, bavlna, polyester, len, vlna a akrylové) a přízí vyrobených z různých technologií byly použity pro ověření navržených matematických modelů pro koeficientem využití napětí vláken. Viskózové, bavlněné a polyesterové příze byly vyrobeny jak prstencovou, tak rotorovou technologií, zatímco lněné, vlněné a polyakrylonitrilové příze byly vypředené pouze na prstencových dopřádacích strojích. Česané prstencové příze z dlouhovlákenné bavlny byly rovněž použity pro ověření modelu.

Bylo zjištěno, že tahové křivky přízí leží vždy pod tahovými křivkami vláken. Experimentální koeficient využití napětí vláken byl ve srovnání se čtyřmi typy teoretických modelů. Dobře známá Gegauffova teorie nadhodnocuje koeficient využití pevnosti vláken v případě všech sledovaných přízí. Model s jednoduchým integrálem predikuje koeficient využití pevnosti vláken v každé hodnotě protažení. Výsledky jsou blízké koeficientům stanoveným na základě Gegauffova modelu, ale není mezi nimi lineární závislost. Částečné zobecnění šroubovicového modelu díky zahrnutí úhlu sklonu vláken přineslo uspokojivý soulad s experimentálními výsledky. Je zřejmé, že orientace vláken hraje důležitou roli při využití pevnosti vláken v přízi. Čím je nižší variabilita sklonu vláken vzhledem k odpovídajícímu sklonu vláken ve šroubovicovému modelu, tím vyšší je využití pevnosti vláken v přízi.

Koeficient využití pevnosti vláken v prstencových přízích byl vyšší v porovnání s koeficientem u rotorových přízí díky lepšímu uspořádání a orientaci vláken v prstencové přízi. Polyesterové příze vykazovaly významně nižší koeficient využití pevnosti vláken díky vyššímu prokluzu a specifické struktuře vláken. Bavlna příze vykazovala vyšší koeficient využití napětí vláken v porovnání s mykanými bavlněnými přízemi z důvodu lepší orientaci vláken z procesu česání.

Dále na základě odvozených vztahů byly predikovány tahové křivky prstencových a rotorových přízí. Křivky byly porovnávány s experimentálně zjištěnými tahovými křivkami. Ukázalo se, že v oblasti před přetrhem příze predikované tahové křivky odpovídají křivkám experimentálním u všech testovaných přízí. Rovněž v případě viskózových prstencových přízí byl navržený matematický model porovnáván s modelem.

Klíčová slova: Průměrná vlákno deformační křivka vlákna, Průměrná příze deformační křivka příze, Koeficient využití napětí vláken. Předpověď specifického napětí příze deformační křivky, orientace vláken.

خلاصہ

موجودہ مطالعہ فائبر اور یارن کی سٹریس-سٹرین منحنی خطوط کی وضاحت کے ساتھ شروع ہوتا ہے. سوت کی ساخت کے اثر سے سوت میں فائبر سٹریس کے استفادہ کا عدّدی سر معلوم کیا جا سکتا ہے. سوت میں فائبر سٹریس کے استفادہ کے عدّدی سر کے لئے ماڈل کی چار اقسام سوت میں ہیلیکل ریشوں کے خیال کی بنیاد پر وضاحت کی جا رہی ہیں. گیگاف کا ماڈل سب سے آسان ہے۔ اور یہ فائبر سٹریس کے استفادہ کا عدّدی سر سٹریس-سٹرین کے تعلق کو لکیری فرض کر کے سوت محوری سٹرین کے بغیر ہی معلوم کر سکتا ہے۔

واحد انضمام مساوات کا حل عدّدی طور پر ممکن ہے۔ اور اِسے فائبر سٹریس کے استفادہ کے عدّدی سر کا اندازہ لگانے کے لیے سوت محوری سٹریس کی بنیاد پر استعمال کیا جا سکتا ہے۔ بشرطیکہ چھوٹے اخترتی، مستقل پیکنگ کثافت اور سکچن تناسب کو فرض کیا جائے۔ ڈبل انضمام ماڈل جنرل ہیلیکل ماڈل کی وضاحت کرتا ہے۔ اور اسے سوت میں فائبر جھکاؤ کے بے ترتیب کردار کو تصور کرتے ہوے سٹیپل کاتے سوت میں فائبر سٹریس کے استفادہ کے عدّدی سر کا اندازہ لگانے کے لیے استعمال کیا جا سکتا ہے۔ اس ماڈل کے حل کے لیے حقیقی فائبر سٹریس-سٹرین فنکشن، سوت بل، سوت قطر اور سوت جہت درّکار ہیں جو کہ تجرباتی طور پر معلوم کیے جا سکتے ہیں۔ اس ماڈل کو حل کرنے کے لیے عدّدی انضمام استعمال کیا گیا۔

ریشوں کی مختلف اقسام (وسکوز، کپاس، پولیئسٹر، لینین، اُون اور ایکریلک) اور مختلف ٹیکنالوجیز سے تیّار کردہ یارن، سوت کے ٹوٹنے کے عمل سے پہلے، فائبر سٹریس کے استفادہ کے عدّدی سر کے لیے مجوّزہ ریاضیاتی ماڈل کی توثیق کے لیے استعمال کیا گیا۔ وسکوز، کپاس اور پالیئسٹر یارن دونوں رنگ اور روٹر ٹیکنالوجی سے تیّار کے گئے۔ جبکہ لینین، اُون اور اکریلک یارن رنگ ٹیکنالوجی سے بنایا گیا تھا۔ طویل سٹیپل کپاس کے ریشے سے تیّار کردہ، کومبڈ کپاس رنگ یارن بھی ماڈل کی تصدیق کے لیے استعمال کیا گیا۔

یہ بات مشاہدہ میں آئی ہے کہ سوت کی سٹریس-سٹرین وکر ہمیشہ ریشہ کی سٹریس-سٹرین وکر کے تحت واقع ہوتی ہے۔ معروف گیگاف کے نظریے سے تمام مطالعہ کیے گئے یارن میں فائبر سٹریس کے استفادہ کے عدّدی سر کی قیمت زیادہ آئی۔ واحد انضمام ماڈل سٹرین کی ہر قیمت پر فائبر سٹریس کے استفادہ کے عدّدی سر کی پیشگوئی کر سکتا ہے۔ جو کہ گیگاف کے ماڈل کے قریب تھا لیکن لیکری نہیں۔ فائبر سٹریس کے استفادہ کا عدّدی سر واحد انضمام ماڈل آخباختی مستقل (K)

گنا، تجرباتی فائبر سٹریس کے استفادہ کے عدّدی سر کے نزدیک پایا گیا لیکن اس میں کوئی منطقی تشریح نہ تھی۔ فائبر کی جہت کو سامنے رکھتے ہوئے ڈبل انضمام ماڈل سے فائبر سٹریس استعمال کے گتانک کی پیشگوئی کی گئی جو کہ تجرباتی نتائج کے ساتھ تسلّی بخش معاہدے میں تھی۔ یہ واضح تھا کہ فائبر جہت سوت میں کشیدگی کے استفادہ کے عدّدہ سر کا فیصلہ کرنے میں اہم کردار ادا کرتی ہے۔ ریشے کی ہیلیکل سمت میں تنوع جتنا کم ہو گا اتنا ہی سوت میں فائبر سٹریس کا استفادہ زیادہ ہو گا۔

رنگ یارن میں فائبر سٹریس کے استفادہ کے عدّدی سر کی تجرباتی قیمت روٹر سوت سے مشاہدہ میں زیادہ آئی جس کی وجہ رنگ یارن میں بہتر فائبر جہت تھی۔ پولیئسٹر سوت میں فائبر سٹریس کے استفادہ کے عدّدہ سر کی قیمت میں نمایاں طور پر کمی، زیادہ فائبر کھسکنے اور فائبر ساخت کی وجہ سے آئی۔ کنگھی کے عمل سے فائبر جہت بہتر ہوئی جس سے کومبڈ کپاس سے تیّار کردہ سوت میں فائبر سٹریس استعمال کے گتانک کی قیمت، کارڈڈ کپاس سے تیّار شدہ یارن کے مقابلے میں زیادہ آئی۔ اس کے علاوہ رنگ، روٹر اور کومبڈ سوت کی ہر ایک قسم سے اخذ کیے گئے سوت کی مخصوص سٹریس-سٹرین منحنی خطوط کا موازنہ تجرباتی منحنی خطوط کے ساتھ کیا گیا۔ یہ نتیجہ نکالا کیا گیا کہ سوت کی تمام اقسام کے لیے اخذ کیے گئے مخصوص سٹریس-سٹرین کے منحنی خطوط، تجرباتی مخصوص سٹریس-سٹرین کے منحنی خطوط کے ساتھ یارن کے ٹوٹنے کے عمل سے پہلے متّفق ہیں۔

مطلوبہ اہم الفاظ:

اوسط فائبر سٹریس-سٹرین منحنی خطوط، اوسط سوت سٹریس-سٹرین منحنی خطوط، فائبر سٹریس کے استفادہ کے عدّدہ سر، فائبر جہت، پیش گوئی شدہ سوت کے مخصوص سٹریس-سٹرین منحنی خطوط

LIST OF TABLES

LIST OF FIGURES

LIST OF SYMBOLS

SYMBOL	DESCRIPTION
$\varphi_{\mathbf{e}}$	Experimental coefficient of fiber stress utilization
φ_{g}	Predicted coefficient of fiber stress utilization according to Gegauff's model
$\varphi_{\mathbf{c1}}$	Predicted coefficient of fiber stress utilization according to single integral
$\varphi_{\mathbf{c2}}$	Predicted coefficient of fiber stress utilization according to double integral model
$k.\varphi_{\mathbf{c1}}$	k times coefficient of fiber stress utilization from single integral model
k	$\frac{\text{Experimental coefficient of fiber stress utilization}}{\text{Coefficient of fiber stress utilization from single integral model}}$
cN	centi-newton
gf	gram-force
CSP	Count strength product
SIM	Single integral model
DIM	Double integral model
GM	Gegauff's model
C.V	Coefficient of variation

CHAPTER 1

INTRODUCTION

1.1 Motivation

Yam mechanics has been considered as an important branch of applied mechanics of textile structures. Because of numerous research in yarn structure, it occupies a significant part of the literature on textile yam mechanics. Being yarn strength a key parameter of staple spun yarns and because of their wide application, yarn strength prediction is very important. Most of research work regarding structure, up to now, is related with the continuous filament yams due to simplest twisted yam structure for theoretical analysis and experimental investigation. Being the extensive applications of staple spun yarns in woven and knitted fabric, it is more important to solve the staple fiber yarn problem.

The discontinuities at the fiber ends and slippage among the fibers in staple fiber yarns have made analysis of staple fiber yarn difficult [1]. Particularly, the effect of yam geometry on the yam behavior has been made the study of staple fiber yarns more complex. The assembly of staple fibers is combined together as a yam due to twist and migration factors. There is huge variation in yarn linear density, yarn twist, fiber arrangement and fiber migration in staple fiber yarns. The above said variables may have a significant influence on the yam behavior which makes the analysis even more difficult.

Many researcher have made attempts to develop satisfactory theoretical basis for practical understanding. Gegauff [2] studied the stress-strain relationship in the twisted yarn taking into account of tensile characteristics of fibers. An analytical expression was derived establishing the relationship among fiber strain, yarn strain and twist angle. Further the coefficient of fiber stress utilization in twisted yarns was predicted as a function of yarn twist angle. This model however did not take into account real stress- strain function and change in yarn diameter during extension of yarn. Considering this Platt [3][4] and Hearle [5] developed more accurate models of stress-strain relation in twisted yarns. Another pioneer work in the area of structural mechanics of yarn include Perice's contribution to the weak link theory for twisted yarns [6]. All theoretical work besides many other empirical researches led to establish a fact that tensile behavior of twisted yarns are by and large determined by constituent fiber properties, yarn structure and testing parameters.

Research work on staple yams so far has mainly focused on the prediction of the yam modulus and the maximum strength. Few studies go beyond these aspects to investigate the

failure response of yams and the whole stress-strain curve for the yarn. Also, a little attention has been paid to the yam behavior under tensile loading. However, the prediction of coefficient of fiber stress utilization in staple yarns is important quality parameter of yarn to improve the yarn strength. The strength of staple yam mainly relate with the twist and fiber properties. The twist level and fiber orientation are the main geometrical parameters which influence the coefficient of fiber stress utilization of staple spun yarns.

The coefficient of fiber stress utilization in yarn depends on yarn axial strain which contradicted the well-known Gegauff's theory [2]. Our proposed mathematical model, based on the assumptions of small deformation, constant packing density and contraction ratio, can be calculated using numerical integration considering real fiber stress-strain relationship and fiber orientation before the process of yarn break when all fibers are mechanically stressed. An attempt is made here to compare and validate our proposed theoretical models discussed in chapter 3 of this work in light of experimental results.

1.2 Objectives

The objective of this research is to apply a mathematical model for prediction of coefficient of fiber stress utilization from stress-strain curves of fiber and yarns considering yarn twist and fiber orientation and to validate the experimental coefficient of fiber stress utilization before yarn break.

This work includes:

1. Understanding the stress-strain behavior of fiber and staple spun yarn before break using different type of fibers, ring and rotor yarns.
2. Analysing behavior of fiber and staple yam, producing the average stress-strain curves for fiber and yams before break using Matlab software.
3. Experimental coefficient of fiber stress utilization will be evaluated from mean experimental fiber and yarn stress-strain curves.
4. Understanding the mathematical model for prediction of coefficient of fiber stress utilization taking into account the concept of nonlinearity in stress-strain curves of textile fibers and yarns and fiber orientation in the staple spun yarns.
5. Comparing the predicted and experimental coefficient of fiber stress utilization on the basis of theoretical model and experimental results for staple spun yarns before breaking process of yarn.
6. Comparing the predicted and experimental yarn specific stress-strain curves before the process of break for staple spun yarns.

7. Comparing the predicted coefficient of fiber stress-strain from our model with Pan's and Frydrych's model.

CHAPTER 2

LITERATURE REVIEW

Numerous literature has been introduced in the studies of yarns mechanics. Most of the models reported are related with complex yarn behavior and mostly literature emphasis on yarn strength, elastic modulus and variation of breaking strength. In this part of thesis the detailed review from the previous researcher will be presented to have deep insight in the field of structure and mechanics of staple spun yarns with some mathematical equations derived earlier by known scientists and researchers.

2.1 Theoretical analysis of yarn mechanical behavior

The research about mechanical behavior of textile yams has been popular by the textile community. The history of modem textile processing machinery dates back two hundred years ago [7]. However, the proper research work was conducted early 1900's for establishing theoretical relationships among fiber properties, yarn structure and material behavior. It can be dated back to the works of Gegauff [2], Gurney [8] and Peirce [9] that as long as the foundation for modem textile mechanics. Since 1940, this field has been established comprehensively by many researchers.

Several logical methods have been used up to now to treat the problem of mechanics of twisted staple spun yams, which can be categorized as energy analysis, finite-element method and force-deformation analysis. Although, the staple fiber yams will be highlighted but some analysis on continuous filament yams will also be elaborated because they are the way for theoretical study of staple spun yams and offer useful information for appropriate understanding of staple yam characteristics. We will deliberate the literature in this area on a sequential basis as follows.

The basic mathematical model of yam was introduced by Gegauff [2] in the form of coaxial helices, all having a pitch equal to the reciprocal of yarn twist. He assumed that the fiber extensions followed Hook's law and derived an expression for the breaking load of a staple fiber yam with higher twist. His equation may be written as

$$\text{Breaking load of yarn} = 2\pi b \int_0^R \frac{r\,dr}{\left(1+\frac{4\pi^2 r^2}{h^2}\right)^2} = \frac{b\pi R^2}{\left(1+\frac{4\pi^2 R^2}{h^2}\right)} \qquad (2.1)$$

Where b is fiber breaking stress, r is distance of circular element of yam from yarn axis of width dr, R stands for radius of yam, and h is length per unit twist in the yam parallel to yarn axis.

A similar model was explained by Gurney [8]. He studied the effect of stress distribution, fiber length, fiber friction and twist on strength of cotton yarns.

Sullivan [10], in his study proposed theoretical approach to relate yam strength with the fiber strength and yam twist considering parallel fibers with and without twisted fiber structures. He also extended the analysis to evaluate the yam strength at any cross section of a yam composed of fibers with varying properties. Later on Sullivan's model was disapproved by other researchers for high twist yarns.

Platt [11] derived an expression for strength of continuous filament yarns similar to the Gegauff except Hook's law was not assumed. The total force on yam can be evaluated in the direction of yam axis by integrating the components of the forces due to individual fibers. The expression for load *P* of yam may be written as

Breaking load of yarn, $P = 2\pi \int_0^R f_r \frac{r\mathrm{d}r}{1+(2\pi NR)^2}$. (2.2)

R is yarn radius, f_r is fiber stress intensity in the yarn at distance *r* from the center as a function of fiber strain, and *N* is yarn twist.

He studied that when the yam is loaded to rapture, the fiber at the center of yam is broken first and then the whole yam is raptured. The maximum force will be reached at this point. In Platt's theory, the strain geometry is such that an axial extension of the yam produces a corresponding change in length of the individual fibers, but does not change their position. This implies that it is based on a small-strain assumption. Platt [12] also studied the variation of yarn modulus with twist and derived an expression which may be written as follows

$$\frac{E_Y}{E_f} = \frac{1}{1+(2\pi NR)^2}\left(\frac{6\pi^2N^2R^2}{(1+4\pi^2N^2R^2)^{\frac{1}{2}}-1}\right). \quad (2.3)$$

Where E_Y is yarn modulus, E_f is fiber modulus, *N* is yarn twist and *R* is yarn radius.

Gregory [13]–[15] modified the formula given by Sullivan for calculation of maximum strength of a parallel strand. He studied that strength of staple spun yarn is less than individual fibers due to variation in load of individual fibers in group of fibers, inclination of fiber to the axis of twisted strand and slippage of fiber in outer layers. Among three the slippage is least important. The cohesion necessary to cause the fiber to break rather than slip is controlled by internal pressure in twisted yarn during tensile load which is function of fiber helix, fiber length and fiber surface properties. He also considered the fact that between a fiber and its adjacent in a yam subjected to a tensile load, some contacting fibers move with,

rather than oppose the motion of that fiber. The yam strength calculated by using his modified formula would be smaller than that given by Sullivan's theory.

Hearle [16] proved that the transverse forces between and through the fibers play an important role in determining mechanical properties of yarns. He analyzed the transverse forces through the yarn, their effect on fiber extension and their contribution to yarn tension from the theoretical model for small strain. The model was not good at higher strain because of change in yarn geometry and deviation of Hook's law. It was concluded that the axial and transverse stresses expressed as function of tensile stress experienced by a filament under same extension as yarn are given as function of twist angle, fiber position in yarn and contraction ratio of fibers. Also, the tensile specific stress of yarn as whole is expressed as similar fraction of fiber stress given by a function of twist angle and contraction ratio. The geometry of the idealized helical yam structure is shown in the figure 2.1 and 2.2.

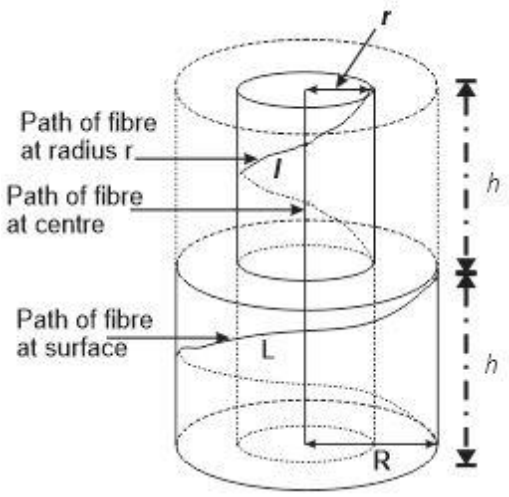

Figure 2.1 Geometry of ideal helical yarn structure [16]

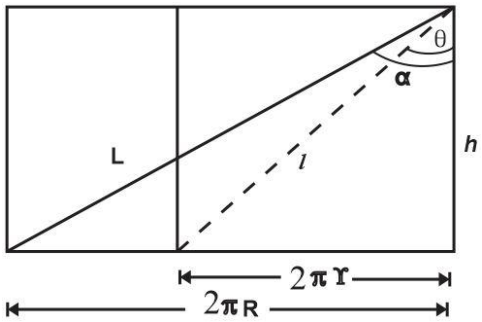

Figure 2.2 Cylinder containing the helices radii r and R opened out into plane [16]

Afterward, Hearle *et al.* [17] modified the previous theory, considering yarn extension and breakage at large extension and also taking into account deviation from Hook's law. Hearle

[18] introduced more simpler energy method similar to Treloar and Riding instead of force method to predict the stress-strain behavior of continuous filament yarns.

Hearle [19], [20] studied the effect of migration in staple fiber yarns and he made a consistent analysis of the behavior and cohesion of an idealized short fiber yams and concluded that yarn twist, fiber arrangement and fiber migration has effect on mechanical properties of yarns.

Later on, Hearle analyzed the conditions in which a fiber will slip or will be gripped and derived the expression for the maximum stress which can be sustained in a fiber at a point E in the yam through the frictional resistance to slippage. The fiber geometry is shown in the figure 2.3 and 2.4.

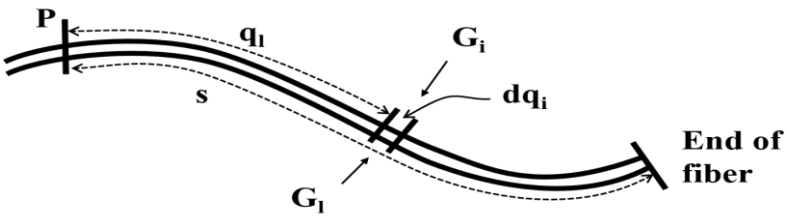

Figure 2.3 Development of frictional forces in a fiber [20]

Maximum specific stress sustained in a fiber at E can be written as

$$\text{Max. Specific Stress} = \frac{2\mu}{a}\int_0^s G\ \left(1 - \frac{2(s-q)}{L_f}\right) dq. \qquad (2.4)$$

Where a is fiber radius, μ is Coefficient of friction, G transverse stress, L_f fiber length, s distance

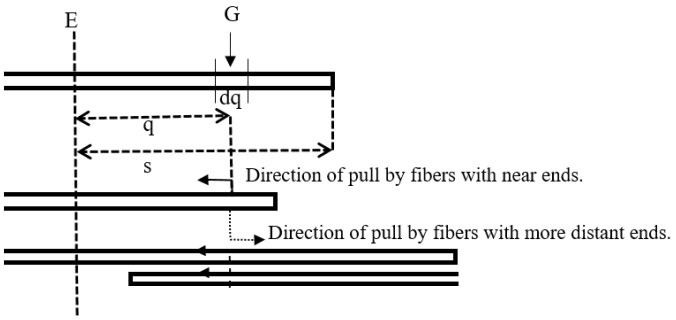

Figure 2.4 Direction of pull on fibers [20]

of a fiber from E to end and q distance along a fiber from element E to dq. According to Hearle the normalized yarn stress is as follow

$$\text{Normalized yam stress} = F = \frac{\text{Yarn modulus}}{\text{Fiber modulus}},$$

Hearle also gives a simplified analysis based on many approximations which yields an explicit equation for the mechanical properties of a staple spun yam.

$$\frac{\text{yarn modulus}}{\text{fiber modulus}} = \cos^2 \alpha\,[1 - k \operatorname{cosec} \alpha\,]. \qquad (2.5)$$

Where $k = \frac{\sqrt{2}}{3L_f}\left(\frac{aQ}{\mu}\right)^{\frac{1}{2}}$, a is fiber radius, μ is coefficient of fiber friction, L_f is fiber length, Q is migration period.

The numerical evaluation of Hearle's equations using k = 0.01 and 0.1 is shown in the figure 2.5.

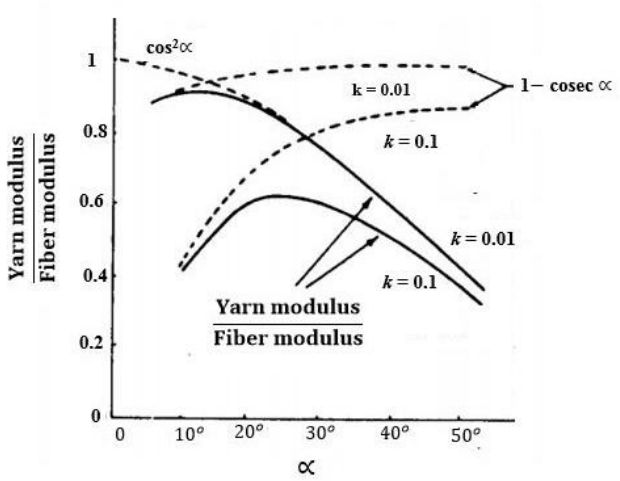

Figure 2.5 Numerical plot of equation, ($\frac{yarn\ modulus}{fiber\ modulus} = \cos^2 \alpha\,[1 - \text{k cosec } \alpha\,]$) [20]

The mechanics of filament yams by energy method was analyzed by Treloar and Riding [21], the work done in stretching the yam was evaluated from the elastic energy stored in the deformed filaments. They assumed in their analysis the ideal yarn geometry in unstrained yam similar to Platt and Hearle, constant volume for both filaments and yam during deformation, and the fibers behave perfectly elastic so that all the work done on the yam is changed into stored elastic energy.

The yarn specific stress, X is given

$$X = \frac{2}{R_o^2}\int_0^{R_o} \sigma_f\,(\varepsilon_f)\,\frac{\partial \varepsilon_f}{\partial \varepsilon_Y}\, r_o dr_o. \qquad (2.6)$$

Where R_o is the yam radius in the unstrained state, $\sigma_f\,(\varepsilon_f)$ is fiber stress as a function of fiber strain, ε_f and ε_Y are fiber and yarn strains, r_o is the yam radial position.

The effect of torsional and bending forces was studied by Treloar [22] in a theoretical analysis of rubber models and it was established that they are negligible in the tensioned yarn.

Later on Treloar [23] applied rubber model to a filament yarn of idealized migration pattern and it was concluded that migration affected slightly the geometrical and tensile properties of filament yam.

Holdaway [24] studied the strength of single worsted yarn and a new concept of "ineffective outer layer" of fibers was introduced. He found that the stretched yarn caused limited lateral pressure immediately below an outer layer of fibers. He considered that such layer have a negligible contribution to the strength of the yam.

A new approach was introduced by White and Cheng *et al.* [25], [26] in mechanics of continuous filament yams using the method of continuum mechanics and tensor matrix analysis. In their model they considered that the stresses acting on a fiber can be divided into axial yarn tensile stress and compressive stresses. Cheng derived an expression for the tensile force *F* which is applicable in static and dynamic deformations of continuous filament yam. The equation can be written as follows

$$F = \int_0^R 2\pi r \, (T^2 \cos 2\theta - P_b \sin 2\theta + 2 f_b \sin\theta \cos\theta) \, dr \qquad (2.7)$$

Where T is tensile stress along the filament, f_b is inter-filament shear stress between the tangent and bi-normal directions, P_b is compressive stress on filament surface along bi-normal direction, θ is angle of fiber tensile stress along the yarn axis, R is yarn radius and r is radius of yarn element. It can be shown that the results of earlier authors are special cases of this general expression. The above equation reduces to Gegauff and Platt's expression for the tensile forces in yam if P_b and f_b are neglected. By putting $f_b = 0$, the above equation is resembled to Hearle's equation for tensile strength.

Carnaby *et al.* [27] studied the tensile behavior of staple-fiber yams at small strains. In their analysis, they considered the effect of large and non-uniform lateral movements of fibers in a tensioned and non-tensioned staple fiber yam that are not initially closely packed. They were also able to predict the internal force and pressure distribution in addition to stress-strain behavior of yarn.

A theoretical model was developed by Thwaites [28] to analyze the tensile and torsional behavior of highly twisted yams. He established an expression for yarn tension assuming that the yam is tightly packed and possessed axial symmetry to avoid relative movement between filaments. His model was only applicable for highly twisted yams. Because of large disagreement for low twist yams, further experimental verification is required for the validity of analysis.

A serious of papers was published by Pan [29]–[32] in the field of mechanics of staple fiber yams. He developed constitutive theory governing the behavior of short fiber yams. He first considered the high twist yams in which the effect of fiber slippage during yam extension can be ignored. By treating a staple yam as a short fiber composite, a fiber is viewed as embedded in a matrix made of the neighbouring fibers as shown in figure 2.6.

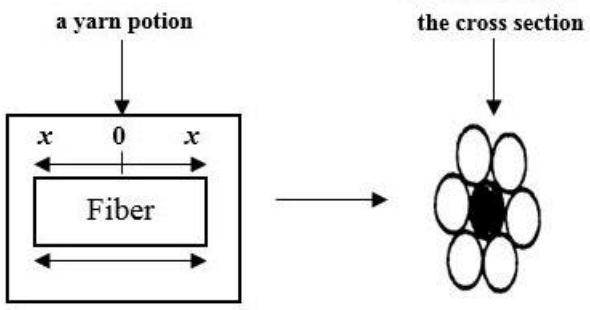

Figure 2.6 Fiber surrounded by adjacent fiber in yarn [19]

Pan [32] established the expression for the ratio between expected strength of staple spun yarn and its constituent fibers as follows

$$\frac{<\sigma_Y>}{<\sigma_f>} = \left(\frac{l_f}{l_c}\right)^{\frac{1}{\beta}} \frac{V_f \eta_q}{\beta^{1/\beta}\left(1/\beta\right)\Gamma\left(1+\left(1/\beta\right)\right)}. \quad (2.8)$$

Where σ_Y is theoretical yarn tenacity, σ_f is fiber tenacity, l_f is mean fiber length, l_c is critical fiber length, V_f is fiber volume fraction of the yarn, β is fiber Weibull shape parameter, η_q is fiber orientation efficiency factor which is obtained according to the following formula,

$$\eta_q = \frac{2q(1-\nu_{LT})+(1+\nu_{LT})\sin 2q}{4q}. \quad (2.9)$$

Where q is fiber helix angle at yarn surface, and ν_{LT} is the associated contraction ratio governing induced yarn transverse strain which can be calculated from equation

$$\nu_{LT} = \frac{\sin^5 q}{2(1-\cos^3 q)\left(q/2 - 1/4 \sin 2q\right)}. \quad (2.10)$$

A statistical theory was developed by Realff *et al.* [33] to explore the relationship between the statistical strength and the properties of the constituent fibers as well as the structural parameters of twisted fiber. The fiber fragmentation process was observed during the breaking process of yam as function of yam strain before complete yarn failure. The critical fiber length was found during fragmentation process which was used to predict the strength of yarn. Their model is applicable equally for filament and staple fiber yarns with high twist level.

Onder and Baser [34], [35] examined the stress-strain behavior and strength of staple yams. A yam model was established in which the fiber migration follows a conical helix path. The stresses acting along the main directions on the yam element are determined. They developed the algorithm describing the slipping and gripping behavior of the fiber. Finally, the yam stress is determined from the sum of tension of gripped fibers. Both transverse and tensile stresses are included. Their approach is like Hearle's model of staple yams.

A theoretical model was developed by Langenhove [36]–[38] to predict the tensile load and untwisting moment of a yarn at a given strain from fiber properties and yarn structure. He transformed yarn into finite elements. He stated that coefficient of friction is most important property of fiber. The stresses and deformations are only functions of the radial coordinate *r*. His model is advantageous over Van Luijk's finite element model in the way that fiber properties do not have to be identical, and the fiber migration pattern is allowed to be variable. The path of the fibers is not necessarily limited to a helix.

Morris *et al.* [39] developed method for yarn modelling by dividing the series of yam cross sections at small intervals along its length. They determined arrangement of fibers in cross section, rotated each cross section by predetermined amount relative to previous one to allow for yarn twist and introduced some random entanglement of fibers. Morris's model provides a new way to represent the yam structure which considers yam migration and yam irregularity. However the stress analysis is based on the assumption that the yam is an isotropic body which is not realistic.

Many researchers [40]–[47] established empirical relationship for yarn strength from fiber and yarn properties for ring and rotor yarns. Some of them also considered process parameters. The equation for estimating yarn tenacity was established by Iyengar *et al.* [48], [49] considering certain factors like fiber length, fineness, tenacity and strength uniformity from scientific considerations under standard processing techniques. Regression equations were also developed for prediction of yarn strength from the fiber properties for ring and rotor yarns [50], [51]. Chasmawala *et al.* [52] introduced regression equation which can determine the breaking load from number of core fibers for air-jet yarn He found that yarn breaking strength in air jet yarns has negative relationship with the number of core fibers. Rajamanickam *et al.* [53] studied the structural and material parameters of air jet spun yarns and derived the regression equation for yarn tenacity. He found that the yarn tenacity is dependent on material and process parameters. Hafez [54] developed the relationship for predicting the lea strength and single yarn strength .

Ramey *et al.* [55] failed to find any significant relationship between count strength product and the micronaire value of the fibre. It is due to a certain range of micronaire for which the change of CSP is insignificant. A mathematical model was developed by Krause *et al.*[56] for coefficient of fiber strength utilization for the air-jet spun yarn. They derived the expression for coefficient of fiber strength utilization for lower fiber friction and higher fiber friction ranges.

Frydrych [57] developed a mechanistic model for prediction of yarn strength. The strength of *y* mm long yarn sample Q_Y was obtained by using the modified Peirce's equation. He evolved the following mathematical equation to estimate yarn strength as

$$Q_Y = Q_h \left[1 - 3.64\, \nu_{Fh}(1 - q^{-\frac{1}{7}})\right]. \quad (2.11)$$

Where Q_Y is the predicted yarn strength (cN / tex), Q_h is stress in the breaking zone of the yarn (cN / tex), ν_{Fh} is the coefficient of variation of breaking force in the length of the fracture zone, which can be found from the following equation

$$\nu_{Fh} = \beta \sqrt{\frac{\text{Yarn fineness in tex } (T_{t_Y})}{\text{Fiber fineness tex } (T_{t_f})}}. \quad (2.12)$$

β is coefficient depending on the spinning system, for carded yarn β = 2 and, β = 1.35 for combed yarns. The parameter *q* can be determined as follow

$$q = \frac{\text{Yarn gauge length } (l_Y)}{\text{Fracture zone length}(l_h)}. \quad (2.13)$$

Most of the Frydrych's model are based on previous work by Zurek [58] and Zurek *et al.* [59]. Das *et al.* [60] used simulated annealing to solve Frydrych's yarn strength equation from fiber properties and twist of ring spun cotton yarns to explore the best combination of parameters that can produce yarn with required strength.

Ghosh *et al.* [61], [62] published the literature regarding prediction of the yarn strength from the properties of its component fibers and other parameters. They explained that the development of predictive model of yarn strength is always significant in theory and practice. He further established the following equation for spun yarn tenacity, Q_t as follows

$$Q_t = \frac{n_h}{n_e} \cdot F_h \cdot \frac{\varphi_b}{100} \cdot \cos^2\theta \cdot \quad (2.14)$$

Where n_h the number of fibers at the place of yarn break, n_e is the average number of fibers in the yarn cross section, F_h is the fiber bundle tenacity measured at a gauge length equal to the actual length of the weakest zone in the yarn, φ_b is the percentage of broken fiber in the yarn failure zone, θ is the average helix angle of fibre at the time of yarn failure.

Sami *et al.* [63] studied the mechanical behavior of yarn using from tensile relaxation tests at different strain levels. They proposed the analytical model to predict the entire stress-strain response of yarn. The model describes the viscoelastic behavior of ring and rotor yarns during traction and retraction. The neural network approach was used for the correlation between the mechanical coefficients of model and process parameters.

Dang *et al.* [64] studied tensile behavior of wool / spandex core spun yarn and introduced theoretical model to determine coefficient of fiber strength utilization considering fiber and yarns properties. Guha *et al.* [65] have compared the mechanistic model described by Frydrych, statistical and a neural network model. These three models are used to predict the tenacity of yarns made from polyester staple fiber. The results indicate the success of all three models in predicting yarn strength.

Cybulska *et al.* [66] developed a mathematical model from the concept of fiber distribution and disposition of fibers from the yarn images before and after yarn break for staple spun yarns. Shao *et al.*[67], [68] developed a mathematical model to predict whole stress-strain curves for low twist staple fiber yarn considering fiber pull out and fiber slippage in staple spun yarns. Further experimental verification was found in good agreement with the theoretical results. Liu *et al.* [69] established a theoretical model to predict tensile and torsional behavior of bulky wool single yarns. They used energy method to calculate the applied force on the yarn from real stress strain behavior of the fiber at large strain. The whole force deformation curve for single yarn was predicted at small strains. Sripateep *et al.* [70], [71] presented a method for modelling the tensile behavior of multifilament twisted yarn using computer aided design approach for tensile analysis. They validated model with experimental stress-strain curves of high tenacity rayon yarn and found reasonable prediction.

CHAPTER 3

THEORETICAL MODELLING

All theoretical models, described in this chapter follows paper series of Neckar *et al.* [72] which is original part of prepared manuscript of the book monographic of yarn modelling.

3.1 Stress-strain diagram of fiber and yarn

Consider a force F_Y acting on yarn of fineness T, then tensile stress $\sigma'_Y = F_Y/S$ where $S = T / \rho$ is the substance cross section of yarn with fiber density ρ. The specific stress of yarn is then

$$\sigma_Y = \frac{F_Y}{T} = \frac{\sigma'_Y}{\rho}. \quad (3.1)$$

Similarly, if the axial force F_f is applied on a fiber with fineness t, then tensile stress of fiber is $\sigma_f = \frac{F_f}{t} = \frac{F_f}{s\rho} = \frac{\sigma'_f}{\rho}$. (3.2)

The force F_Y applied on the yarn causes an axial deformation by increasing initial length L_o to the elongated length L_Y. The difference $\Delta L = L_Y - L_o$ is called yarn elongation and the relative strain is known as yarn axial strain and can be written as

$$\varepsilon_Y = \Delta L / L_o . \quad (3.3)$$

Strain is preferred as dimensionless values instead of percentage. Similar quantities will be used for axial fiber strain. If the initial fiber length l_o increases to l_f then the difference $\Delta l = l_f - l_o$ is fiber elongation and the ratio is called fiber axial strain and is given by

$$\varepsilon_f = \Delta l / l_o . \quad (3.4)$$

By yarns as well as by fibers, the specific stresses are functions of strain and such functions are named as stress-strain functions or curves as shown in figure 3.1.

Let us suppose that each such function starts from origin as an increasing function. The maximum points of specific stress on stress-strain curves determine the breaking specific stress of fiber σ_f^* (fiber strength) and the breaking specific stress σ_Y^* of yarn (yarn tenacity). The strain values corresponding to these points are a_f and a_Y and known as breaking strains. Figure 3.1 illustrates schematically the specific stress-strain curve of twisted staple yarn and similar curve of corresponding fiber.

The yarn curve has more or less similar shape to the fiber curve in twisted staple yarns but the yarn curve lies under fiber curve. It is inconsequence to a very specific fibrous arrangement and fiber to fiber interaction in the yarn. The corresponding stress difference is $h_1$at the yarn

breaking strain $\varepsilon_Y = a_Y$. However the yarn breaking strain a_Y is mostly smaller then fiber breaking strain a_f.

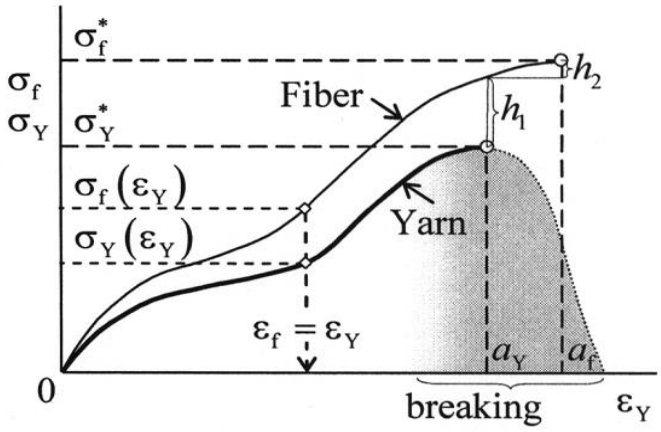

Figure 3.1 Schematic of specific stress-strain curves [72]

So the fiber specific stress increases usually more to h_2 to the final value σ_f^* on the distance from a_Y to a_f. This mechanism is related to the difference in process, yarn structure and yarn variation. Thus the coefficient of fiber stress utilization is consequence of two different influences: process in yarn structure by its tensional deformation (without significant fiber breakage) and process of fiber breakage due to yarn destruction. There are two regions on specific stress-strain curve of yarn in figure 3.1. Original structural character of a yarn remains relatively stable and all fibers are mechanically workable in first part (white). However the structure is prominently changed and more and more fibers break in the second part (gray). Of course, the border between these two regions is not too clear, the first portion is continuously changing to the second type as illustrated in the figure 3.1. However, this idea of separation of both processes reveals for building of theoretical models.

3.2 Explaining coefficient of fiber stress utilization

Let us imagine a yarn from one type of fibrous material. The ratio between the yarn tenacity and mean fiber strength is called coefficient of fiber strength utilization, which is smaller than one in all practical cases and is represented as follows

$$\varphi_\sigma^* = \frac{\sigma_Y^*}{\sigma_f^*}. \qquad (3.5)$$

Similarly we can define also the coefficient of fiber strain utilization as the ratio between the breaking strain of yarn and breaking strain of fiber i.e. , $\varphi_a^* = \frac{a_Y}{a_f}$. Generally the coefficient of strain utilization can be smaller but sometimes may be higher than one. The coefficient of

fiber stress utilization in yarn can be evaluated in the same way**.** Let us study the area before break of fiber and yarn. By the same strain $\varepsilon_f = \varepsilon_Y$, we can find experimentally the specific stress in fiber $\sigma_f(\varepsilon_Y)$ and specific stress in yarn $\sigma_Y(\varepsilon_Y)$. The ratio between two is "experimental coefficient of fiber stress utilization" in yarn and can be expressed as follows

$$\varphi_e(\varepsilon_Y) = \frac{\sigma_Y(\varepsilon_Y)}{\sigma_f(\varepsilon_Y)}. \qquad (3.6)$$

Generally this expression is not constant and it is function of yarn strain.

We will study the regulations in the next sections which are valid in the white part in figure 3.1, where original structural characteristics of yarn remains relatively stable and all fibers are mechanically workable, although the border of this part is very indistinct. Based on different experiences, the grey part of tearing process is relatively most significant in staple yarns.

3.3 Tensile behavior of twisted yarn from helical models

The helical model of fibers in yarn of fineness T, diameter D, twist Z and number of fibers in cross section *n* is based on the following assumptions: (1) All fibers have same cross-sectional area *s*; (2) all fibers are 'infinitely' long; (3) the axis of all fibers create helices with same direction of rotation; (4) all coils have one common axis which is yarn axis; (5) the height of each coil of fiber is constant and equal to $1/Z$. According to these assumptions of helical model we can proceed as follows.

3.3.1 Fiber element

The figure 3.2 displays a general thick element of a helical fiber having length d*l* and angle β, which is lying at its starting radius *r* before tensile straining. This is determining an elementary (dark grey) cylindrical surface with dimensions *r* dφ and dζ. After yarn elongation, this element shifts to a new position at smaller radius r' with a news angle β′ and with a new set of dimensions r'dφ and dζ of new elementary (light grey) cylindrical surface also mentioned separately on right hand side of figure 3.2. The following relation are then valid to write

$$\tan\beta = r\,d\varphi / d\zeta. \qquad (3.7)$$

$$\tan\beta' = r'd\varphi / d\zeta'. \qquad (3.8)$$

Considering relative characteristic of shifting we can introduce following relative dimensionless quantities of fiber element. We assume that axial strain of each fiber element is similar to axial strain of yarn. It is expressed as follows

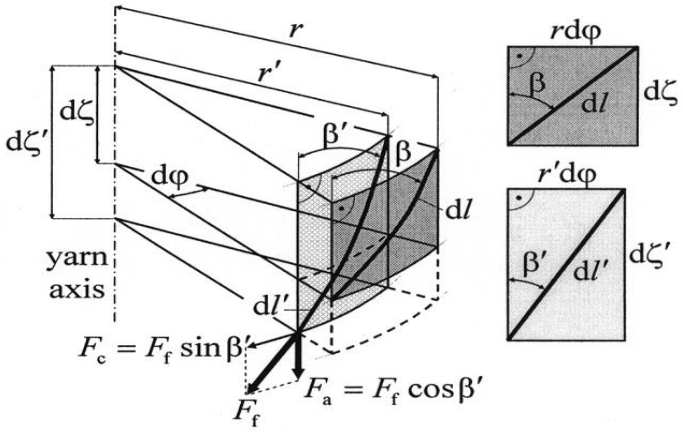

Figure 3.2 Coordinates of fiber element in a yarn before and after deformation [72]

$\varepsilon_Y = (d\zeta' - d\zeta) / d\zeta$ or $d\zeta' = (1 + \varepsilon_Y)\, d\zeta.$ (3.9)

The radial strain ε_r of fiber element takes the form

$$\varepsilon_r = \frac{r' - r}{r} = \frac{r'}{r} - 1 \text{ or } r' = (1 + \varepsilon_r)\, r. \quad (3.10)$$

The radius $r' < r$ in almost all cases so that $\varepsilon_r < 0$. The contraction ratio or Poisson's ratio can be defined as follows

$$\eta_r = -\varepsilon_r / \varepsilon_Y. \quad (3.11)$$

The value of $\eta_r \geq 0$ because $\varepsilon_r \leq 0$. We assume that value of radial strains ε_r as well as contraction ratio η_r are same for fiber element on same radius but can be generally different on different radius. Both are function of radius r. It is well known that $\eta_r \in (0, 0.5)$ in continuum mechanics and for small deformations. The contraction ratio of 0.5 means the constant volume strained body. In other cases, the contraction ratio can have higher values than 0.5. The fiber strain is defined as follows

$$\varepsilon_f = \frac{dl' - dl}{dl} = \frac{dl'}{dl} - dl, \quad dl' = dl\,(1 + \varepsilon_f). \quad (3.12)$$

3.3.2 Geometrical expression of fiber strain

According to Pythagorean's theorem the following relation can be written with a view to the elemental cylindrical surfaces on figure 3.2.

$$d^2 l = d^2\zeta + (r.\, d\varphi)^2, \quad (3.13)$$

$$d^2 l' = d^2\zeta' + (r'.d\varphi)^2. \quad (3.14)$$

Arranging equation (3.14) by using equations (3.9) to (3.12), we obtain

$$[(1+\varepsilon_f)\, dl]^2 = [(1 + \varepsilon_Y)\, d\zeta\,]^2 + [(1+\varepsilon_r)\, r\, d\varphi], \quad (3.15)$$

$$(1+\varepsilon_f)^2 = [(1 + \varepsilon_Y)\, d\zeta\,]^2 + [(1+\varepsilon_r)\, r\, d\varphi] / d^2 l. \quad (3.16)$$

Applying equation (3.7) and (3.13) we can obtain

$$(1+\varepsilon_f)^2=1+2\varepsilon_Y(\cos^2\beta-\eta_r\sin^2\beta)+\varepsilon_Y^2(\cos^2\beta+\eta_r{}^2\sin^2\beta)\,. \quad (3.17)$$

The highest fiber strain value is obtained by $\beta = 0$, due to central fibers. i.e. $\varepsilon_f = \varepsilon_Y$. Moreover, $\eta_r < 1$ and if $\beta > 0$ then $\cos^2\beta + \eta_r{}^2\sin^2\beta < 1$, and so $\varepsilon_f < \varepsilon_Y$ according to equation (3.14). The oblique fiber elements have their strain less than the axial strain of yarn. The higher is the angle β the smaller is fiber strain.

3.3.3 Relation between the angles

We can use equations (3.7) and (3.9) to (3.12) in equation (3.8). We can find the following relation among angles

$$\tan\beta' = \frac{1+\varepsilon_r}{1+\varepsilon_Y}\tan\beta = \frac{1-\eta_r\varepsilon_Y}{1+\varepsilon_Y}\tan\beta. \quad (3.18)$$

However, the relation $\tan\beta = 2\pi rZ$ is valid for starting angle β in case of helical model. So we can write

$$\tan\beta = 2\pi rZ,\ \tan\beta' = \frac{1-\eta_r\varepsilon_Y}{1+\varepsilon_Y}2\pi rZ. \quad (3.19)$$

$$\cos\beta = \frac{1}{\sqrt{(1+\tan^2\beta)}} = \frac{1}{\sqrt{1+(2\pi rZ)^2}},\ \sin\beta = \frac{2\pi rZ}{\sqrt{1+(2\pi rZ)^2}}\,. \quad (3.20)$$

$$\cos\beta' = \frac{1}{\sqrt{(1+\tan^2\beta')}} = \frac{1}{\sqrt{\left[1+\frac{1-\eta_r\varepsilon_Y}{1+\varepsilon_Y}(2\pi rZ)^2\right]}}\,. \quad (3.21)$$

The relation between the two angles is given as follow

$$\frac{\cos\beta'}{\cos\beta} = \frac{\sqrt{(1+(2\pi rZ)^2}}{\sqrt{\left[1+\frac{1-\eta_r\varepsilon_Y}{1+\varepsilon_Y}(2\pi rZ)^2\right]}}\,. \quad (3.22)$$

3.3.4 Fiber force and stress

The tensional force F_f in fiber is an increasing function of fiber strain ε_f. We can represent such function as follows

$$F_f = F_f(\varepsilon_f). \quad (3.23)$$

Though, the stress-strain relation of fiber can be characterized more frequently. The specific engineering tensile stress in fiber is possible to represent as follows

$$\sigma_f = \sigma_f(\varepsilon_f). \quad 3.24)$$

The fiber specific stress can be expressed as follow

$$\sigma_f(\varepsilon_f) = \frac{F_f(\varepsilon_f)}{t} = \frac{F_f(\varepsilon_f)}{s\rho}\,. \quad (3.25)$$

Where t is fiber fineness, s is the cross sectional area of fiber, ρ is the fiber density and ε_f is the fiber strain estimated by equation (3.17).

3.3.5 Component of the force

The force F_f can be decomposed into two perpendicular components in figure 3.2. The component of force F_a in yarn direction is parallel with yarn axis and F_c in cross direction of yarn is vertical to the yarn axis. So

$$F_a = F_f(\varepsilon_f)\cos\beta'. \tag{3.26}$$

The force F_a is contributing to the whole yarn axial force from studied fiber. The cross directional force $F_c = F_f(\varepsilon_f)\sin\beta'$, along with all other fibers creates torsional moment of yarn.

3.3.6 Differential layer

The fiber cross-sectional area s^* of one fiber in the yarn cross-section illustrated in figure 3.3a is $s^* = s/\cos\beta$. The concept of differential layer in the yarn according to helical model is shown in the figure 3.3b and we can find number of fiber d_n in cross section of differential layer according to the following equation

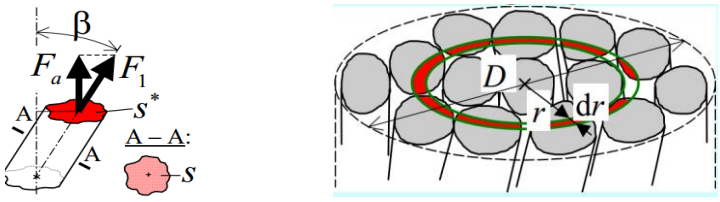

(a) (b)

Figure 3.3 a) Inclined fiber b) Differential annulus in yarn cross section[72]

$$d_n = \frac{\text{Sectional area of all fibers in differential anulus}}{\text{Sectional area of one fiber}} = \frac{2\pi r dr \mu_r}{s/\cos\beta}. \tag{3.27}$$

After elongation of the yarn the differential layer changed its position from starting radius r to the new radius $r'$and it "takes its own fiber with". Such differential layer contributes to total axial force of yarn with

$$dF_Y = F_a\, d_n. \tag{3.28}$$

The total axial force F_Y of the yarn diameter D is then the integral over the whole differential layers from radius $r = 0$ to radius $r = D/2$. All fibers lie inside of a yarn cylinder with diameter D in the case of helical model.

3.3.7 Force of yarn

Using equations from (3.25) to (3.28) and by considering equations (3.21) and (3.22) we can express the total axial force F_Y of yarn as function of yarn strain ε_Y as follows

$$F_Y(\varepsilon_Y) = \int_{r=0}^{r=D/2} dF_Y = \int_{r=0}^{r=D/2} F_a \, d_n = 2\pi\rho \int_0^{D/2} \sigma_f(\varepsilon_f) \cos\beta' \cos\beta \, \mu_r r dr,$$

$$F_Y(\varepsilon_Y) = 2\pi\rho \int_0^{D/2} \sigma_f(\varepsilon_f) \frac{\cos\beta'}{\cos\beta} \cos^2\beta \, \mu_r r \, dr. \quad (3.29)$$

Where ε_f is determined by equation (3.17). The angle β and ratio $\frac{\cos\beta'}{\cos\beta}$ are given according to equations (3.19), (3.20), (3.21) and (3.22). The force F_Y is function of ε_Y which is contained in equation (3.17) determining ε_f as function of ε_Y.

3.3.8 Specific stress-strain relation of yarn

In case of helical model the substance cross section of yarn which is the sum of sectional area of all fibers present in yarn cross section. So we can write

$$S = \int_0^{D/2} dS = 2\pi \int_0^{D/2} \mu_r r dr. \quad (3.30)$$

The stress of yarn is $\sigma'_Y = F_Y / S$ and the specific stress is then $\sigma_Y = \sigma'_Y / \rho = F_Y / S\rho$. Using now equations (3.29) and (3.30), we can write the expression as follows

$$\sigma_Y(\varepsilon_Y) = \frac{F_Y(\varepsilon_Y)}{S\rho} = \frac{2\pi\rho \int_0^{D/2} \sigma_f(\varepsilon_f) \frac{\cos\beta'}{\cos\beta} \cos^2\beta \, \mu_r r dr}{2\pi\rho \int_0^{D/2} \mu_r r dr},$$

$$\sigma_Y(\varepsilon_Y) = \frac{\int_0^{D/2} \sigma_f(\varepsilon_f) \frac{\cos\beta'}{\cos\beta} \cos^2\beta \, \mu_r r dr}{\int_0^{D/2} \mu_r r dr}. \quad (3.31)$$

This expression shows that σ_Y is function of ε_Y because this variable contains equation (3.17) determining ε_f as function of ε_Y.

3.3.9 Non-twisted bundle

The angle $\beta = 0$ for all radii in non-twisted bundle of fibers. Then $\cos\beta = 1$ and $\sin\beta = 0$ according to equation (3.20) and (3.21), $\frac{\cos\beta'}{\cos\beta} = 1$ and $\varepsilon_f = \varepsilon_Y$ according to equation (3.17). Then equation (3.31) can be written as follows

$$\sigma_Y(\varepsilon_Y) = \frac{\int_0^{D/2} \sigma_f(\varepsilon_f) \, \mu_r r dr}{\int_0^{D/2} \mu_r r dr} = \sigma_f(\varepsilon_f) \frac{\int_0^{D/2} \mu_r r dr}{\int_0^{D/2} \mu_r r dr} = \sigma_f(\varepsilon_f). \quad (3.32)$$

We can write the $\sigma_f(\varepsilon_f)$ before integral because we assumed that all fibers have the same properties.

3.3.10 Coefficient of fiber stress utilization in yarn

The coefficient of fiber stress utilization in the yarn is defined according to equation (3.6). Applying equation (3.31) in equation (3.6). We can have

$$\varphi(\varepsilon_Y) = \frac{\sigma_Y(\varepsilon_Y)}{\sigma_f(\varepsilon_Y)} = \frac{\int_0^{D/2} \sigma_f(\varepsilon_f) \frac{\cos\beta'}{\cos\beta} \cos^2\beta\, \mu_r\, r dr}{\sigma_f(\varepsilon_Y) \int_0^{\frac{D}{2}} \mu_r\, r dr}. \quad (3.33)$$

The coefficient of fiber stress utilization is unity by non-twisted bundle because equation (3.32) is valid in this special case. The solving of the equation (3.33) is possible but practically extra ordinary difficult. It is because we usually do not know the necessary input of radial functions μ_r and η_r. Experimental specific stress-strain function of fiber $\sigma_f(\varepsilon_f)$ can be evaluated easily in modern fiber and textile laboratories.

The radial function η_r could be possible to derive based on experimental knowledge of starting radial function of packing density μ_r and final radial function of packing density μ'_r in tensioned yarn.

3.4 Coefficient of fiber stress utilization from Gegauff

Beside all previous simplification Gegauff [2] assumed that specific stress σ_f by axial tension of fiber is a linear function of fiber strain ε_f as follows

$$\sigma_f = k\,\varepsilon_f. \quad (3.34)$$

$k = E / \rho$ = constant, the constant k is the ratio between fiber Young's modulus and fiber density.

The axial force in the fiber is

$$F_f = \sigma_f\, s = k\,\varepsilon_f\, s. \quad (3.35)$$

The component of force in yarn direction using equations (3.34) and (3.35) can be written as follows

$$F_a = F_f \cos\beta = k\,\varepsilon_f\, s \cos\beta. \quad (3.36)$$

The fiber sectional area $s^* = s / \cos\beta$ and the normal stress on this area is

$$\sigma_a = \frac{F_a}{s^*} = \frac{k\,\varepsilon_f\, s \cos\beta}{s / \cos\beta} = k\,\varepsilon_f \cos^2\beta. \quad (3.37)$$

For small strains $\varepsilon_f = \varepsilon_Y(\cos^2\beta - \eta \sin^2\beta)$, so we can rewrite the equation (3.37) as follow

$$\sigma_a = k\,\varepsilon_Y\,(\cos^4\beta\ -\eta\cos^2\beta\sin^2\beta). \tag{3.38}$$

The fiber sectional area inside the differential annulus is $ds = 2\pi r dr\mu$, then the yarn axial force is

$$F_Y\ =\ \int_{r=0}^{r=D/2}\sigma_a ds\ =\ \int_0^{D/2}\sigma_a\,2\pi\,\mu\,r dr. \tag{3.39}$$

From equation (3.39) and using equation (3.38), we can obtain

$$F_Y = \int_0^{D/2} k\,\varepsilon_Y\,(\cos^4\beta\ -\eta\cos^2\beta\sin^2\beta)\,2\pi\,\mu\,r dr,$$

$$F_Y = 2\pi\,\mu\,k\,\varepsilon_Y\int_0^{D/2}(\cos^4\beta\ -\eta\cos^2\beta\sin^2\beta)\,r dr. \tag{3.40}$$

By substitution $r = \frac{2\pi rZ}{2\pi Z} = \frac{D\tan\beta}{2\pi DZ} = \frac{D\tan\beta}{2\tan\beta_D}$, $dr = \frac{D}{2\tan\beta_D}\ \frac{d\beta}{\cos^2\beta}$, $r\,dr = [\frac{D}{2\tan\beta_D}]^2\ \frac{\sin\beta}{\cos^3\beta}\,d\beta$.

Putting the values of rdr in equation (3.40) and rearranging, we obtain

$$F_Y = 2\pi\,\mu\,k\,\varepsilon_Y\,[\frac{D}{2\tan\beta_D}]^2\int_0^{\beta_D}(\cos^4\beta\ -\eta\cos^2\beta\sin^2\beta)\frac{\sin\beta}{\cos^3\beta}\,d\beta. \tag{3.41}$$

The yarn contraction ratio is usually function of radius and twist angle, but we assume η = constant.

$$F_Y = 2\pi\,\mu\,k\,\varepsilon_Y\,[\frac{D}{2\tan\beta_D}]^2[\int_0^{\beta_D}\sin\beta\cos\beta\,d\beta\ -\eta\ \int_0^{\beta_D}\frac{\sin^3\beta}{\cos\beta}\,d\beta] \tag{3.42}$$

Solving the indefinite integral by substitution method, we have

$\sin\beta = t$, $\cos\beta\,d\beta = dt$,

$$\int\cos\beta\sin\beta\,d\beta = \int t dt = \frac{t^2}{2} = \frac{\sin^2\beta}{2} = \frac{1-\cos^2\beta}{2},$$

$$\int\frac{\sin^3\beta}{\cos\beta}\,d\beta = \int\frac{1-\cos^2\beta}{\cos\beta}\sin\beta\,d\beta = \int\frac{1-t^2}{t}(-dt)\ \ (\text{By substitution } \cos\beta = t\ ,\ -\sin\beta\,d\beta = dt\ ),$$

$$= -\int\frac{dt}{t} + \int t dt = -\ln|t| + \frac{t^2}{2} = -\ln|\cos\beta| + \frac{\cos^2\beta}{2}\int\cos\beta\sin\beta\,d\beta - \ \eta\int\frac{\sin^3\beta}{\cos\beta}\,d\beta,$$

$$= \frac{1-\cos^2\beta}{2} + \eta\ \ln|\cos\beta| - \ \frac{\eta\cos^2\beta}{2},$$

$$F_Y = \pi\,\mu\,k\,\varepsilon_Y\,[\frac{D}{2}]^2\ \left[(1+\eta)(\cos^2\beta_D) + \ \frac{\eta\ln\cos^2\beta_D}{\tan^2\beta_D}\right]. \tag{3.43}$$

At the same strain ε_Y, untwisted bundle of same fineness has the axial force as follows

$$F_Y^* = \sigma_Y\,S = k\,\varepsilon_Y\,\mu\,\pi\ \frac{D^2}{4} \tag{3.44}$$

The coefficient of fiber stress utilization in the twisted yarn is

$$\varphi_g(\varepsilon_Y) = \frac{F_Y}{F_Y^*} = (1+\eta)(\cos^2\beta_D) + \frac{\eta\ln\cos^2\beta_D}{\tan^2\beta_D}\ . \tag{3.45}$$

The solving of Gegauff's equation is very simple just evaluate the twist angle β_D from yarn diameter D, twist per meter Z, contraction ratio η and using equation (3.45) we can determine the coefficient of fiber stress utilization φ_g of the fiber in yarn independent of yarn strain ε_Y.

3. 5. Coefficient of fiber stress utilization considering real stress-strain function

The complete solution of equations (3.29), (3.31) and (3.33) is not usually possible because we have not the necessary input information regarding radial function of packing density μ_r and radial function of contraction ratio η_r. Experimental determination of the third function, specific stress-strain function of fiber $\sigma_f(\varepsilon_f)$ is possible in modern fiber and textile laboratories. However, we can make this problem easier by means of certain simplifying assumptions.

3.5.1 Small strains

At first let us assume that the yarn strain ε_Y is small. Then the corresponding strain ε_f of the fiber from the starting radius of *r* is even smaller then ε_Y. Then it is possible to represent fiber strain ε_f in an assembly of fibers twisted at some arbitrary angle according to equation (3.17) as follows

$$(1+\varepsilon_f)^2 = 1 + 2\varepsilon_Y\left(\cos^2\beta - \eta_r\sin^2\beta\right) + \varepsilon_Y{}^2\left(\cos^2\beta + \eta_r{}^2\sin^2\beta\right).$$

On simplification $$\varepsilon_f + \frac{\varepsilon_f{}^2}{2} = \varepsilon_Y\left(\cos^2\beta - \eta\sin^2\beta\right) + \frac{\varepsilon_Y{}^2}{2}\left(\cos^2\beta + \eta^2\sin^2\beta\right).$$

It can be shown that at very low fiber and yarn strains (0 ~ 0.1), the second term on the right hand side in the above expression becomes negligible while the first term is little affected. Since for small strains $\varepsilon_f^2 = 0$ and $\varepsilon_Y^2 = 0$. Then we can write as follow

$$\varepsilon_f = \varepsilon_Y\left(\cos^2\beta - \eta_r\sin^2\beta\right). \qquad (3.46)$$

Equation (3.20) explains the ratio $\frac{\cos\beta'}{\cos\beta}$, figure 3.4 show the mentioned relation in typical area of common staple yarns. The majority of the fibers in yarn has usually angle β smaller then 30^o, the contraction ratio of yarns is usually not far from 0.5, and the axial strain of the yarn is used to be under 0.2. Then the quantity $\frac{\cos\beta'}{\cos\beta}$ differs from value 1 not more then 3 % in such situation. So we observe that

$$\frac{\cos\beta'}{\cos\beta} = 1. \qquad (3.47)$$

It can be obviously the good approximation of this ratio.

3.5.2 Independency to radius

In spite of the fact that the packing density μ_r and contraction ratio η_r of differential layer depends generally on the radius, we assume for the simplification that these quantities are independent to the radius *r* similar to yarn strain ε_Y. Thus

$$\mu_r = \mu = \text{constant} \qquad (3.48)$$

$\eta_r = \eta$ = constant (3.49)

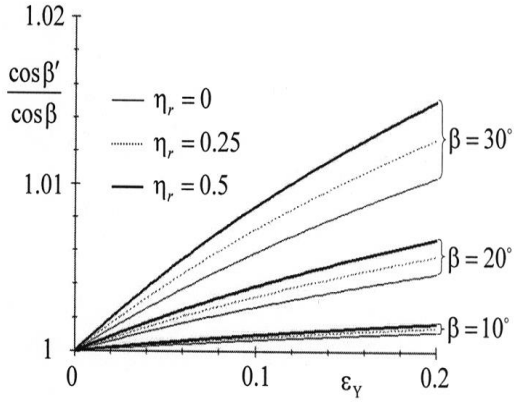

Figure 3. 4 Ratio $\frac{cos\,\beta'}{cos\,\beta}$ as function of ε_Y [72]

3.6 Simplified equation for coefficient of fiber stress utilization

Using equations (3.47) and (3.48), we can formulate corresponding equations for the total axial force of yarn and for coefficient of fiber stress utilization in the yarn.

The total axial force $F_Y\,(\varepsilon_Y)$ of yarn follows equation (3.29). So it is valid to write as follows

$$F_Y\,(\varepsilon_Y) = 2\pi\,\rho\,\mu\int_0^{D/2}\sigma_f\,(\varepsilon_f)\cos^2\beta\;r dr. \tag{3.50}$$

Substitution of r and dr similar to equation (3.40) in the equation (3.50) and subsequent rearrangement yields below

$$F_Y\,(\varepsilon_Y) = 2\pi\,\rho\,\mu\int_0^{\beta_D}\sigma_f\,(\varepsilon_f)\cos^2\beta\,\left[\frac{D}{2\tan\beta_D}\right]^2\frac{\sin\beta}{\cos^3\beta}\,d\beta,$$

$$= 2\pi\rho\mu\left[\frac{D}{2\tan\beta_D}\right]^2\int_0^{\beta_D}\sigma_f\,(\varepsilon_f)\tan\beta\,d\beta. \tag{3.51}$$

According to equation (3.31), the expression for yarn specific stress can be written as follows

$$\sigma_Y\,(\varepsilon_Y) = \frac{\mu\int_0^{D/2}\sigma_f\,(\varepsilon_f)\;\cos^2\beta\;r dr}{\mu\int_0^{D/2} r dr} = \frac{\left[\frac{D}{2\tan\beta_D}\right]^2\int_0^{\beta_D}\sigma_f\,(\varepsilon_f)\tan\beta\,d\beta}{\left[\frac{D}{2\tan\beta_D}\right]^2\int_0^{\beta_D}\frac{\sin\beta}{\cos^3\beta}d\beta},$$

$$\sigma_Y\,(\varepsilon_Y) = \frac{\int_0^{\beta_D}\sigma_f\,(\varepsilon_f)\;\tan\beta\,d\beta}{\int_0^{\beta_D}\frac{\sin\beta}{\cos^3\beta}d\beta} \tag{3.52}$$

Let us solve the integral in denominator of equation (3.52) by substituting

$\cos\beta = t$, $-\sin\beta\,d\beta = dt$.

$$\int_0^{\beta_D}\frac{\sin\beta}{\cos^3\beta}d\beta = -\int_1^{\cos\beta_D}\frac{dt}{t^3} = \left[\frac{1}{2t^2}\right]_1^{\cos\beta_D} = \frac{1}{2}\left(\frac{1}{\cos^2\beta_D} - 1\right) = \frac{\tan^2\beta_D}{2}. \tag{3.53}$$

Applying equation (3.53) in equation (3.52), we can obtain

$$\sigma_Y(\varepsilon_Y) = \frac{\int_0^{\beta_D} \sigma_f(\varepsilon_f) \tan\beta \, d\beta}{\int_0^{\beta_D} \frac{\sin\beta}{\cos^3\beta} d\beta} = \frac{2}{\tan^2\beta_D} \int_0^{\beta_D} \sigma_f(\varepsilon_f) \tan\beta \, d\beta \quad (3.54)$$

We can write the coefficient of fiber stress utilization $\varphi_{c1}(\varepsilon_Y)$ in yarn using equation (3.6) as follows.

$$\varphi_{c1}(\varepsilon_Y) = \frac{\sigma_Y(\varepsilon_Y)}{\sigma_f(\varepsilon_Y)} = \frac{\frac{2}{\tan^2\beta_D} \int_0^{\beta_D} \sigma_f(\varepsilon_f) \tan\beta \, d\beta}{\sigma_f(\varepsilon_Y)}$$

$$= \frac{2}{\sigma_f(\varepsilon_Y) \tan^2\beta_D} \int_0^{\beta_D} \sigma_f(\varepsilon_f) \tan\beta \, d\beta. \quad (3.55)$$

Fiber strain ε_f should be calculated from equation (3.46) for small deformations to determine the fiber specific stress $\sigma_f(\varepsilon_f)$.

3.7 Calculation of coefficient of fiber stress utilization from single integral

The single integral equation (3.55) was solved using the input parameters fiber stress-strain function $\sigma_f(\varepsilon_f)$, surface twist angleβ_D, yarn strain ε_Y and contraction ratio η. The twist angle β_D was evaluated from yarn diameter *D* and yarn twist per millimetre *Z*. The fiber strain ε_f at each value of angle β from 0 ~ β_D with hundred steps was determined to prepare the look up table. The fiber specific stress $\sigma_f(\varepsilon_f)$ was evaluated at each value of fiber strain from look up table. Multiplication of fiber specific stress-strain function $\sigma_f(\varepsilon_f)$ and tan β was followed by numerical integration, $\left[\sum_0^{\beta_D}(\sigma_f(\varepsilon_f)\tan\beta)\right]$. The output from the numerical integration was finally multiplied by $\frac{2}{\sigma_f(\varepsilon_Y)\tan^2\beta_D}$ to obtain the coefficient of fiber stress utilization from single integral model. The calculation scheme is shown in the figure 3.5.

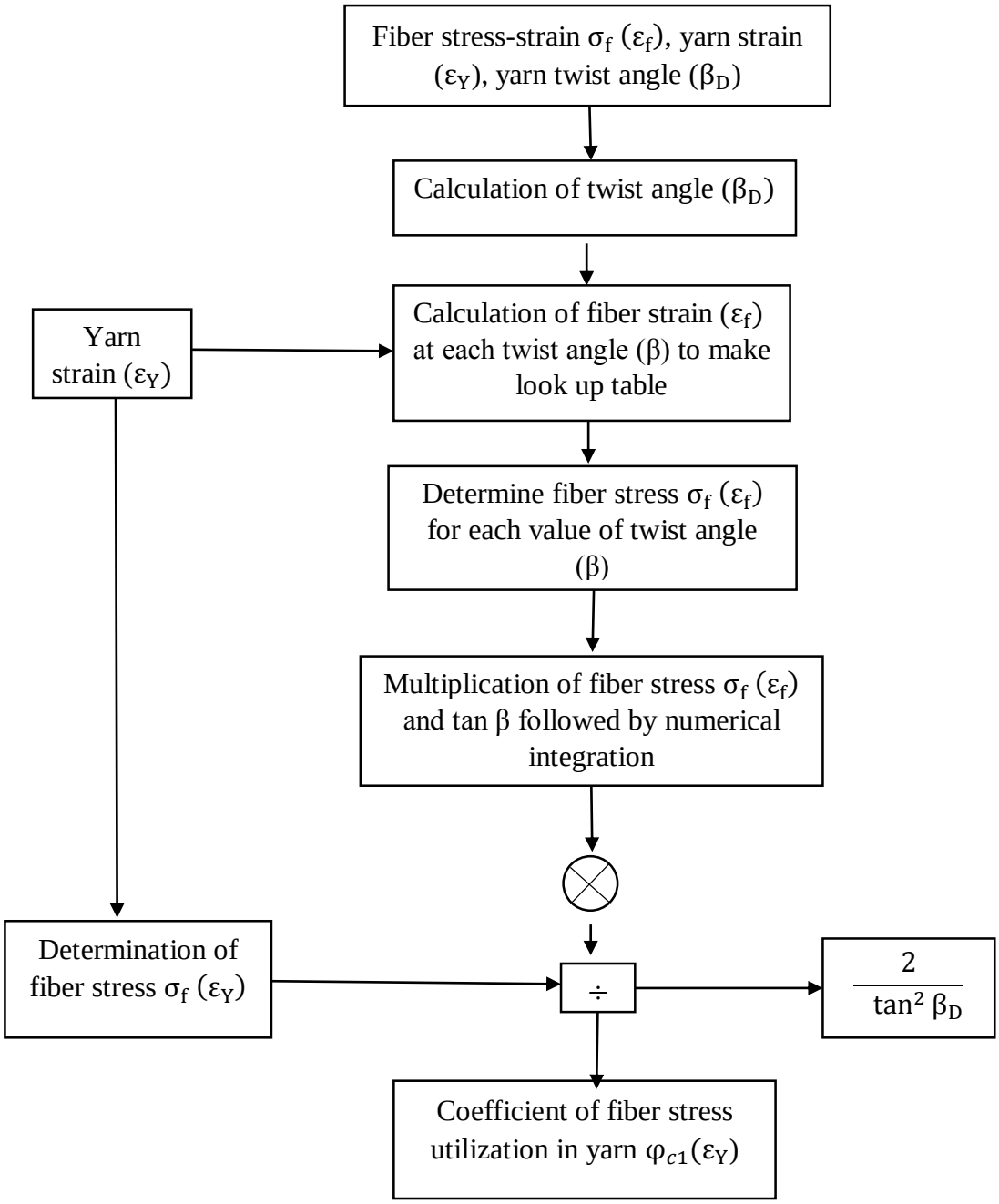

Figure 3. 5 Calculation scheme for coefficient of fiber stress utilization from single integral

3.8. Partial generalization of helical model

Up to now, it is considered that all the fibers in the yarn are inclined at a given radius *r* with same angle β in accordance with the helical model. Now this model will be partly generalized. Let us imagine that all the fibers in the differential layer situated at radius *r* are lying on the corresponding cylindrical surface, but they do not have the same angle β, rather they form different angles θ from yarn axis.

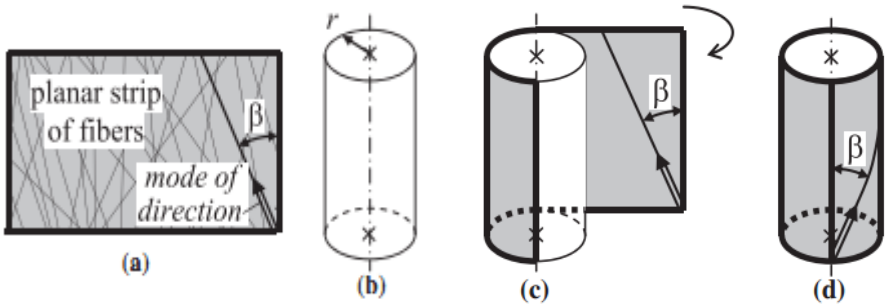

Figure 3. 6 Originating differential fiber layer in yarn [72]

3.8.1 Idea of generalization

The above equations are based on idea of helical model that all fibers have same twist angle β, but in actual twist angle varies at elemental radius. Let us imagine that all fibers in differential annulus on radius *r* permanently lying on the corresponding cylindrical surface and do not change their path. The differential thin layer is shown in the figure 3.6. Let us have gray planer strip (a) of fibers with varying angle θ such that $\theta = \beta$. Further let us have cylinder (b) round yarn axis at radius *r* and the strip is rolled up on the cylindrical surface in (c) , so that we obtained differential layer of yarn where fibers have different angles θ and model angle $\beta = \theta$ in the direction of yarn axis.

3.8.2 Distribution of angle θ

The distribution of fiber directions by planer orientation of fibers was derived in [73]. It was found that uni modal probability density function of non-oriented angle $\theta \in (0, \frac{\pi}{2})$ is as follows

$$u(\theta) = \frac{1}{\pi} \frac{C}{C^2-(C^2-1)\cos^2(\theta+\beta)} + \frac{1}{\pi} \frac{C}{C^2-(C^2-1)\cos^2(\theta-\beta)} . \qquad (3.56)$$

$C \geq 1$ is costant, "measure" of preference of model direction. The graphical display of function is shown in the figure 3.6.

The higher is the parameter *C*, more is the concentration of fiber near to the modal angle β. *C* is unlimitedly higher and higher then fiber directions are more and more concentrated in smaller and smaller vicinity round the modal direction given by angle β. Finally, all fibers will have the same angle $\theta = \beta$ in the limit of such process. The probability density function $u(\theta)$ is then limited to Direac delta-function $\delta(\theta - \beta)$. It is valid $\delta(\theta - \beta) = \infty$ if $\theta = \beta$, $\delta(\theta - \beta) = 0$ for $\theta \neq \beta$, and $\int_{-\infty}^{\infty} \delta(\theta - \beta)\, d\theta = 1$.

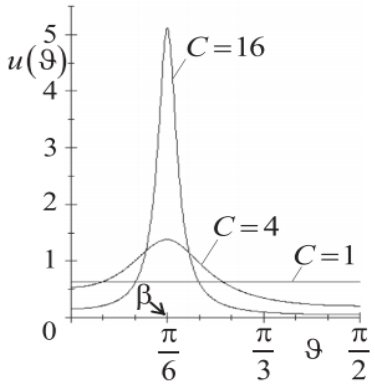

Figure 3. 7 Behavior of equation 3.56 at β = 30° [72]

Finally, it is valid for each general function

$$\int_{-\infty}^{\infty} f(\theta)\ \delta\ (\theta - \beta)\ d\theta = f\ (\beta). \qquad (3.57)$$

In our case, the probability density function $u\ (\theta)$ according to equation (3.56) represents also the probability density function of fiber inclination in differential layer of yarn.

The distribution of fiber directions in cross-section differs from the distribution of fiber direction in whole planar strip of fibers. The probability density function of such angles θ was explained by Neckar [73]. The relation is given as follows

$$u^*\ (\theta) = \frac{\cos\theta\ u\ (\theta)}{k_n}\ . \qquad (3.58)$$

Where $k_n = \int_0^{\frac{\pi}{2}} \cos\theta\ u(\theta)\ d\theta$. (3.59)

Now $u^*(\theta)$ represents also the probability density function of fiber inclination in cross section of differential layer of yarn.

3.8.3 Number of fibers in section of differential layer

A section of very thin planar strip of unit length with a thickness of δh is shown in figure 3.7. The number of sectioned fibers hatched fiber islands per unit sectional length was derived by Neckar [72] as follows

$$\nu = \delta h \frac{\mu\rho}{t} k_n\ . \qquad (3.60)$$

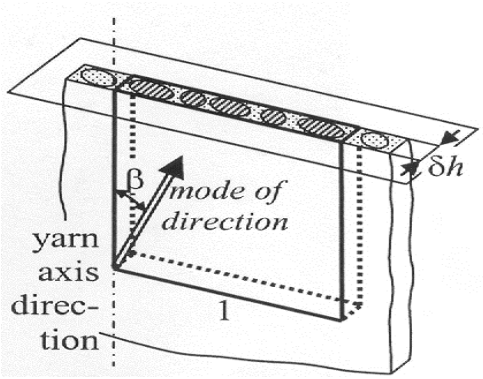

Figure 3. 8 Section of planar fiber assembly [72]

Where t is fiber fineness, ρ is fiber mass density and μ is packing density of the mentioned planar strip. The fiber cross sectional area $s = t / \rho$. Further if the thickness of the planar strip is elemental $\delta h \rightarrow \mathrm{d}h$, then the number of fibers per unit sectional length is also elemental $\nu \rightarrow \mathrm{d}\nu$, and we can write equation (3.60) as follow

$$\mathrm{d}\nu = \frac{\mathrm{d}h\ \mu\ k_\mathrm{n}}{s} \tag{3.61}$$

After rolling of the starting planar strip on cylindrical surface, the elemental thickness dh is changed to the elemental increment radius dr. Moreover, the length of differential layer on radius r *is* $2\pi r$, so that the number dn of sectioned fibers in studied differential layer by cross section of yarn is

$$\mathrm{d}n = \mathrm{d}\nu\ 2\pi r = \mathrm{d}r\ \mu\ \frac{k_n}{s}\ 2\pi r = \frac{2\pi\ \mu\ r\mathrm{d}r}{s}\ k_\mathrm{n} \tag{3.62}$$

The mean sectional area of fiber in the differential layer $s^* = s / k_n$, so it is valid to write $\mathrm{d}n = 2\pi\mu\ r\mathrm{d}r\ / s^*$. Only the constant sectional area, s / cos β was used in place of present mean sectional area of fiber $s^* = s / k_\mathrm{n}$.

3.8.4 Simplified Assumptions

We will use simplified assumptions as follows.

I. Quantities $\mu_r = \mu$ and $\eta_r = \eta$ are constant, independent to radius according to equations (3.48) and (3.49).

II. Small deformations: It allows approximately to use the starting geometry of yarn in place of geometry of tensioned yarn. Especially $\theta' = \theta$, $\beta' = \beta$, $\beta'_\mathrm{D} = \beta_\mathrm{D}$, $r' = \mathrm{r}$, $D' = D$.

III. The yarn strain ε_Y and fiber strain ε_f are small and related similar to equation (3.46) as follow

$\varepsilon_f = \varepsilon_Y (\cos^2 \theta - \eta \sin^2 \theta)$. (3.63)

There exists an upper limit of angle $\theta = \theta_u$ by which the fiber strain is equal to zero, $\varepsilon_f = 0$. So it is valid to write

$0 = \varepsilon_Y (\cos^2 \theta_u - \eta \sin^2 \theta_u)$, $\theta_u = \text{arc sin} \frac{1}{\sqrt{(1+\eta)}}$. (3.64)

If $\theta \in (\theta_u, \frac{\pi}{2})$ then the fiber strain is negative according to equation (3.63), fiber should be axially compressed. The situation is illustrated in the figure 3.7. Where $\theta > \theta_u$ so that $dl' < dl$ and $\varepsilon_f = (dl' - dl)/dl < 0$ according to equation (3.12). However, we can assume that

- Number of such fibers is very small so that their influence to the mechanical properties of yarn is not too significant.
- The axial component of fiber is difficult to imagine due to fiber slippage, waviness, and or another similar processes in this situation.

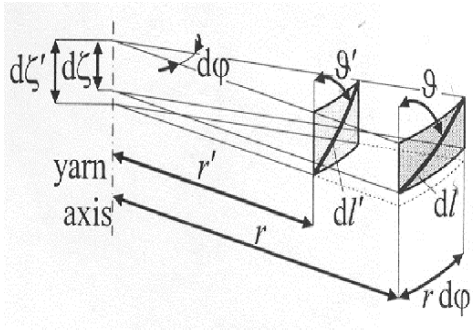

Figure 3. 9 Shortening of fiber element by yarn straining (if $\theta > \theta_u$) [72]

Going out from previous assumptions, if $\theta \in (\theta_u, \pi/2)$ then the contribution to the axial yarn specific stress is zero from fiber under consideration.

3.8.5 Force in yarn

Specific stress of fiber $\sigma_f(\varepsilon_f)$ determines the force in fiber $F_f(\varepsilon_f) = \sigma_f(\varepsilon_f)\, s\rho$ according to equation (3.25). A fiber has the angle θ to the yarn axis so that its component to the yarn direction is

$F_a = F_f(\varepsilon_f) \cos\theta$, and $F_a = 0$ if $\theta \in (\theta_u, \frac{\pi}{2})$.

However, fibers have lot of directional angles θ on a given radius. In the cross-section of differential layer, the distribution of their angles θ is described according to equation (3.56). So, the mean force component per one fiber to the yarn direction using equation 3.58 is as follows.

$$\bar{F}_a = \int_0^{\theta_u} F_a u^*(\theta)\, d\theta = \frac{s\rho}{k_n} \int_0^{\theta_u} \sigma_f\,(\varepsilon_f) \cos^2\theta\, u\,(\theta) d\theta. \quad (3.65)$$

Using equations (3.62) and (3.65) and rearranging, the whole differential layer is carrying the force

$$dF_Y = dn\, \bar{F}_a = 2\pi\mu\rho r dr \int_0^{\theta_u} \sigma_f\,(\varepsilon_f) \cos^2\theta\, u\,(\theta)\, d\theta. \quad (3.66)$$

The complete axial force in the yarn is then

$$F_Y(\varepsilon_Y) = \int_{r=0}^{r=D/2} dF_Y = 2\pi\mu\rho \int_0^{D/2} \left[\int_0^{\theta_u} \sigma_f\,(\varepsilon_f) \cos^2\theta\, u\,(\theta) d\theta\right] r dr. \quad (3.67)$$

In the last equation (3.67):

- Helical angle β is determined by equation $\tan\beta = 2\pi r Z$ where Z is the yarn twist. Similarly, the twist intensity $\tan\beta_D = \pi D Z$.
- Fiber strain $\varepsilon_f = \varepsilon_Y(\cos^2\theta - \eta\sin^2\theta)$ is the function of angle θ through ε_f. The axial force in yarn depends on the yarn strain ε_Y.
- The upper limit of angle θ, i.e. angle θ_u follows equation (3.67) as the function of the contraction ratio, η.
- The probability density function $u\,(\theta)$ determines equation (3.56) as the function of θ and the modal value β.

Equation (3.67) can also be rearranged by substitution as follows.

$$r = \frac{2\pi r Z}{2\pi Z} = \frac{\tan\beta}{2\pi Z} = \frac{D\tan\beta}{2\pi D Z} = \frac{D\tan\beta}{2\tan\beta_D}, \quad dr = \frac{D}{2\tan\beta_D}\frac{d\beta}{\cos^2\beta},$$

$$r dr = \frac{D\tan\beta}{2\tan\beta_D}\frac{D}{2\tan\beta_D}\frac{d\beta}{\cos^2\beta} = \left[\frac{D}{2\tan\beta_D}\right]^2 \frac{\sin\beta}{\cos^3\beta},$$

$$F_Y(\varepsilon_Y) = 2\pi\mu\rho\left[\frac{D}{2\tan\beta_D}\right]^2 \int_0^{\beta_D} \left[\int_0^{\theta_u} \sigma_f\,(\varepsilon_f) \cos^2\theta\, u\,(\theta) d\theta\right] \frac{\sin\beta}{\cos^3\beta} d\beta. \quad (3.68)$$

Let us imagine that all angles θ are limited to the angle β in a special case. Then the probability density function $u\,(\theta)$ is limited to Dirac delta-function $\delta\,(\theta - \beta)$ and equation (3.57) is valid. Let us especially select the function $f\,(\theta) = \sigma_f\,(\varepsilon_f)\cos^2\theta$ according to the expression in equation (3.68). Then

$$\int_{-\infty}^{\infty} \sigma_f\,(\varepsilon_f)\cos^2\theta\, \delta\,(\theta - \beta)\, d\theta = \sigma_f\,(\varepsilon_f)\cos^2\beta, \text{ where } \varepsilon_f = \varepsilon_Y(\cos^2\beta - \eta\sin^2\beta).$$

Thus $$F_Y(\varepsilon_Y) = 2\pi\mu\rho\left(\frac{D}{2\tan\beta_D}\right)^2 \int_0^{\beta_D} \sigma_f\,(\varepsilon_f)\cos^2\beta \frac{\sin\beta}{\cos^3\beta} d\beta,$$

$$= 2\pi\mu\rho\left(\frac{D}{2\tan\beta_D}\right)^2 \int_0^{\beta_D} \sigma_f\,(\varepsilon_f)\tan\beta\, d\beta.$$

This expression is identical with earlier derived equation (3.51).

3.8.6 Coefficient of fiber stress utilization from partial generalization of helical model

The packing density of yarn is, $\mu = 4T / (\pi D^2 \rho)$ where T is the yarn fineness. Using this expression in equation (3.67) we find

$$F_Y(\varepsilon_Y) = 2\pi \frac{4T}{\pi D^2 \rho} \rho \left(\frac{D}{2\tan \beta_D}\right)^2 \int_0^{\beta_D} \left[\int_0^{\theta_u} \sigma_f(\varepsilon_f) \cos 2\theta \, u(\theta) \, d\theta\right] \frac{\sin \beta}{\cos^3 \beta} \, d\beta ,$$

$$= T \frac{2}{\tan^2 \beta_D} \int_0^{\beta_D} \left[\int_0^{\theta_u} \sigma_f(\varepsilon_f) \cos^2 \theta \, u(\theta) d\theta\right] \frac{\sin \beta}{\cos^3 \beta} \, d\beta . \quad (3.69)$$

However, the specific stress is defined as the ratio of force and fineness. So we obtain the following expression from the above equation

$$\sigma_Y(\varepsilon_Y) = \frac{F_Y(\varepsilon_Y)}{T} = \frac{2}{\tan^2 \beta_D} \int_0^{\beta_D} \left[\int_0^{\theta_u} \sigma_f(\varepsilon_f) \cos^2 \theta \, u(\theta) d\theta\right] \frac{\sin \beta}{\cos^3 \beta} \, d\beta. \quad (3.70)$$

The coefficient of fiber stress utilization in the yarn is defined according to equation (3.6), applying equation (3.70), we find

$$\varphi_{c2}(\varepsilon_Y) = \frac{\sigma_Y(\varepsilon_Y)}{\sigma_f(\varepsilon_Y)} = \frac{2}{\sigma_f(\varepsilon_Y) \tan^2 \beta_D} \int_0^{\beta_D} \left[\int_0^{\theta_u} \sigma_f(\varepsilon_f) \cos^2 \theta \, u(\theta) \, d\theta\right] \frac{\sin \beta}{\cos^3 \beta} \, d\beta. \quad (3.71)$$

3.9 Calculation scheme for fiber stress utilization from double integral

The total axial force $F_Y(\varepsilon_Y)$ of yarn, specific stress of yarn $\sigma_Y(\varepsilon_Y)$, and coefficient of fiber stress utilization in yarn $\varphi_{c2}(\varepsilon_Y)$ can be practically calculated as the function of axial strain of yarn ε_Y, when we know:

a. Specific stress-strain function of fiber $\sigma_f(\varepsilon_f)$.
b. Yarn twist Z, yarn diameter D, contraction ratio η, and the 'measure' of preference of modal direction C.

The calculation according to equations (3.68), (3.70) and (3.71) needs also to use equations (3.63) for ε_f and (3.64) for θ_u and β_D from relation $\tan \beta_D = \pi DZ$. The double integrals in previous equations are usually necessary to solve by means of suitable numerical method using Simulink technique in Matlab. The calculation scheme for double integral model is given in the figure 3.10. The input parameters used in the Simulink model are maximum yarn twist β_D, contraction ratio η, constant parameter C, and yarn strain ε_Y. The yarn surface twist β_D, angle θ_u and $u(\theta)$ are also calculated in the Simulink model. The fiber strain ε_f was determined at each value of angle θ. For each value of fiber strain the fiber stress was also calculated from different value of θ using look up table. The look up table was prepared from the fiber stress and strain calculated at different angle θ for step of hundred values. Fiber stress-strain function $\sigma_f(\varepsilon_f)$, $\cos^2 \theta$ and $u(\theta)$ were multiplied followed by numerical integration. The factor $\sin \beta / \cos^3 \beta$ was computed for hundred values of angle β from 0 ~ 100

steps. Both were multiplied with the factor $\left(\frac{2}{\sigma_f(\varepsilon_Y)\tan^2\beta_D}\right)$ to evaluate the coefficient of fiber stress utilization in yarn.

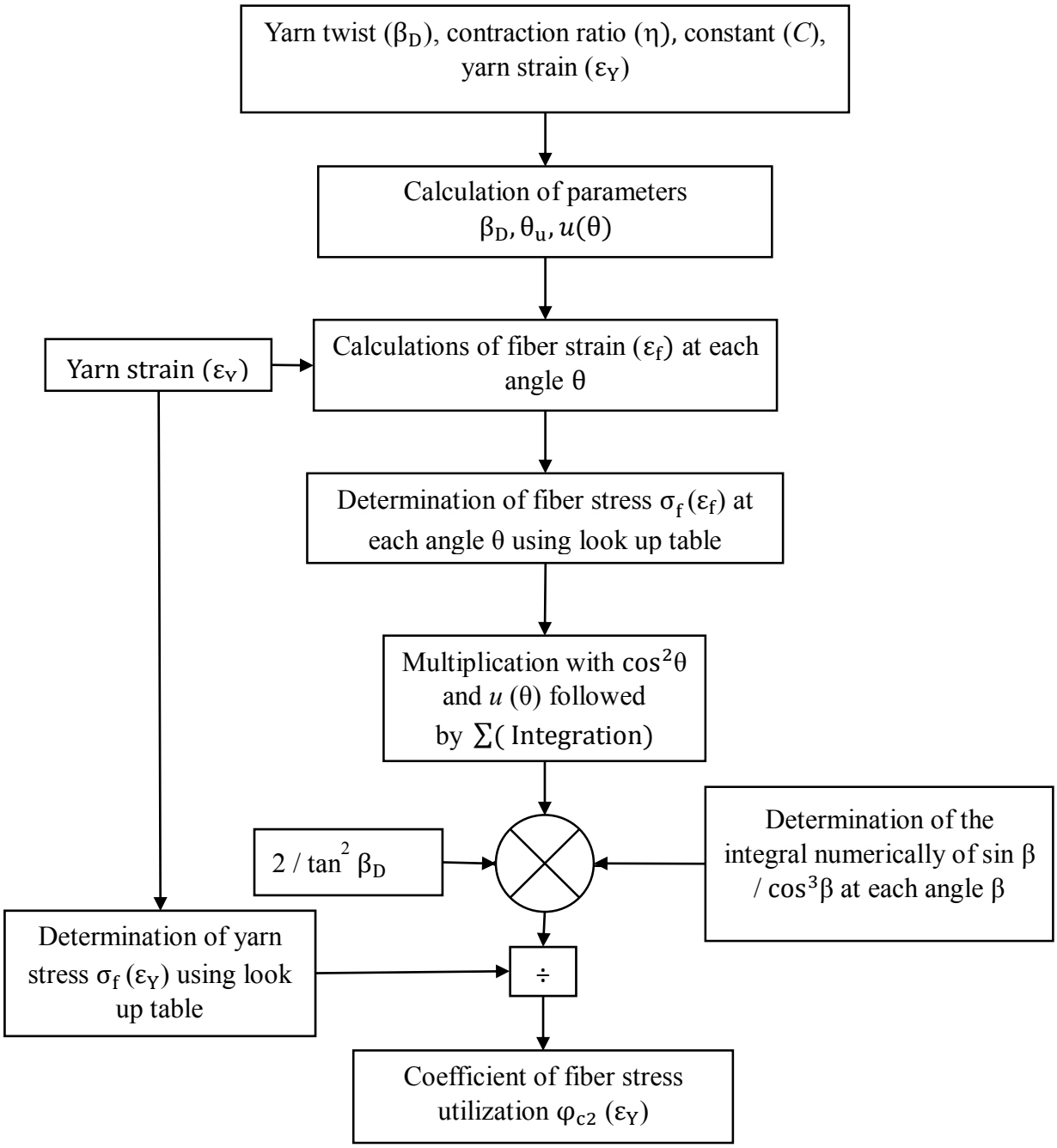

Figure 3. 10 Calculation Scheme for coefficient of fiber stress utilization from double integral

3.10 Yarn specific stress

From the idea of coefficient of fiber stress utilization, the yarn specific stress-strain curves can be predicted from the relation as follows

$$\sigma_Y(\varepsilon_Y) = \varphi_{c2}(\varepsilon_Y).\ \sigma_f(\varepsilon_Y). \qquad (3.72)$$

Where σ_Y (ε_Y) is yarn specific stress-strain function before break, σ_f (ε_Y) is fiber specific stress-strain from the experiment and φ_{c2} (ε_Y) is coefficient of fiber stress utilization from double integral equation (3.71).

3.11 Summary of model

Basic concepts of stress-strain relation are derived first with introductory concepts of stress-strain relations. The coefficient of fiber stress utilization based on Gegauff's concept has been derived first and then modified to single integral equation considering nonlinear stress-strain behavior of fiber and yarns**.** The single integral equation predict the coefficient of fiber stress utilization as function of yarn strain and does not account for the fiber orientation in yarn. So to investigate the effect of fiber orientation the double integral model was introduced from our single integral equation using the concept of direct delta function. From the theoretical coefficient of fiber stress utilization, the predicted yarn specific stress can be evaluated from the equation (3.72). The overview of models is given in figure 3.10

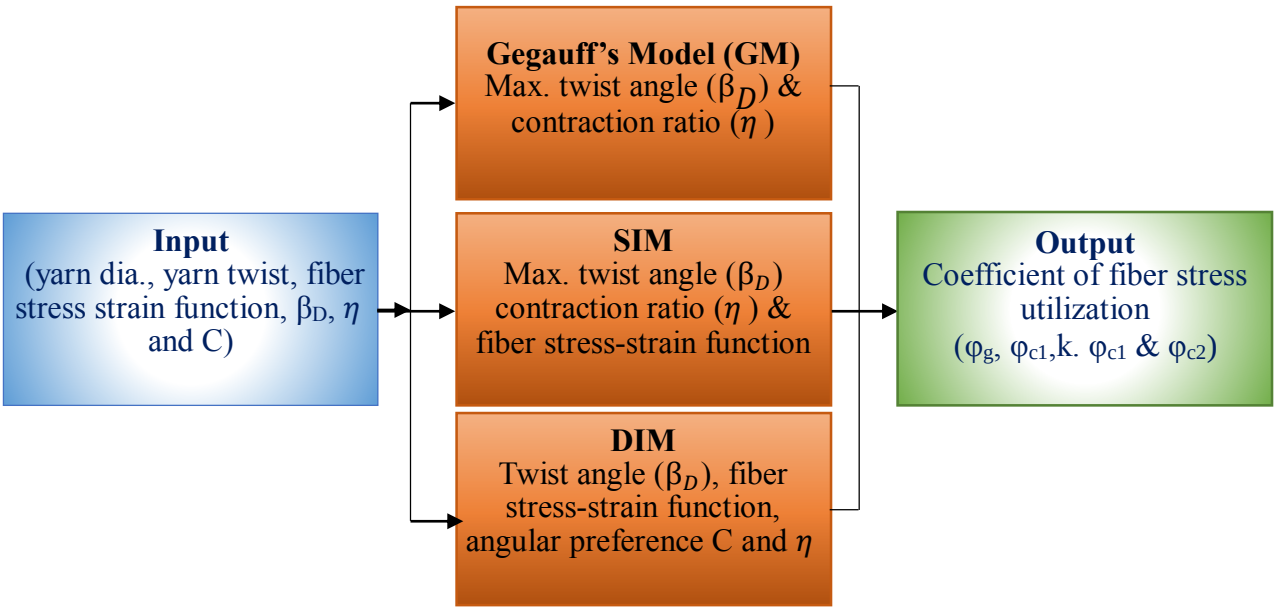

Figure 3.11 Overview of mathematical models

CHAPTER 4.

METHODOLOGY

Experiments were carried out to verify the theoretical model described in Chapter 3.The different types of fibers and staple spun yarns with different linear densities and materials were used for validation of the mathematical model and brief procedures for the measurement of the necessary parameters are being explained in this section. The important parameters that were considered in the experiment include: fiber fineness, fiber force and elongation, yarn fineness, yam force and elongation, yarn diameter and yarn twist. The mean curves and experimental coefficient of fiber stress utilization are also elaborated in this section.

4.1 Material

The six types of fibers cotton, polyester, viscose, worsted, acrylic and linen were used to produce staple spun yarns. The yarns were produced by ring and rotor technologies with different linear densities.

4.1.1 Fiber

The six types of fibers cotton, polyester, viscose, worsted, acrylic and linen were used for validation of model. The measured and / or nominal specification of the fibers are given in the table 4.1.

Table 4.1 Fiber specifications

Yarn type / Parameters	Viscose fiber	Carded cotton fiber	Combed cotton fiber	Polyester fiber	Linen fiber*	Worsted fiber	Acrylic fiber
Breaking force [cN]	3.66	4.88	6.40	6.11	23.52	5.90	4.71
Breaking strain [%]	18.04	6.35	6.93	18.35	2.39	31.07	26.21
Tenacity [cN / tex]	29.53	30.5	44.28	42.98	68.92	15.43	35.3
St. dev. of breaking force	0.53	1.88	2.08	0.64	1.07	1.8	0.82
C.V of breaking force [%]	14.51	29.64	26.36	10.42	26.72	30.50	17.31
Fineness [d tex]	1.29	1.6	1.46	1.43	3.47	3.81	1.34
Test speed [mm / min]	10	10	10	10	10	10	10
Gauge length [mm]	20	10	20	20	20	20	20
Pre-Tension wt. [mg]	100	100	100	100	200	200	100
Staple length [mm]	38	25	35	38	40	50	40

∗) Technical fiber

4.1.2 Yarns

The different yarn linear densities produced from various types of materials viscose, cotton, polyester, worsted, acrylic and linen from ring and rotor technologies are given in the table 4.2.

Table 4.2 Yarn linear densities (Tex)

Material &	Viscose yarn		Polyester yarn		Carded cotton yarn		Combed cotton yarn		Linen yarn*		Worsted yarn		Acrylic fiber	
Ring yarns	Nom.	Act.	Nom.	Act.	Nom.	Act.	Nom.	Act.	Nom.	Act.	Nom.	Act.	Nom.	Act.
	45	46.8	45	43.8	73.8	72.2	20.0	19.70	28	27.66	20	20.0	18	17.9
	29.5	32.5	29.5	30.0	59.0	58.4	11.50	11.28	36	36.82	23	23.3	14	13.9
	20	20.1	20	20.4	___	___	___	___	___	____	____	____	12	12.7
Rotor yarns	50	52.2	50	50.5	98.4	101.7	___	___	___	____	___	____	____	___ _
	29.5	30.7	42	41.6	73.8	73.5	___	___	___	____	___	____	____	___ _
	20	20.0	33	33.8	59.0	58.5	___	___	___	___	____	____	____	___ _

∗) Technical yarn, Nom.: Nominal, Act. : Actual

4.2 Method

The standard test methods for evaluation of different parameters fiber fineness, fiber force and elongation, yarn fineness, yam force and elongation, yarn diameter and yarn twist are described in the following lines.

4.2.1 Vibrodyn-400

Tensile force, elongation, titre and tenacity of all types of fibers were measured on LENZING Vibrodyn-400 according to the standard test method CSN-ENISO 1973. A total of fifty measurements were made for all types of fibers. The gauge length was 10 mm and force was applied at a rate of 10 mm / min. The stress-strain curves and data for each type of the staple fibers were obtained from the equipment software which was used to produce mean curve for each fiber.

4.2.2 Instron-4411

All types of yarns were tested on Instron-4411 in accordance with standard test method CSN-ENISO 2060. The yarns were tested for force and elongation at the corresponding speeds depending upon the yarn type and the gauge length being 500 mm for all type of yarns. The

tensile force application time was kept from 17 to 22 seconds for all types of yarns. A total of fifty tests were performed on each of the yarns. The force and elongation was measured directly from the instrument. The individual raw force-strain curves and breaking force and elongation for some samples of yarns is given in the Appendix B. The individual raw force-strain data of each yarn was used to obtained average stress-strain curve using linear interpolation and Matlab.

The yarn linear density was measured from a lea of one hundred meters according to standard test procedure CSN 80 0050. Five samples for each type of yarn were prepared on lea making machine and each sample was weighed in grams on weighing balance and yarn tex was determined from average of five samples. Raw data for linear density of polyester yarn is given in the Appendix C.4.

The yarn diameter was determined by image analysis method with the help of instrument as shown in the figure 4.1 according to the standard test method (Interni Norma) C.22.102-01/01. Image of yarn at different places were saved in the software and then measured for each sample. Average value of diameter from one hundred observations were taken and recoded.

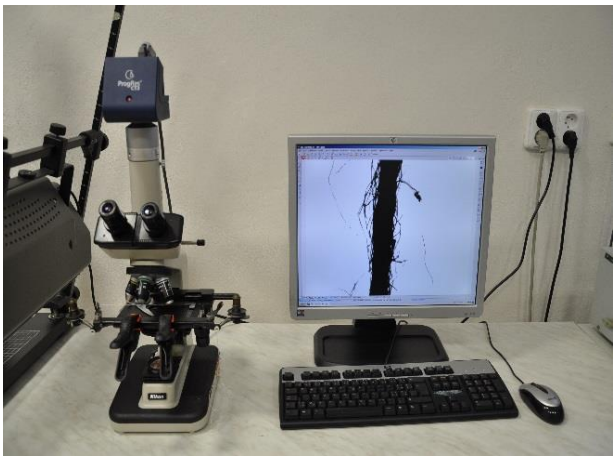

Figure 4. 1 Microscope for yarn diameter measurement

The measured diameter was used to determine the twist angle by using equation $\tan \beta_D = \pi DZ$. Raw data for diameter of cotton yarn is given in the Appendix C.5.Twist per meter were measured on twist testing machine according to standard procedure CSN 80 0701.Thirty samples from each type of yarn were measured and mean value of twist was recorded. Raw data for cotton yarns is given in the Appendix C.6. The mean values of all parameters obtained from equipment were recorded in the tables 4.3, 4.5, 4.7, 4.9, 4.11, 4.12, and 4.14.

4.3 Evaluation of specific stress-strain curves

The brief procedures to plot the average specific stress-strain curves both for fiber and yarn are explained as follows.

4.3.1 Average specific stress-strain curve for fiber

The preliminary fiber stress-strain curve data for fifty fiber samples obtained from vibrodyn-400 was used to produce average specific stress-strain curve in Matlab for each type of fiber. The specimen of fiber mean stress-strain curves obtained from Matlab are given in Appendix-A. The mean fiber specific stress-strain curve was evaluated at each strain with a step of 0.001using linear interpolation before the fiber break occurred.

4.3.2 Average specific stress-strain curve for yarn

The individual raw stress-strain curve data for all type of yarns from fifty specimens from Instron-4411 was used to produce the average specific stress-strain curve for yarn in Matlab. The raw mean and individual stress-strain curves for some yarns are mentioned in the Appendix-B. The elongation was converted into strain and the yarn force before break was interpolated linearly at each strain value with a step of 0.001. The yarn force at each strain value was converted into cN/tex and the data was used in the micro soft excel to obtain the average stress-strain curve for yarn.

About 10 % of individual stress-strain curves, having smallest and highest breaking strains were excluded from the experiment data for all fiber and yarn specimens as outlier curves.

4.4 Experimental coefficient of fiber stress utilization

The six types of fibers viscose, cotton, polyester, worsted, acrylic and linen yarns from same materials produced from ring and rotor technology were used for verification of theoretical model. The average specific stress-strain curves for fiber and yarns were produced according to the section 4.3 and will be used to evaluate experimental coefficient of fiber stress utilization.

The experimental coefficient of fiber stress utilization curves for various ring and rotor staple spun yarns were determined dividing specific stress of yarns by specific stress of fiber at same strain value according to the equation 3.6 in chapter 3. The prior theoretical relations are not fully valid in the area of very small strains probably as consequence of relative imperfections by process of measurement and / or fiber crimp. Liu *et al.* [69] presented the similar conclusion for fiber and yarns strains. They also studied stress-strain curves beyond the limit of 2 %. Therefore, we shall analyse the mutual relations starting from strain value of

0.02 (2 %). The respective experimental coefficient of fiber stress utilization curves will also be explained in this section with the help of graphs.

4.4.1 Experimental coefficient of fiber stress utilization of viscose yarns

Standard viscose fibers of 1.3 dtex fineness and 38 mm staple length and two sets of viscose staple spun yarns one ring and other rotor were tested for investigation of coefficient of fiber stress utilization. The different specifications of viscose ring and rotor yarns were measured and recorded in the Table 4.3.

Table 4.3 Parameters of viscose staple yarns

Yarn type	Yarn linear densities		Yarn twist	Yarn dia.	Twist angle	Twist coefficient	Test speed
	Nominal[tex]	Actual[tex]	Z [m^{-1}]	D[mm]	β_D[deg.]	$\propto$ [$m^{-1}ktex^{1/2}$]	[mm/min]
	45	46.78	515	0.263	22	111	220
Ring	29.5	32.45	650	0.210	21	117	220
	20	20.07	840	0.169	23	119	220
Rotor	50	52.15	550	0.294	27	126	170
	29.5	30.71	680	0.222	23	119	170
	20	20.03	900	0.177	27	127	170

The average experimental specific stress-strain curves for viscose fiber and yarns before the process of break are shown in the figure 4.2. The mean fiber specific stress-strain curve occupies on higher position and all position of yarn specific stress-strain curves are lower than the fiber curves while rotor yarns lie slightly under the ring yarns. The shape of specific stress-strain curves both for fiber and yarn are similar in shape. All ring yarn curves occupy same position and same is true for rotor yarns.

The experimental coefficient of fiber stress utilization for all types of viscose ring and rotor yarns was evaluated at each strain and was plotted against the different values of strain as shown in the figure 4.3. The experimental coefficient of fiber stress utilization for all viscose ring yarns is lying at higher position because of the better orientation of fibers in that yarn due to the true twist in ring yarns which is not expected in the rotor yarns. The end points of the rotor yarns finish before ring yarns due to their lower tenacity and elongation. The coefficient of fiber stress utilization curves of all the ring yarns are at same position and same is true for rotor yarns.

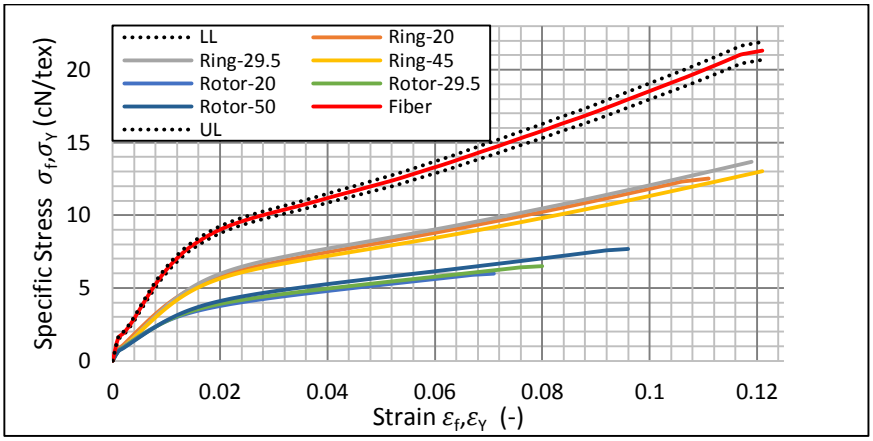

Figure 4.2 Experimental stress-strain curves for viscose fiber and yarns

More over all experimental curves possess similar shape and trend. The shape of the viscose fiber and yarn curves show less nonlinear behaviour as compared with the polyester fiber and yarns because of its cellulosic composition.

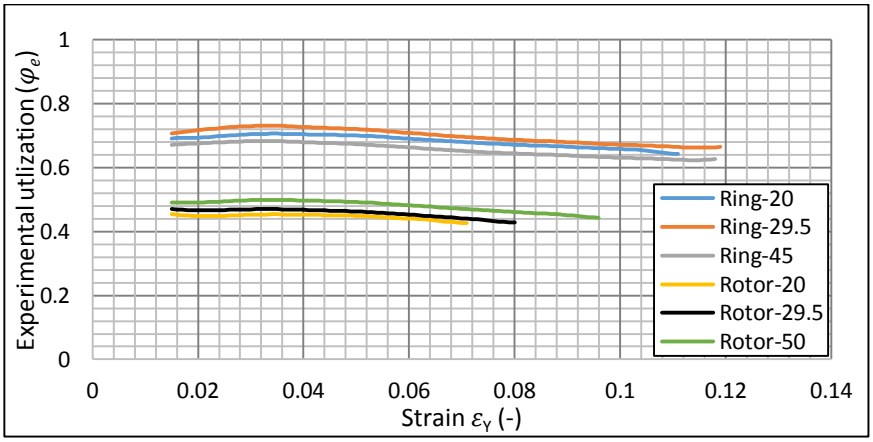

Figure 4.3 Experimental coefficient of fiber stress utilization for viscose yarns

The experimental peak coefficient of fiber stress utilization and strain at peak coefficient of fiber stress utilization for all ring and rotor viscose yarns is given in the table 4.4. All ring viscose yarns have same peak coefficient of fiber stress utilization and strain at peak coefficient of fiber stress utilization and the same is true for rotor viscose yarns. The slight difference in peak coefficient of fiber stress utilization in both the yarns might be due to the variation in strength of the yarns.

Table 4.4 Experimental peak coefficient of fiber stress utilization of viscose yarns

Yarn tex	Peak coefficient of fiber stress utilization (φ_e)		Strain at peak coefficient of stress utilization (φ_e)	
	Ring yarn	Rotor yarn	Ring Yarn	Rotor yarn
20	0.706	0.452	0.037	0.038
29.5	0.732	0.468	0.038	0.038
45/50	0.681	0.497	0.038	0.038

4.4.2 Experimental coefficient of fiber stress utilization of polyester yarns

Standard polyester fibers of 1.5 dtex fineness and 38 mm staple length and two sets of polyester staple yarns one ring and other rotor were tested for investigation of coefficient of fiber stress utilization. The polyester ring and rotor yarn parameters are given in the table 4.5.

Table 4.5 Parameters of polyester staple yarns

Yarn type	Yarn linear densities		Yarn twist	Yarn dia.	Twist angle	Twist coefficient	Speed
	Nominal[tex]	Actual[tex]	Z [m^{-1}]	D[mm]	β_D[deg.]	$\propto$ [$m^{-1}ktex^{1/2}$]	[mm/min]
Ring	20	20.39	836	0.176	24.50	118	230
	29.5	30.02	661	0.223	24.84	114	230
	45	43.84	543	0.274	25.50	115	230
Rotor	33	33.77	720	0.250	29.48	131	230
	42	41.56	615	0.288	29.09	126	230
	50	50.54	593	0.313	30.24	133	230

The average fiber stress-strain curve occupies on higher position and all position of yarn curves are lower than the fiber curves while rotor yarns lie slightly under the ring yarns as described for viscose. The shape of average curves for polyester fiber and yarn are different from the viscose staple fiber and yarn as shown in the figure 4.4 due to different chemical nature of polyester fiber from viscose.

The experimental coefficient of fiber stress utilization for all polyester ring and rotor yarns is presented in the figure 4.5. Coefficient of fiber stress utilization curves for all ring yarns are at the same position and also all rotor yarn curves exists at the same level. The trend of all curves has some analogy. The higher position of stress-strain curves in ring yarns might be

due to the better orientation of fibers in that yarn because of proper twist which is not observed in the rotor yarns.

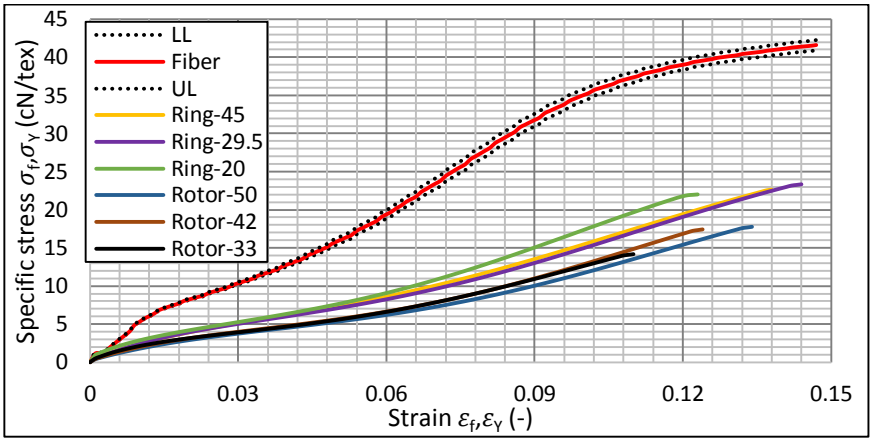

Figure 4.4 Experimental stress-strain curves for polyester fiber and yarn

The shape of experimental coefficient of fiber stress utilization curves of the polyester yarn present nonlinear behaviour which might be due to the unique chemical composition of that material. The coefficient of fiber stress utilization is higher at the start then decreases at the middle at strain of 0.07~0.08 and again increase before break.

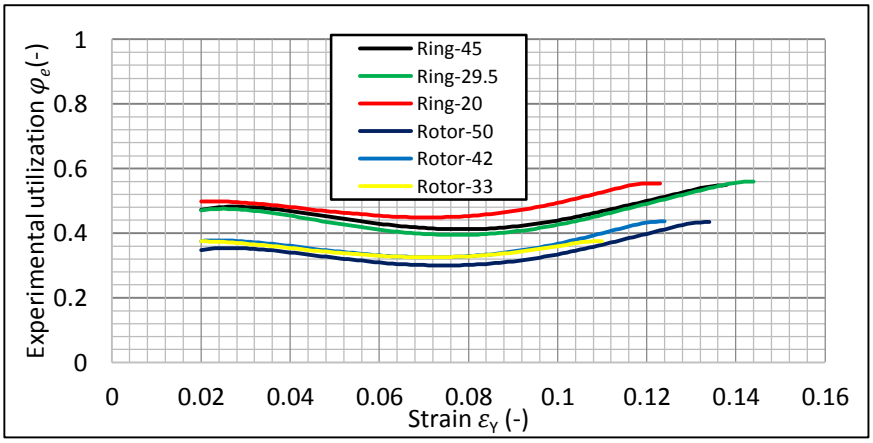

Figure 4.5 Experimental coefficient of fiber stress utilization for polyester yarns

The experimental least coefficient of fiber stress utilization and strain at that utilization for all ring and rotor polyester yarns is given in the table 4.6. All ring polyester yarns have same least coefficient of fiber stress utilization and strain at that utilization and the same is true for all rotor polyester yarns. The slight difference among the least coefficient of fiber stress utilization and strain at that coefficient of fiber stress utilization might be due to the variation in those yarns.

Table 4.6 Experimental least fiber stress utilization of polyester yarns

Yarn tex	Least coefficient of fiber stress utilization (φ_e)		Strain at least coefficient of utilization (φ_e)	
	Ring yarn	Rotor yarn	Ring Yarn	Rotor yarn
20 ring / 33 rotor	0.448	0.326	0.072	0.077
29.5 ring / 42 rotor	0.395	0.325	0.082	0.077
45 ring / 50 rotor	0.412	0.300	0.082	0.077

4.4.3 Experimental coefficient of fiber stress utilization of cotton yarns

Carded and combed cotton yarns were used for experimental evaluation of coefficient of fiber stress utilization. The carded and combed cotton yarns were produced from short and long staple cotton fiber respectively. The experimental coefficient of fiber stress utilization for both types of cotton staple spun yarns is being explained in the following lines.

4.4.3.1 Experimental coefficient of fiber stress utilization of carded cotton yarns

Standard cotton fibers of 1.6 dtex fineness and 28 mm staple length and two sets of cotton staple yarns ring and rotor were tested for investigation of coefficient of fiber stress utilization. Cotton fiber stress-strain curve data was obtain from the vibrodyn-400. The fineness could not be measured on Vibrodyn-400 due to smaller staple length of cotton fiber. So the cotton fiber fineness was measured with the help of micron air equipment according to the standard procedure, IS-3674-1966 and value was converted into dtex. The parameter of both ring and rotor yarns are given in the table 4.7.

Table 4.7 Parameters of cotton staple yarns

Yarn type	Yarn linear densities		Yarn twist	Yarn dia.	Twist angle	Twist coefficient	Speed
	Nominal[tex]	Actual[tex]	Z [m^{-1}]	D[mm]	β_D[deg.]	$\propto$ [$m^{-1}ktex^{1/2}$]	[mm/min]
Ring	59.0	58.4	532	0.258	23.3	128	120
	73.8	72.2	493	0.301	25.0	133	120
Rotor	59.0	58.5	529	0.337	29.5	128	95
	73.8	73.5	454	0.380	28.5	123	95
	98.4	101.7	415	0.434	29.5	132	95

The figure 4.6 shows the experimental mean stress-strain curves of cotton fiber and yarns. The average cotton fiber stress-strain curve occupies on higher position and all position of cotton yarn curves are lower than the fiber curves while rotor yarns lie under ring yarns analogous to viscose and polyester. The shape of stress-strain curves for cotton yarn exhibits more linearity and is dissimilar from the viscose and polyester staple fiber and yarns due its chemical composition.

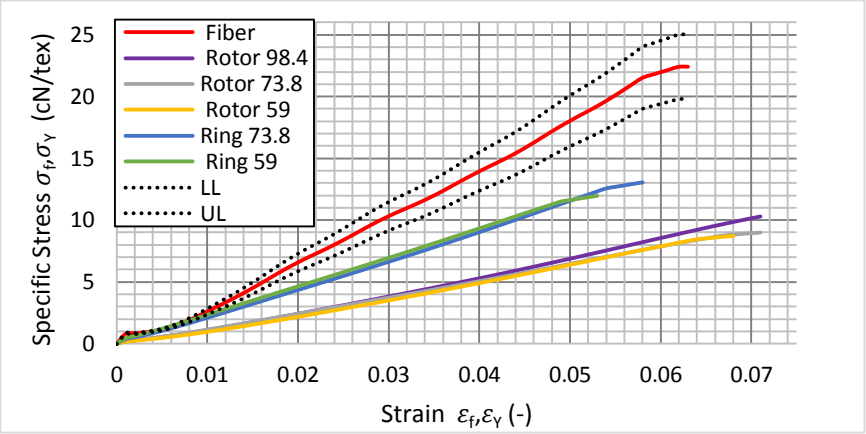

Figure 4.6 Experimental stress-strain curves of cotton fiber and yarn

The experimental coefficient of fiber stress utilization curves for all types of cotton yarns are presented in the figure 4.7. All experimental coefficient of fiber stress utilization curves for ring yarns are lying at higher position and for rotor yarns at lower level due to the better orientation of fibers in ring yarn similar to viscose and polyester yarns. The shape of the coefficient of fiber stress utilization curves for ring and rotor are similar. The experimental coefficient of fiber stress utilization curves for cotton yarns also reveal more linear behaviour as compared with the viscose and polyester yarns.

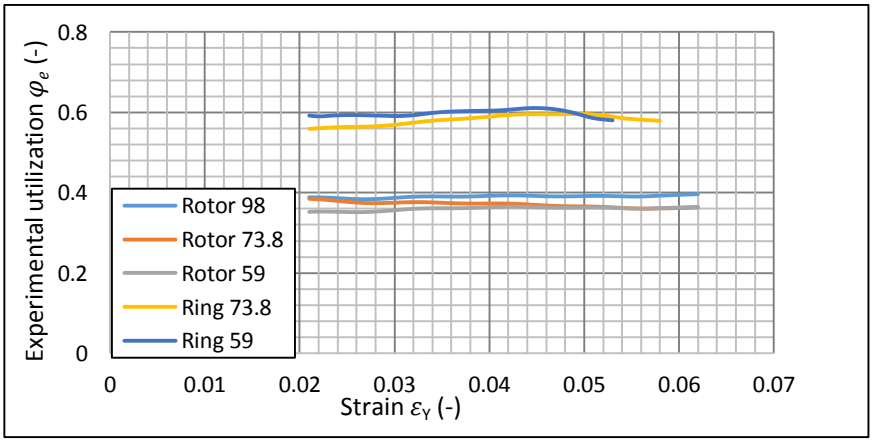

Figure 4.7 Experimental coefficient of fiber stress utilization of carded cotton yarns

The experimental peak coefficient of fiber stress utilization and strain at peak coefficient of fiber stress utilization for all ring and rotor cotton yarns is given in the table 4.8. All ring cotton yarns have same peak coefficient of fiber stress utilization and strain at peak coefficient of fiber stress utilization which is also true for rotor yarns.

Table 4.8 Experimental peak coefficient of fiber stress utilization of carded cotton yarns

Yarn tex	Peak coefficient of fiber stress utilization (φ_e)		Strain at peak coefficient of fiber stress utilization (φ_e)	
	Ring yarn	Rotor yarn	Ring Yarn	Rotor yarn
98.4	N/A	0.394	N/A	0.044
73.8	0.596	0.374	0.046	0.044
59	0.611	0.366	0.045	0.044

4.4.3.2 Experimental coefficient of fiber stress utilization by combed cotton yarns

Standard combed cotton fibers of fineness 1.68 dtex and 35 mm staple length with one set of combed cotton staple yarns were tested for investigation of coefficient of fiber stress utilization. The specifications of combed cotton yarns are presented in Table 4.9.

Table 4.9 Parameters of combed cotton staple spun yarns

Yarn type	Yarn linear densities		Yarn twist	Yarn dia.	Twist angle	Twist coefficient	Speed
	Nominal[tex]	Actual[tex]	Z [m^{-1}]	D[mm]	β_D[deg.]	α [$m^{-1}ktex^{1/2}$]	[mm/min]
Ring	11.5	11.28	955	0.13	21.30	101	65
	20.0	19.78	726	0.17	21.20	102	65

The figure 4.8 shows the measured average stress-strain curves for long staple cotton fiber and combed yarns. The highest position is occupied by the mean fiber specific stress-strain curve. All position of combed cotton yarn curves exist at lower position than the fiber curves. Again, the specific stress-strain curves for long staple cotton fiber and yarns are similar to short staple cotton fiber and carded yarns due to their similar composition.

The mean specific stress-strain curves for both the yarns are similar with respect to position and shape except the finer yarn of 11.5 tex has less elongation as compared with the coarser yarn so the curves disappear soon as compared with the 20 tex yarn.

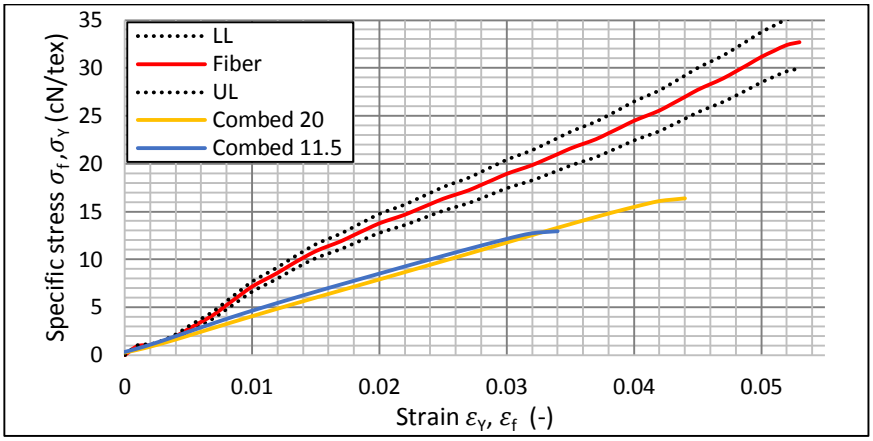

Figure 4.8 Experimental stress-strain curves of linen fiber and yarns

The experimental coefficient of fiber stress utilization curves are presented in figure 4.9.

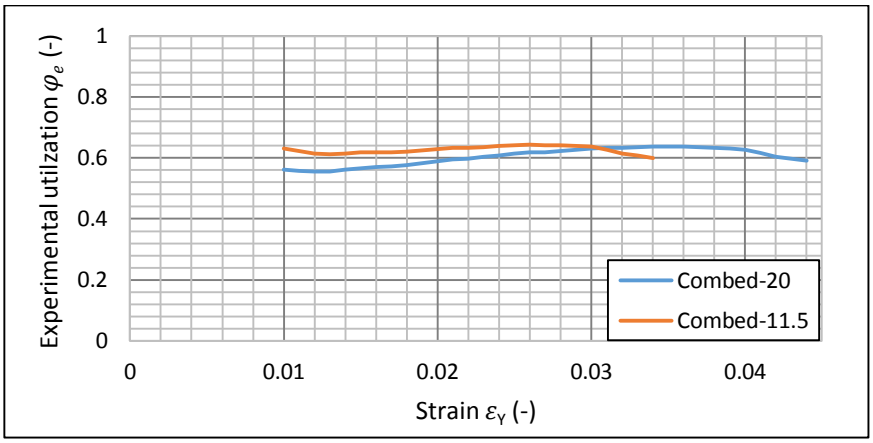

Figure 4.9 Experimental coefficient of fiber stress utilization of combed cotton yarns

Both the experimental coefficient of fiber stress utilization curves for combed cotton yarn lie on the same position and also exhibit same shape. The coefficient of fiber stress utilization for both yarns is about 60~64% which is higher than carded cotton ring spun yarns (54~60%).

The experimental peak coefficient of fiber stress utilization and strain at peak coefficient of fiber stress utilization for combed cotton yarns is given in the table 4.10. Both the combed cotton yarns have same peak coefficient of fiber stress utilization and only the strain at peak coefficient of fiber stress utilization is less for finer yarn because of low elongation of that yarn.

Table 4.10 Experimental peak coefficient of fiber stress utilization for combed cotton yarns

Yarn linear density[tex]	Peak coefficient of fiber stress utilization (φ_e)	Strain at peak coefficient of fiber stress utilization (φ_e)
11.5	0.643	0.026
20	0.637	0.034

4.4.4 Experimental coefficient of fiber stress utilization of linen yarn

We also performed the same experiments to evaluate the experimental and theoretical coefficient of fiber stress utilization for technical fiber like linen. The standard linen staple fibers with 3.5 dtex were taken randomly from different places of staple spun linen yarns. Two types of spun yarns were used to validate the results of the mathematical model. The specifications of both linen yarns were presented in table 4.11.

Table 4.11 Parameters of linen staple spun yarns

Yarn type	Yarn linear densities		Yarn twist	Yarn dia.	Twist angle	Twist coefficient	Speed
	Nominal[tex]	Actual[tex]	Z [m^{-1}]	D[mm]	β_D[deg.]	$\propto$ [$m^{-1}ktex^{1/2}$]	[mm/min]
Ring	28	27.66	535	0.21	19.50	89	25
	36	36.82	489	0.24	20.25	94	25

The figure 4.10 shows the measured average specific stress-strain curves for linen fiber and yarns. The mean linen fiber specific stress-strain curve occupies on higher position and all position of linen yarn curves are lower than the fiber curves as discussed in previous sections for all other fibers. The curves for linen fiber and yarns are similar to the cotton fiber and yarns because both are cellulosic fiber and somehow display linear relationship. The linen fiber and yarn both possess low elongation because of higher stiffness of flex fibers. The curves for both the yarns are alike with respect to position and shape.

The experimental coefficient of fiber stress utilization curves for both the linen yarns are shown in the figure 4.11. Both curves lie on the same position and also have compare able shape. The coefficient of fiber stress utilization of linen yarns is 32~38 % which is less as compared with the other studied yarns. The results were too different from our experience of viscose, cotton and polyester fibers due to variability in fineness and lack of the elemental fiber of this technical yarn.

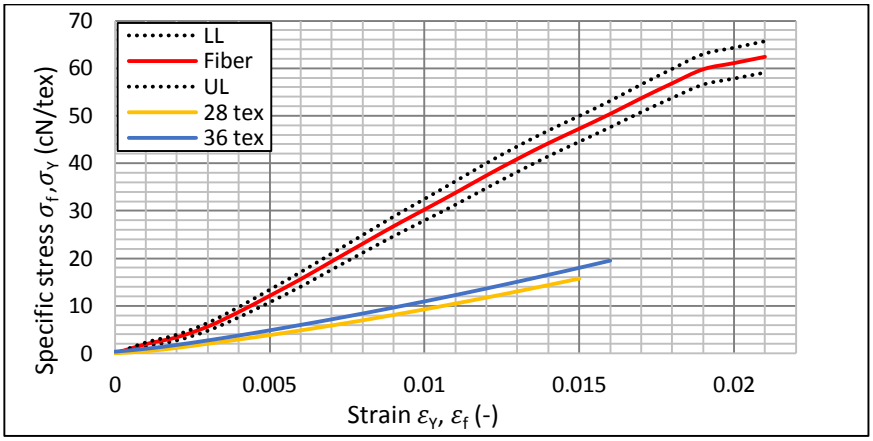

Figure 4.10 Experimental stress-strain curves of linen fiber and yarns

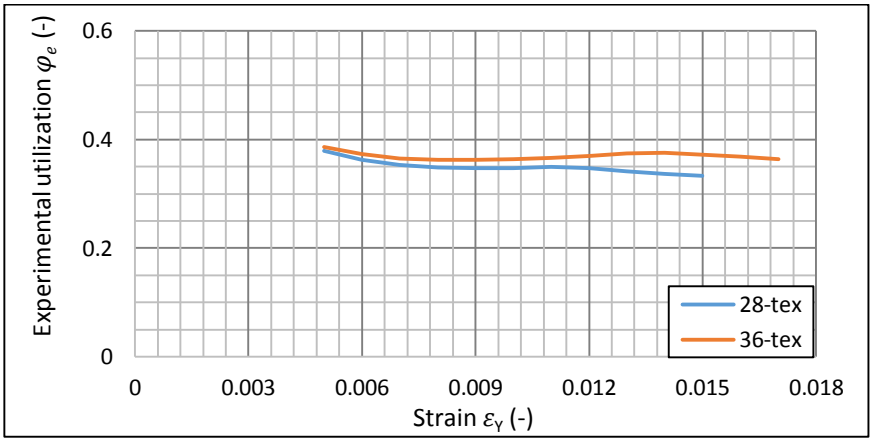

Figure 4.11 Experimental coefficient of fiber stress utilization of linen yarns

4.4.5 Experimental coefficient of fiber stress utilization of worsted yarn

We also performed the similar experiments to evaluate the experimental coefficient of fiber stress utilization for worsted ring spun yarn. The standard wool staple fibers with 3.81 dtex were used in worsted spun yarn. Two worsted yarns were used to validate the results of the mathematical model. The specifications of both worsted yarns were presented in table 4.12.

Table 4.12 Parameters of worsted staple spun yarns

Yarn type	Yarn linear densities		Yarn twist	Yarn dia.	Twist angle	Twist coefficient	Speed
	Nominal[tex]	Actual[tex]	Z [m^{-1}]	D[mm]	β_D[deg.]	$\propto$ [$m^{-1}ktex^{1/2}$]	[mm/min]
Ring	20	20.03	790	0.177	23.7	112	230
	23	23.25	640	0.190	21.0	98	230

Figure 4.12 shows the measured average stress-strain curves for wool fiber and yarns. The position and shape of average wool fiber and yarn specific stress-strain curve occupies on

higher position and all position of worsted yarn curves are at lower position than the wool fiber curves as discussed in previous sections for other fibers. The curves for wool fiber and yarns are different from all other fiber and yarns because of their chemical nature. The wool fiber and yarn both possess higher elongation as compared with cellulosic natural and synthetic fibers. The curves for both the yarns are alike with respect to position and shape only the finer yarn has less elongation as compared with the coarser worsted yarn.

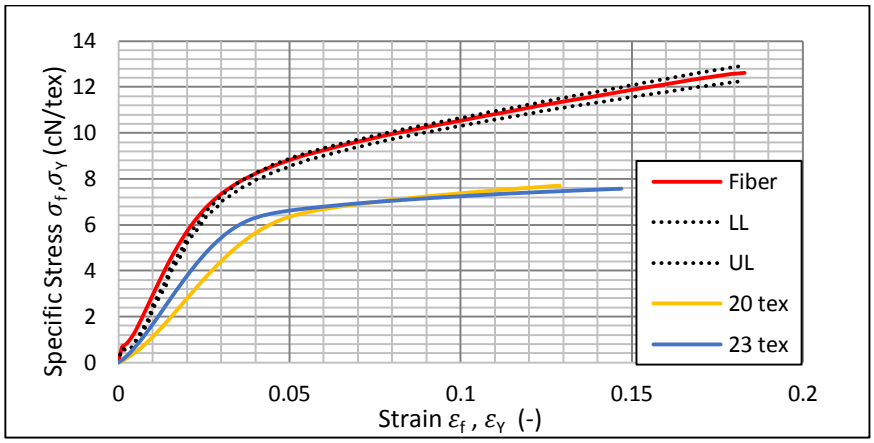

Figure 4.12 Experimental stress-strain curves of wool fiber and yarns

The experimental coefficient of fiber stress utilization curves for both the worsted yarns are shown in the figure 4.13. Experimental coefficient of fiber stress utilization curves for both the yarns lie on the same position and also have similar shape. The coefficient of fiber stress utilization of worsted yarns is more than 65 % which is higher as compared with the natural fiber yarns. The variation in strain up to 5 % is higher which might be due to high crimp in wool fiber.

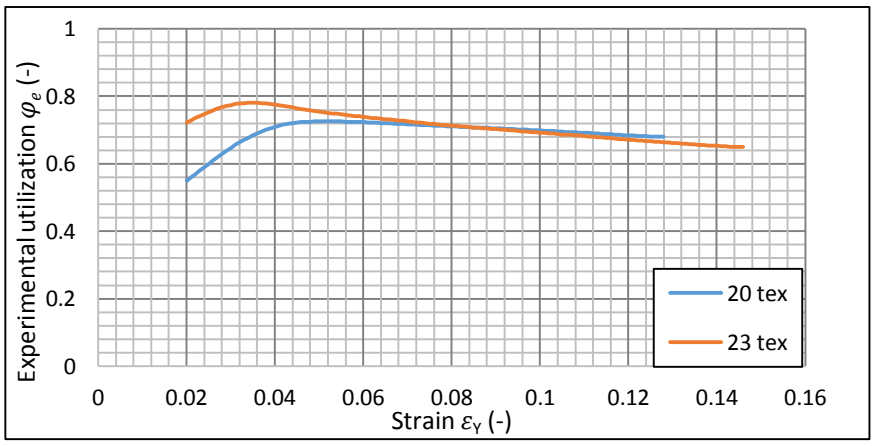

Figure 4.13 Experimental coefficient of fiber stress utilization of worsted yarns

The experimental peak coefficient of fiber stress utilization and strain at peak coefficient of fiber stress utilization for worsted yarns is given in the table 4.13. Both the worsted yarns

have same peak coefficient of fiber stress utilization and the strain at peak coefficient of fiber stress utilization.

Table 4.13 Experimental peak coefficient of fiber stress utilization for worsted yarns

Yarn linear density[tex]	Peak coefficient of fiber stress utilization (φ_e)	Strain at peak coefficient of fiber stress utilization (φ_e)
20 tex	0.715	0.075
23 tex	0.777	0.041

4.4.6 Experimental coefficient of fiber stress utilization of acrylic yarns

Standard acrylic fibers of 1.3 dtex fineness and 50 mm staple length and acrylic ring spun yarns were measured for investigation of coefficient of fiber stress utilization in yarn. The different specifications of acrylic yarns were measured and recorded in the table 4.14.

Table 4.14 Parameters of acrylic staple spun yarns

Yarn type	Yarn linear densities		Yarn twist	Yarn dia.	Twist angle	Twist coefficient	Speed
	Nominal[tex]	Actual[tex]	Z [m^{-1}]	D[mm]	β_D[deg.]	$\propto$ [$m^{-1}ktex^{1/2}$]	[mm/min]
Ring	12	12.70	725	0.141	22	82	280
	14	13.90	742	0.150	21	88	280
	18	17.95	568	0.167	23	76	280

The experimental average stress-strain curves produced for acrylic fiber and yarns from the equipment software data are shown in the figure 4.14.

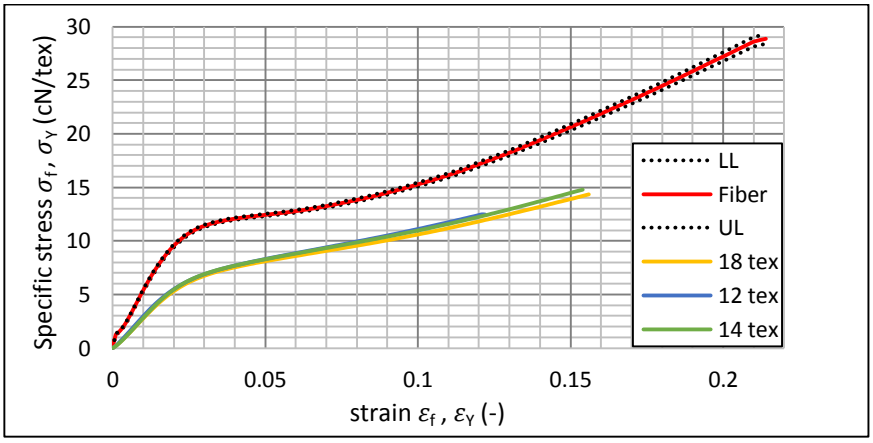

Figure 4.14 Experimental stress-strain curves of acrylic fiber and yarns

The experimental coefficient of fiber stress utilization for all acrylic ring spun yarns was evaluated at each strain value and plotted against the different values of strain as shown in the figure 4.15. The experimental coefficient of fiber stress utilization curves for all acrylic ring yarns are lying at same position and possess similar shape and trend but exhibit nonlinear behavior.

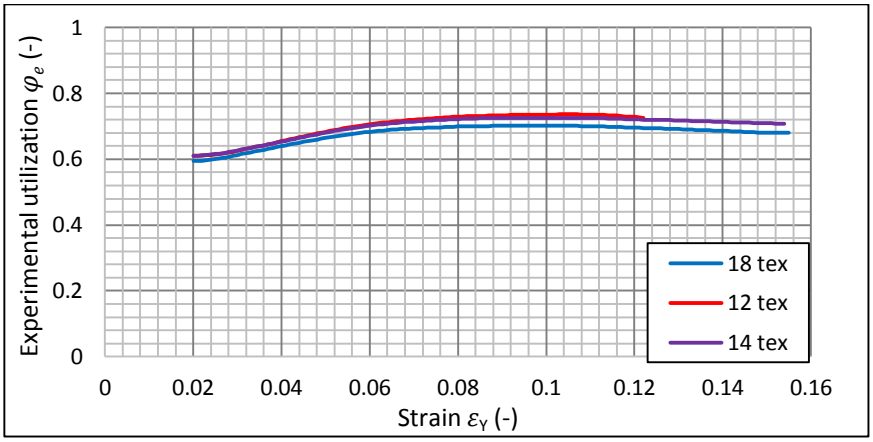

Figure 4.15 Experimental coefficient of fiber stress utilization for acrylic yarns

The experimental peak coefficient of fiber stress utilization and strain at peak coefficient of fiber stress utilization coefficient for all acrylic ring yarns is given in the table 4.15. All three types of acrylic ring yarns have same peak coefficient of fiber stress utilization and strain at peak coefficient of fiber stress utilization.

Table 4. 15 Experimental peak coefficient of fiber stress utilization of acrylic yarns

Yarn linear density[tex]	Peak coefficient of fiber stress utilization (φ_e)	Strain at peak coefficient of fiber stress utilization (φ_e)
12 tex	0.736	0.104
14 tex	0.726	0.104
18 tex	0.701	0.095

CHAPTER 5

RESULTS AND DISCUSIONS

In this section the predicted and experimental coefficient of fiber stress utilization for all types of yarns is explained in brief. The experimental coefficient of fiber stress utilization from all types of yarns φ_e is compared with predicted coefficient of fiber stress utilization from Gegauff's model φ_g from single integral model φ_{c1} double integral model φ_{c2} and k times single integral model φ_{c1} with the help of graphs. In addition, we have also compared experimental and theoretical yarn specific stress-strain curves from all type of yarns. Further the results of the proposed mathematical model were compared with Pan and Frydrych's model.

5.1 Predicted and experimental coefficient of fiber stress utilization

We have predicted the coefficient of fiber stress utilization of all the yarn samples using the theoretical model developed in Chapter 3. The curves of coefficient of fiber stress utilization in yarn as function of yarn strain obtained from equations (3.45), (3.55) and (3.71) are being explained here along with the experimental results for six types of staple spun yarns. The theoretical results are actually the result of relatively complicated process. The proposed mathematical model is implemented using Simulink technique in the Matlab software. The reason that why we choose Simulink for computation is that it can easily provide the information for coefficient of fiber stress utilization by changing the block parameters like fiber specific stress-strain function, twist angle, yarn contraction ratio and angular preference *C*. Fiber response in the yam and its contribution to the coefficient of fiber stress utilization in yarn can be investigated both in the form of curve and data. Only at the initial strain up 0.02 (2%), the difference between experimental and predicted coefficient of fiber stress utilization is higher which might be due to pre-tension yarn, fiber crimp and /or process of measurement. Treloar *et al.* [21] also studied the stress-strain relationship beyond strain of 0.02 for high twist yarns. Similar conclusions were drawn by Liu *et al.* [69] for coefficient of fiber stress utilization in staple spun yarns. Therefore we shall analyse the mutual relations starting from strain value of 0.02 (2 %). The coefficient of fiber stress utilization behavior for all types of yarns is studied before the process of fiber and yarn breakage. The fiber and yarn parameter used for the model are summarized in the table 5.1. The parameters from table 5.1 and $\eta = 0.5$ were used for calculations.

Table 5.1 Yarn parameters used for model validation

Yarn type		**Yarn linear density**	**Yarn twist (Z)**	**Yarn diameter (D)**	**Twist angle (β_D)**
		[tex]	**[m^{-1}]**	**[mm]**	**[deg.]**
Viscose yarn	Ring	46.78	840	0.169	23.59
		32.45	650	0.210	20.93
		20.07	515	0.263	22.89
	Rotor	20.03	900	0.177	26.97
		30.71	680	0.222	23.13
		52.15	550	0.294	26.61
Polyester yarn	Ring	20.39	836	0.181	24.80
		30.02	661	0.225	24.84
		43.84	543	0.281	25.05
	Rotor	33.77	720	0.250	29.48
		41.56	615	0.288	29.09
		50.54	593	0.313	30.24
Carded cotton yarn	Ring	58.40	532	0.258	23.30
		72.20	493	0.301	25.00
	Rotor	58.50	529	0.337	29.50
		73.50	454	0.380	28.50
		101.70	415	0.434	29.50
Combed cotton yarn	Combed	11.28	955	0.13	21.30
		19.78	726	0.17	21.20
Linen	Ring	27.66	535	0.21	19.50
		36.82	489	0.24	20.25
Worsted	Ring	20.03	790	0.177	23.70
		23.25	640	0.190	21.00
Acrylic	Ring	12.70	725	0.141	22.00
		13.90	742	0.150	21.00
		17.85	568	0.167	23.00

5.2 Predicted and experimental coefficient of fiber stress utilization of viscose yarns

A reasonably good inferred regular trend of coefficient of fiber stress utilization was observed by viscose staple yarns. Zubair *et al.* [74] compared the similar results for viscose ring and rotor yarns and found good agreement for predicted and experimental coefficient of fiber stress utilization. There are six graphs in figure 5.1 related to three ring yarns (a, b, c) and three rotor yarns (d, e , f).The experimental coefficient of fiber stress utilization curve φ_e was evaluated experimentally according to equation (3.6). Both functions in the numerator and denominator are determined experimentally.

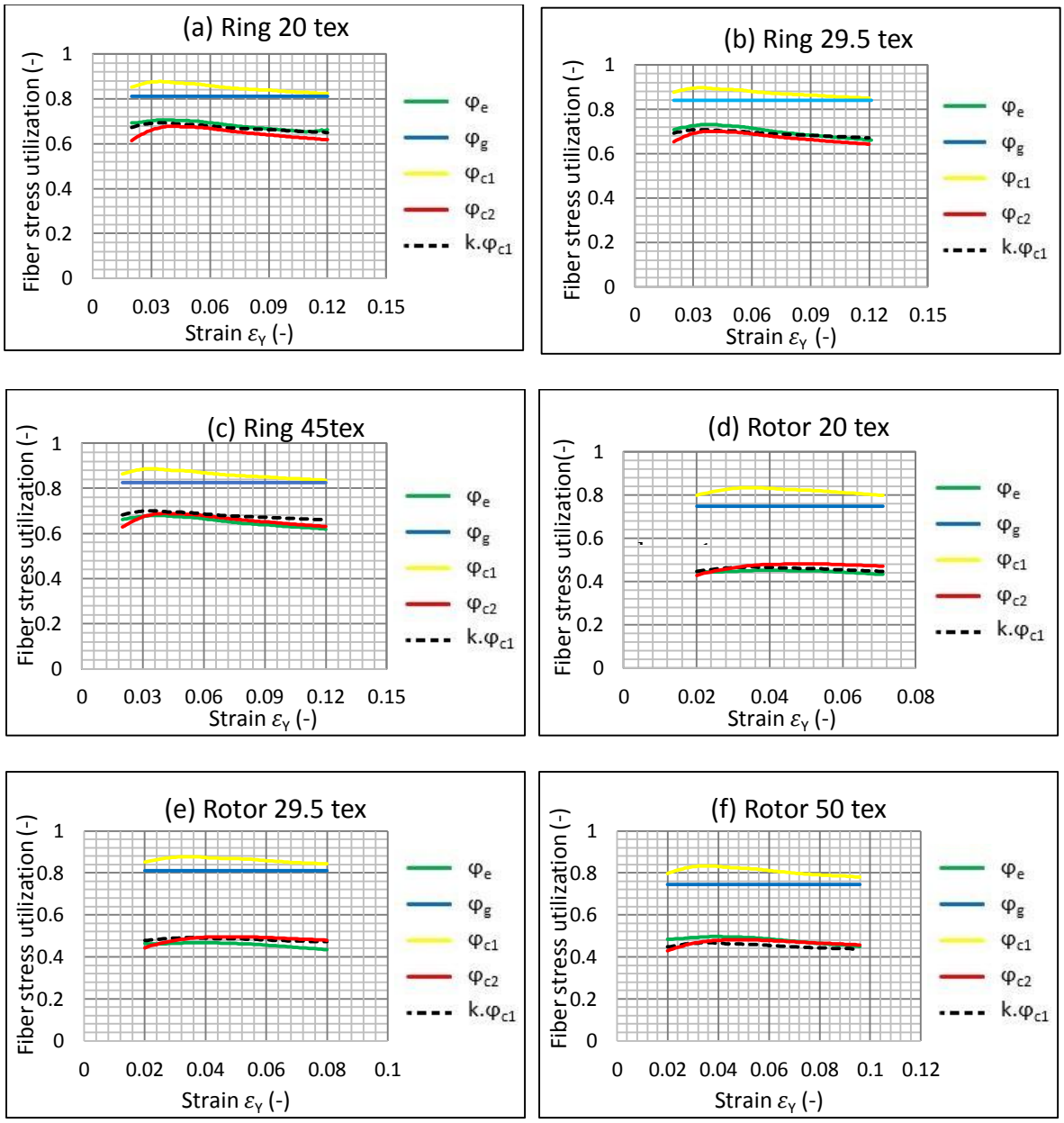

Figure 5.1 Predicted and experimental coefficient of fiber stress utilization in viscose staple spun yarn; ring yarns a, b, c; rotor yarns d, e, f.

The calculated Gegauff's model φ_g according to equation (3.45) represents straight lines on the graph. The coefficient of fiber stress utilization curves φ_{c_1}correspond to equation (3.55) single integral equation. Also, k-multiple of φ_{c_1} that is the lines k. φ_{c_1} work naturally with the same single integral equation (3.55). The coefficient of fiber stress utilization curves φ_{c_2} corresponds to equation (3.71). The empirical common values C = 4.9 and k = 0.79 for all ring yarns and C = 1.6 and k = 0.55 for all rotor yarns were used for predicting theoretical coefficient of fiber stress utilization coefficient as shown by curves φ_{c_2} and k. φ_{c_1}.

Similar flat experimental curves for coefficient of fiber stress utilization by viscose staple yarns were published in the research report [75]. However, the level of experimental curves was a little higher about 0.75 for ring yarns, 0.55 for rotor yarns from same type of viscose fibers and 0.4 for woollen yarns.

The workable range of strain for viscose yarns is maximum value of 0.12 before break. At lower yarn strain coefficient of fiber stress utilization is high which is due to low slippage among the fibers. Dang [2] published as the yarn extension is increased force along the fiber axis reduces resulting lower coefficient of fiber stress utilization due to more fiber slippage especially for outer layer fibers. The lower coefficient of fiber stress utilization at the yarn surface might be due to the low pressure and less gripping among the fibers which is consistent with Hearle' theory. The coefficient of fiber stress utilization for viscose ring yarns has increasing trend for the strain value of 0.02 ~ 0.048, then decreasing from 0.049 to 0.12 but lies within the average range before break of yarn. The coefficient of fiber stress utilization for rotor yarns has increasing trend from 0.02 ~ 0.038, then decreases from 0.039 ~ 0.096. The decreasing trend of coefficient of fiber stress utilization may be due to the combined effect of fiber to fiber contacts and more slippage among the fiber in this region. It might be due to the difference between the point modulus of fiber and yarns at higher value of strain.

We can observe from figure 5.1 that coefficient of fiber stress utilization curves from Gegauff φ_g are relatively far from experimental coefficient of fiber stress utilization curves φ_e on graph in term of their position as well as their shape. The coefficient of fiber stress utilization curve φ_{c1} has a similar shape to the experimental curves but these are lying too high in our graph near Gegauff's line. A suitable k-multiple of φ_{c1} curves are very near to the experimental curves φ_e. It is interesting that one common value empirically determined parameter k = 0.79 satisfies to all ring yarns as well as another common value k = 0.55 satisfies to all rotor yarns.

There is a question what is the cause of the last observed phenomenon by the viscose yarns. The analysis offers one idea of distribution of fiber orientation expressed by the coefficient of fiber stress utilization curve φ_{c2} . These curves lie in close contact with curves $k.\varphi_{c1}$ in all graphs. The suitable value of characteristic *C* in equation (3.71) of fiber angular preference is also interesting. The relatively high common value *C* = 4.9 was necessary to choose for viscose ring yarns in which by consequence to intensive drafting process fiber directions are concentrated mostly round helical model angle β. For rotor yarns we must choose much smaller common value *C* = 1.6 which corresponds to the level of orientation of short fiber portion in carded web [76]. In other words free flying moving fibers in air channel of spinning unit of rotor technology produce at last the structure like carded web on the internal surface of rotor yarn.

It is evident from figure 5.1a, b, c and table 5.2 that all the viscose ring yarns exhibits similar mean peak coefficient of fiber stress utilization and strain at peak coefficient of fiber stress utilization both experimental and predicted.

Table 5.2 Peak coefficient of fiber stress utilization of viscose ring yarns

Sample	Peak coefficient of fiber stress utilization		Strain at peak coefficient of utilization	
	Experimental	Predicted	Experimental	Predicted
20 tex	0.706	0.677	0.037	0.041
29.5 tex	0.732	0.700	0.038	0.038
45 tex	0.681	0.689	0.038	0.041

It is evident from figure 5.1d, e, f and table 5.3 that all the viscose rotor yarns produced similar peak coefficient of fiber stress utilization and strain at peak coefficient of fiber stress utilization both experimental and predicted.

Table 5.3 Peak coefficient of fiber stress utilization of viscose rotor yarns

Sample	Peak coefficient of fiber stress utilization		Strain at peak coefficient of fiber stress utilization	
	Experimental	Predicted	Experimental	Predicted
20 tex	0.452	0.481	0.038	0.050
29.5 tex	0.468	0.495	0.038	0.050
50 tex	0.497	0.481	0.038	0.050

5.3 Predicted and experimental coefficient of fiber stress utilization of Cotton yarns

Two sets of cotton yarns one from carded and other from combed technology were used for validation of mathematical model. The carded yarns were produced from ring and rotor technologies. We can explain the coefficient of fiber stress utilization for carded and combed yarns as follows..

5.3.1 Predicted and experimental coefficient of fiber stress utilization of carded cotton yarns

The experimental and theoretical coefficient of fiber stress utilization for various cotton ring and rotor yarns are calculated at a range of strain values and the results are presented graphically in figure 5.2a, b for ring yarns and figure 5.2c, d, e for rotor yarns.

The calculated Gegauff's model φ_g according to equation (3.45) represents straight lines on the graph in figure 5.2. The coefficient of fiber stress utilization curves φ_{c1} correspond to equation (3.55) single integral equation. The parameters from table 5.1 and $\eta = 0.5$ were used for calculations. Moreover, empirical common values, $k = 0.79$ for all ring yarns and $k = 0.55$ for all rotor yarns were used for estimation of curve $k.\varphi_{c1}$. The coefficient of fiber stress utilization curve φ_{c2} corresponds to double integral equation (3.71) which is analogous with the experimental curve φ_e with respect to shape and position. It is interesting that values of C for both ring and rotor cotton yarns were used similar to viscose yarns, $C = 4.9$ and $C = 1.6$ respectively.

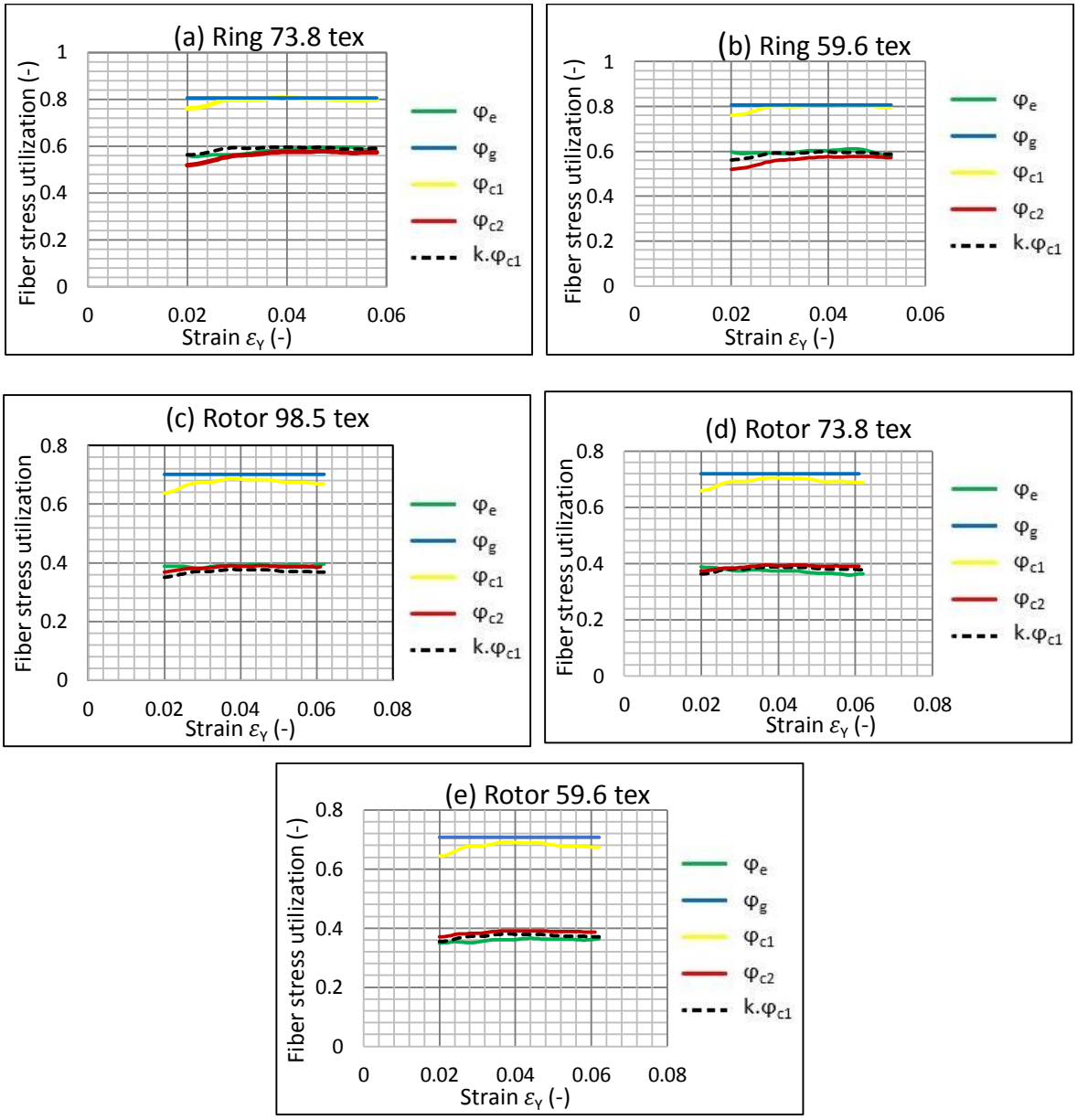

Figure 5.2 Predicted and experimental coefficient of fiber stress utilization in cotton staple spun yarn; ring yarns a, b, c and rotor yarns d, e.

It is evident from figure 5.2a, b and table 5.4 that all the cotton ring yarns reveals similar peak coefficient of fiber stress utilization and strain at peak coefficient of fiber stress utilization both experimental and predicted. The strain before break in the workable range for all ring cotton yarns is 0.06. The shape and position of all the predicted and experimental coefficient of fiber stress utilization curves is similar. The predicted coefficient of fiber stress utilization curves φ_{c1} determined from the single integral equation (3.55) for all ring yarns is function of yarn strain and is not linear as the curve φ_g from the Gegauff's equation (3.45). All the coefficient of fiber stress utilization curves φ_{c2} as function of yarn strain predicted from equation (3.71) are similar in shape to experimental curves.

The comparison between the experimental and theoretical results in figure 5.2a, b and table 5.4 for ring cotton yarns indicates that predicted peak coefficient of fiber stress utilization and strain at peak coefficient of fiber stress utilization are in good agreement with the experimental results.

Table 5.4 Peak coefficient of fiber stress utilization of cotton ring yarns

Sample	Peak fiber stress utilization		Strain at peak utilization	
	Experimental	Predicted	Experimental	Predicted
73.8 tex	0.596	0.578	0.046	0.046
59.0 tex	0.611	0.578	0.045	0.046

Similarly, comparison between the experimental and theoretical results in figure 5.2c, d, e and table 5.5 for rotor cotton yarns also show the prediction of coefficient of fiber stress utilization, peak coefficient of fiber stress utilization behavior and strain at peak coefficient of fiber stress utilization. In general, the theoretical prediction agreed well with the experimental results.

Table 5.5 Peak coefficient of fiber stress utilization of cotton rotor yarns

Sample	Peak coefficient of fiber stress utilization		Strain at peak coefficient of fiber stress utilization	
	Experimental	Predicted	Experimental	Predicted
98.4 tex	0.394	0.390	0.044	0.045
73.8 tex	0.374	0.394	0.044	0.045
59.0 tex	0.366	0.391	0.044	0.045

The ring and rotor cotton yarn coefficient of fiber stress utilization, general shape and the trends of the experimental results are well captured.

5.3.2 Predicted and experimental coefficient of fiber stress utilization of combed cotton yarns

Two combed yarns from long staple cotton fiber were used for validation of model. The experimental and theoretical coefficient of fiber stress utilization for both combed cotton yarns was calculated at a range of strain values and the results are presented graphically in figure 5.3. The theoretical relations are not fully valid in the area of very small strains due to relative variations by process of measurement and pre tensioned yarn. Therefore, we shall analyse the mutual relations starting from strain values of 0.01 (1%).

The calculated Gegauff's model φ_g according to equation (3.45) represents thin straight lines on the graph in figure 5.4. The coefficient of fiber stress utilization curves φ_{c1} correspond to equation (3.55) single integral equation. The parameters from table 5.1 and $\eta = 0.5$ were used for calculations. Moreover, empirical common values, $k = 0.73$ for both combed yarns was used for prediction of theoretical coefficient of fiber stress utilization $k.\ \varphi_{c1}$. The coefficient of fiber stress utilization curve φ_{c2} resembles to equation (3.71) our double integral equation. The relative higher value of C = 5.5 and lower value of empirical constant k was used in equation (3.71) for evaluation of coefficient of fiber stress utilization because of better orientation of fibers in combed yarn.

The comparison between the experimental and theoretical results in figure 5.3 and table 5.6 for combed cotton yarns show the prediction of coefficient of fiber stress utilization and yarn peak coefficient of fiber stress utilization behavior are reasonable. In general, the theoretical prediction agrees well with experimental results.

Table 5.6 Peak coefficient of fiber stress utilization of combed cotton yarns

Sample	Peak coefficient of fiber stress utilization		Strain at peak coefficient of fiber stress utilization	
	Experimental	Predicted	Experimental	Predicted
11.5 tex	0.643	0.649	0.026	0.026
20 tex	0.637	0.648	0.034	0.030

The coefficient of fiber stress utilization for combed cotton yarn is higher as compared with carded cotton yarns which might be due to the longer cotton fiber and better orientation and migration of fibers in such yarns due to combing process.

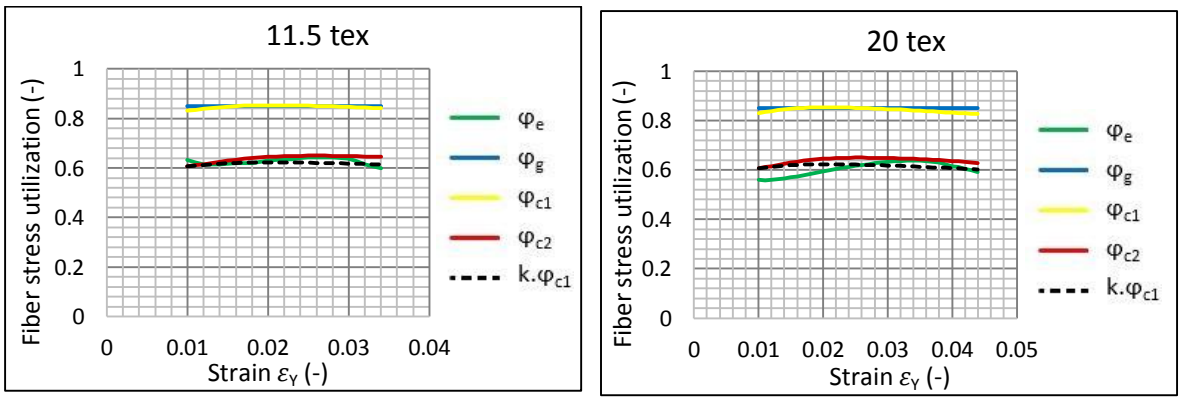

Figure 5.3 Predicted and experimental coefficient of fiber stress utilization in combed cotton staple spun yarn

5.4 Predicted and experimental coefficient of fiber stress utilization of polyester yarns

The six graphs for experimental and theoretical coefficient of fiber stress utilization related to individual polyester yarns are presented in figure 5.4. The graphs (a, b, c,) are for ring yarns and (d, e, f) for rotor yarns. The calculated Gegauff's model φ_g according to equation (3.45) represents straight lines on the graph in figure 5.5. The coefficient of fiber stress utilization curves φ_{c1} and φ_{c2} correspond to equation (3.55) and (3.71) single and double integral equations respectively.

On the face of it, these graphs have more or less similar logic then the previous curves of viscose and cotton yarns. Of course, it was necessary to use another parameter specific for these polyester yarns. The values from the table 5.1 and $\eta = 0.5$, more common values $C = 2.0$ and $k = 0.60$ for ring yarns and $C = 1.17$ and $k = 0.51$ for rotor yarns were used for prediction of theoretical coefficient of fiber stress utilization.

It is also valid that coefficient of fiber stress utilization from Gegauff's model is relatively far from experimental curves. The coefficient of fiber stress utilization curve φ_{c1} have roughly similar shapes to the experimental coefficient of fiber stress utilization curves but these are lying too high in our graphs near Gegauff's line. By suitable empirical values of k, the black dotted curves $k.\varphi_{c1}$ are lying near to the experimental curves φ_e especially by smaller values of strain ε_Y. The predicted coefficient of fiber stress utilization curves φ_{c2} from double integral equation (3.71) are lying with respect to position and shape with dotted black curves $k.\varphi_{c1}$.

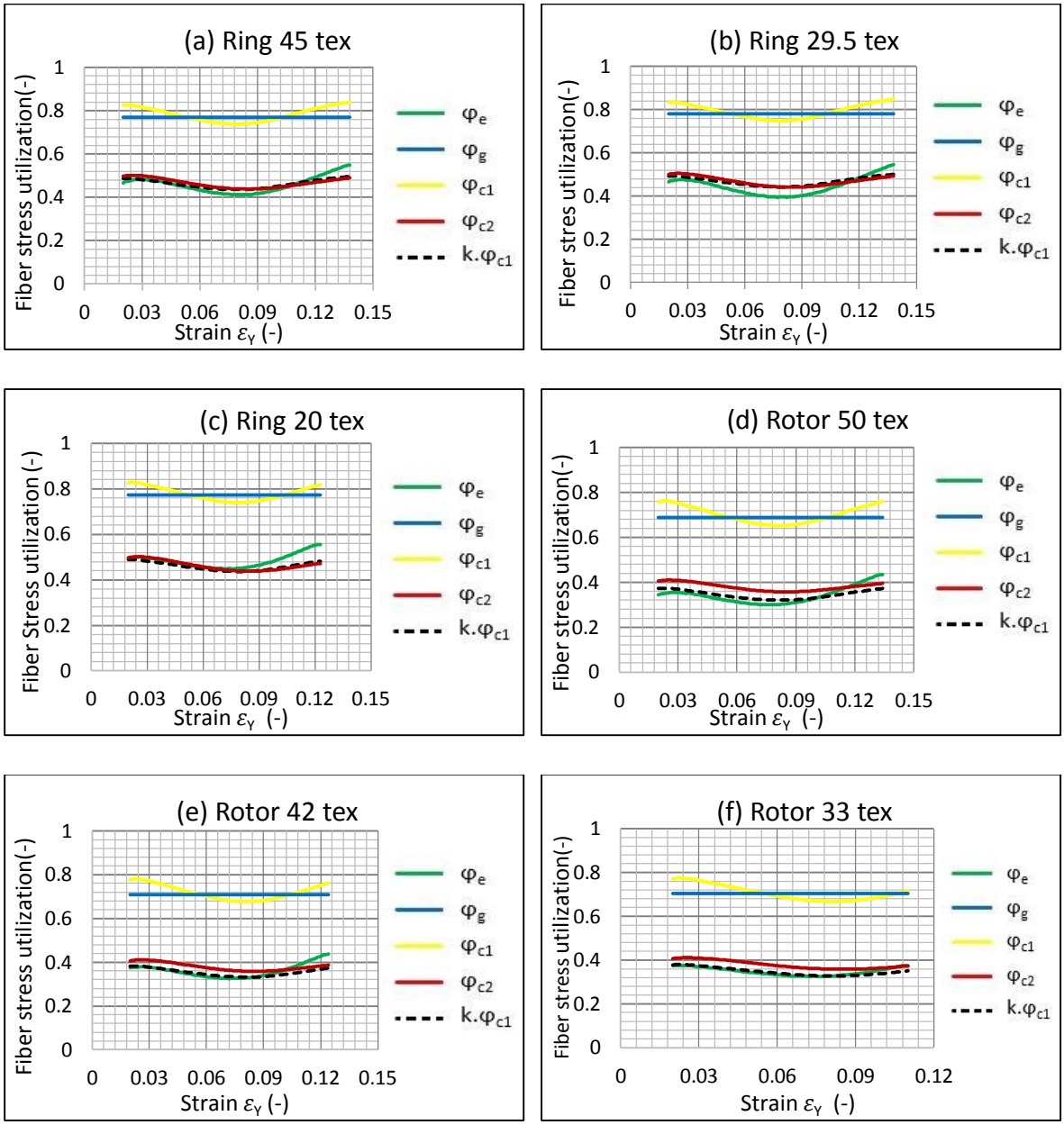

Figure 5.4 Predicted and experimental coefficient of fiber stress utilization in polyester staple spun yarn; ring yarns a, b, c and rotor yarns d, e, f.

The comparison between the experimental and theoretical results in figure 5.4a, b, c and table 5.7 for ring spun polyester yarns show the prediction of coefficient of fiber stress utilization, least coefficient of fiber stress utilization behavior and strain at least coefficient of fiber stress utilization are in good agreement.

Table 5.7 Least coefficient of fiber stress utilization of polyester ring yarns

Sample	Least coefficient of fiber stress utilization		Strain at least coefficient of fiber stress utilization	
	Experimental	Predicted	Experimental	Predicted
20 tex	0.448	0.437	0.072	0.083
29.5 tex	0.395	0.441	0.082	0.084
45tex	0.412	0.436	0.082	0.080

The comparison between the experimental and theoretical results in figure 5.4d, e, f and table 5.8 for rotor polyester yarns show the prediction of coefficient of fiber stress utilization, yarn least coefficient of fiber stress utilization behavior and strain at least utilization.

Table 5.8 Least coefficient of fiber stress utilization of polyester rotor yarns

Sample	Least coefficient of fiber stress utilization		Strain at Least coefficient of fiber stress utilization	
	Experimental	Predicted	Experimental	Predicted
33 tex	0.326	0.358	0.077	0.082
42 tex	0.325	0.358	0.077	0.082
50 tex	0.300	0.357	0.077	0.084

The polyester yarns presented low coefficient of fiber stress utilization when compared with viscose and cotton yarns. The shape of the experimental coefficient of fiber stress utilization curves is different at higher strains from predicted coefficient of fiber stress utilization curves due to the slippage among the polyester fiber near the breaking point which may be attributed to specific structure of polyester. The behavior of coefficient of fiber stress utilization was found different for polyester fiber and yarn as compared with other studied fibers and yarns.

5.5 Experimental and predicted coefficient of fiber stress utilization of linen yarns

The predicted and experimental coefficient of fiber stress utilization for two linen yarns is presented in the figure 5.5. The position of the experimental curve φ_e is far from the Gegauff's straight line φ_g. The position of the coefficient of fiber stress utilization curve φ_{c1} is near to the Gegauff's line but it is not linear. The predicted coefficient of fiber stress utilization curve φ_{c2} from double integral equation (3.71) is similar in position as well as in shape to the experimental curve. The coefficient of fiber stress utilization for linen yarn is very low. We have to use the value of angular preference C = 1.6 like cotton and viscose

rotor yarn and small value of empirical constant k = 0.43. The low coefficient of fiber stress utilization in linen yarns might be due to the poor orientation of linen fiber like rotor yarn and variation in the linen fiber fineness due to lack of elemental fiber.

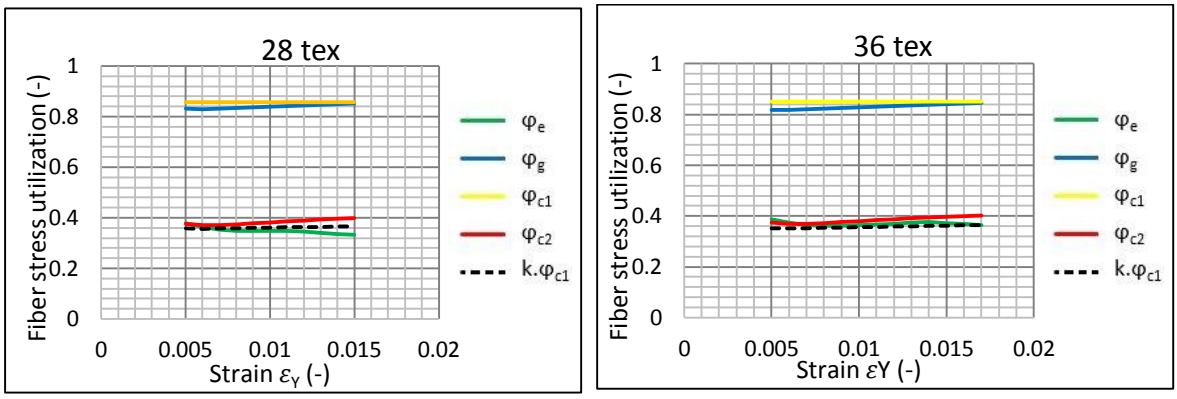

Figure 5.5 Predicted and experimental coefficient of fiber stress utilization in linen staple spun yarn

5.6 Experimental and predicted coefficient of fiber stress utilization of worsted yarns

The predicted and experimental coefficient of fiber stress utilization for two worsted yarns is presented in the figure 5.6. The position of the experimental coefficient of fiber stress utilization curve φ_e is far from the Gegauff's straight line φ_g. The position of the coefficient of fiber stress utilization curve φ_{c1} is near to the Gegauff's line but it is not linear. The predicted coefficient of fiber stress utilization curve φ_{c2} from double integral equation (3.71) is similar in position as well as in shape to the experimental curve. The coefficient of fiber stress utilization for worsted yarn is about 65%. We used the parameter C = 4.9 and k = 0.79 similar to cotton and viscose ring yarn. The higher coefficient of fiber stress utilization in worsted yarns might be attributed to its fiber surface properties.

The comparison between the experimental and theoretical results in figure 5.6 and table 5.9 for worsted yarns show the prediction of coefficient of fiber stress utilization, peak coefficient of fiber stress utilization behavior and strain at peak utilization are reasonable.

Table 5.9 Peak coefficient of fiber stress utilization of worsted ring yarns

Sample	Peak coefficient of fiber stress utilization		Strain at peak coefficient of fiber stress utilization	
	Experimental	Predicted	Experimental	Predicted
20 tex	0.716	0.686	0.073	0.073
23 tex	0.756	0.699	0.051	0.051

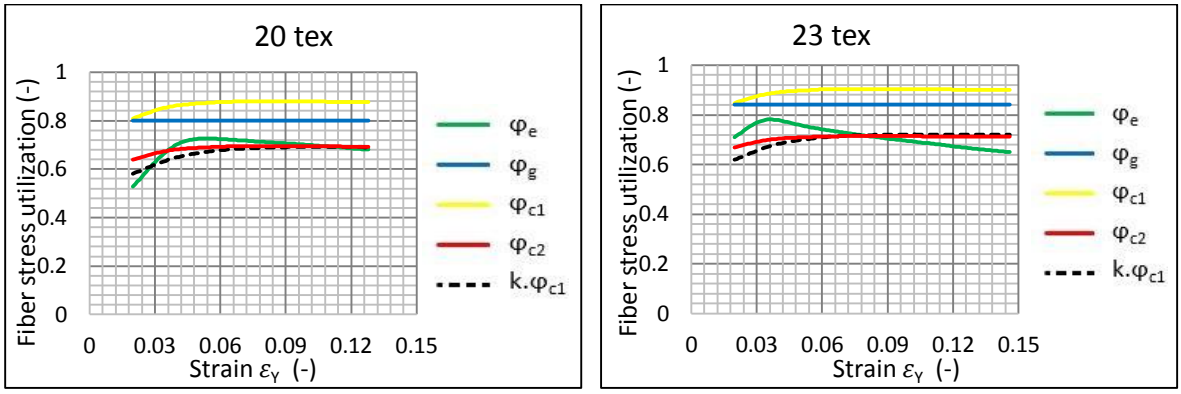

Figure 5.6 Predicted and experimental coefficient of fiber stress utilization in worsted staple spun yarn

5.7 Predicted and experimental coefficient of fiber stress utilization of acrylic yarns

The predicted and experimental coefficient of fiber stress utilization for three acrylic ring yarns is presented in the figure 5.7. The position of the experimental coefficient of fiber stress utilization curve φ_e is far from the coefficient of fiber stress utilization from Gegauff φ_g. The position of the coefficient of fiber stress utilization curve φ_{c1} is near to the Gegauff's line but it is not linear. The predicted coefficient of fiber stress utilization curve φ_{c2} from double integral equation (3.71) is similar in position as well as in shape to the experimental coefficient of fiber stress utilization curve. The coefficient of fiber stress utilization for acrylic yarn is about 70 %. We used the parameter C = 4.9 and k = 0.76 similar to cotton and viscose ring yarns. The higher coefficient of fiber stress utilization in acrylic yarns might be attributed to uniform and longer staple length of acrylic fibers. The comparison between the experimental and theoretical results in figure 5.7 and table 5.10 for all ring acrylic yarns show the prediction of coefficient of fiber stress utilization, peak coefficient of fiber stress utilization behavior and strain at peak utilization. The comparison is found better near the end points of the coefficient of fiber stress utilization curves.

Table 5.10 Peak coefficient of fiber stress utilization of acrylic ring yarns

Sample	Peak coefficient of fiber stress utilization		Strain at peak coefficient of fiber stress utilization	
	Experimental	Predicted	Experimental	Predicted
12 tex	0.73	0.76	0.078	0.078
14 tex	0.72	0.74	0.086	0.086
18 tex	0.70	0.76	0.085	0.085

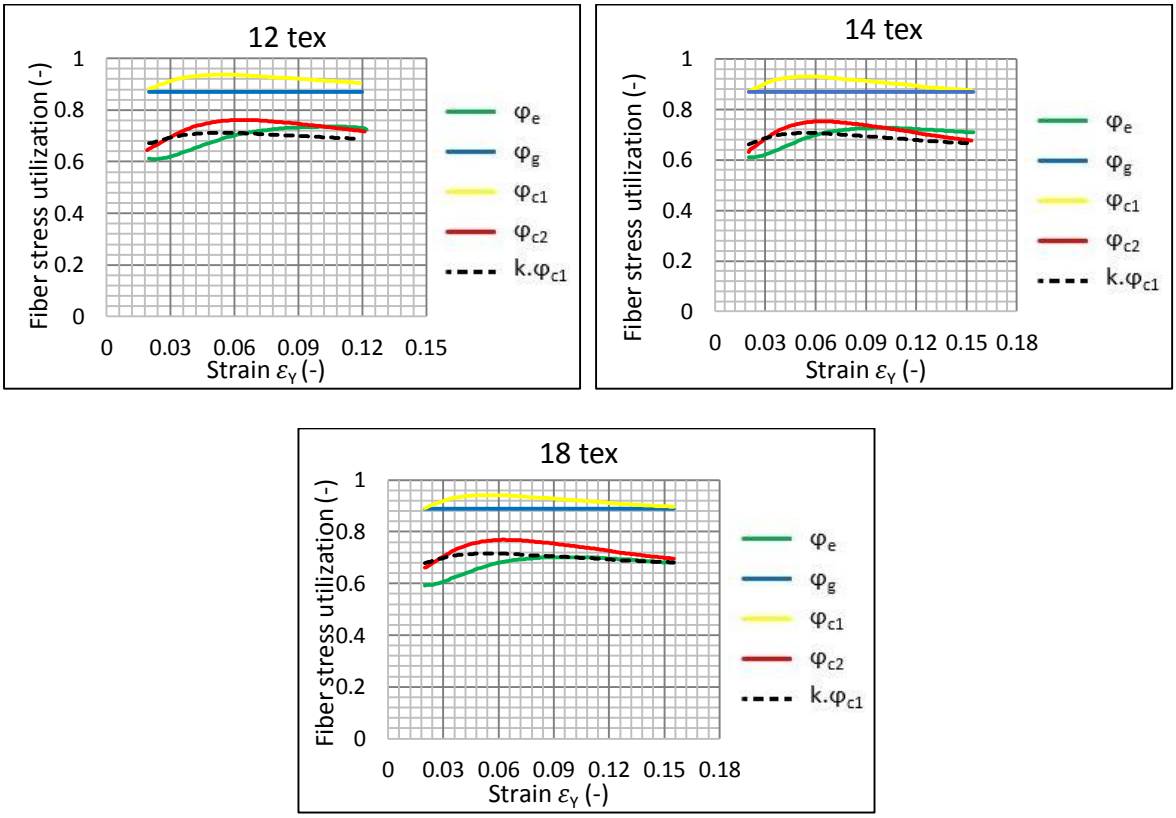

Figure 5.7 Predicted and experimental coefficient of fiber stress utilization in acrylic staple spun yarn

5.8 Comparison of mathematical models for coefficient of fiber stress utilization

We compared our mathematical model explained in Chapter 3 with other mathematical models from Pan, Frydrych and Gegauff. The comparison of four mathematical models for coefficient of fiber stress utilization was done before process of break for two types of viscose ring spun yarns. The comparison for both type of viscose yarns is presented in figure 5.8.

It can be revealed that the results of our model for coefficient of fiber stress utilization are in good agreement with the experimental results with respect to shape and position as compared with other three mathematical models. Zubair *et al.* [77] published similar results for comparison of mathematical models. The Pan and Frydrych's models under estimate the coefficient of fiber stress utilization and same value of coefficient of fiber stress utilization is obtained at each strain, while Gegauff's model over estimates that coefficient and cannot evaluate as a function of strain.

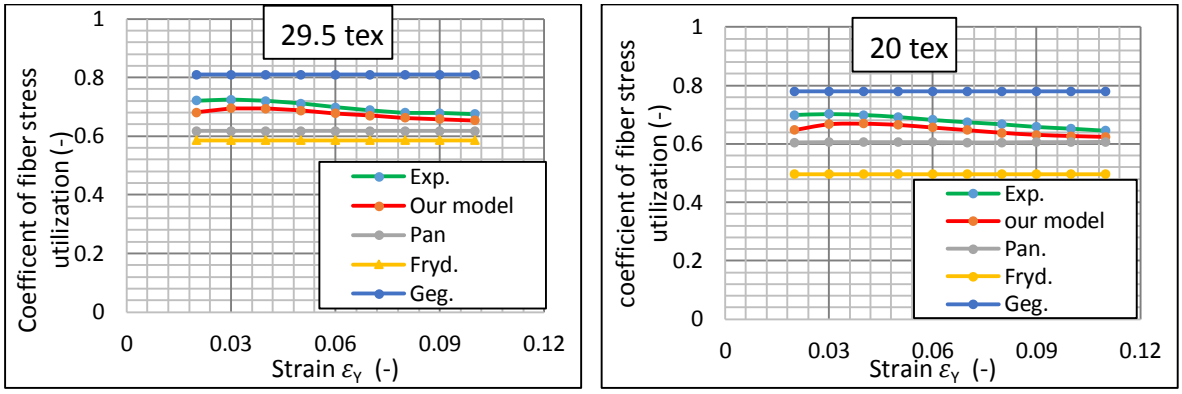

Figure 5.8 Comparison of mathematical models for coefficient of fiber stress utilization in viscose ring spun yarns

5. 9 Experimental and predicted yarn specific stress-strain curves

The theoretical coefficient of fiber stress utilization obtained from our model equation (3.72) was used to evaluate the yarn specific stress-strain curves from the fiber stress-strain curve data for each type of ring and rotor yarns. The equation (3.72) was used to predict the yarn specific stress-strain curve for all types of yarns. The predicted and experimental specific stress-strain curve before break for viscose, cotton, polyester, linen, wool and acrylic yarns are described in this section.

5.9.1 Predicted and experimental specific stress-strain curves of viscose yarns

The experimental and theoretical specific stress-strain curves for viscose ring and rotor yarns are shown in the figure 5.9. For all viscose yarns, predicted yarn specific stress-strain curves have good agreement with the experimental specific stress-strain curves both in position and shape before break. Zubair *et al.* [78] compared the predicted and experimental specific stress-strain curves for cotton and polyester staple spun ring and rotor yarns and found reasonable agreement.

The slight difference in predicted and experimental specific stress-strain curves in case of rotor yarn might be the result of yarn structure due to rotor technology.

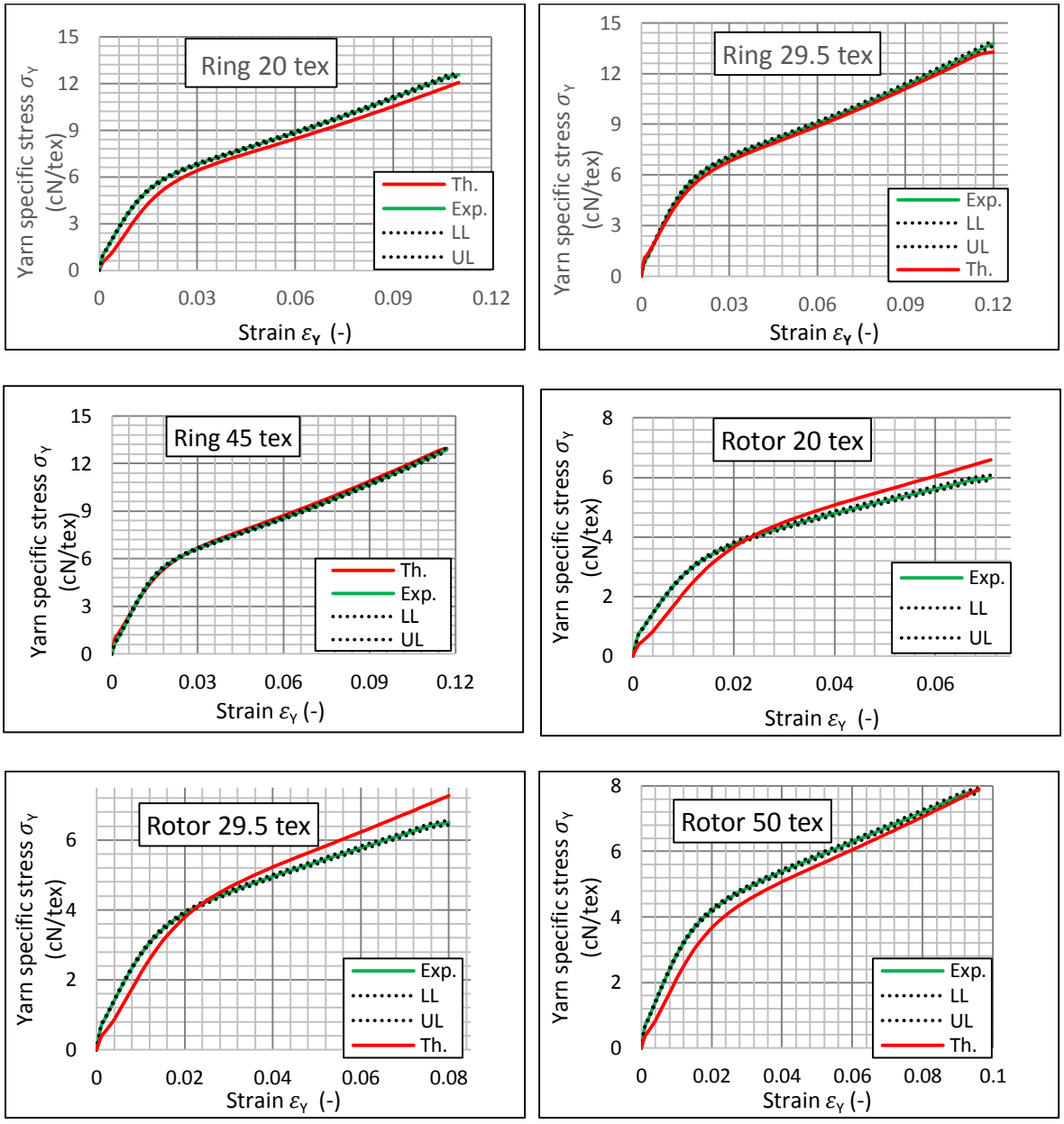

Figure 5.9 Predicted and experimental specific stress-strain curves of viscose ring and rotor staple spun yarns

Variation of migration and twist between both inner and outer layer in rotor yarn causes its structure to separate into two phases unlike unified helical structure in ring spun yarn [79].

5.9.2 Predicted and experimental specific stress-strain curves of polyester yarns

The experimental and theoretical specific stress-strain curves for polyester ring and rotor yarns are drawn in the figure 5.10. The polyester yarns could not present good results as by viscose yarn for yarn specific stress-strain curves. Results indicate that predicted yarn specific stress-strain curves captured well the experimental results before yarn break.

However, differences are observed at higher strains in both ring and rotor yarns which might be the result of higher slippage among the polyester fibers.

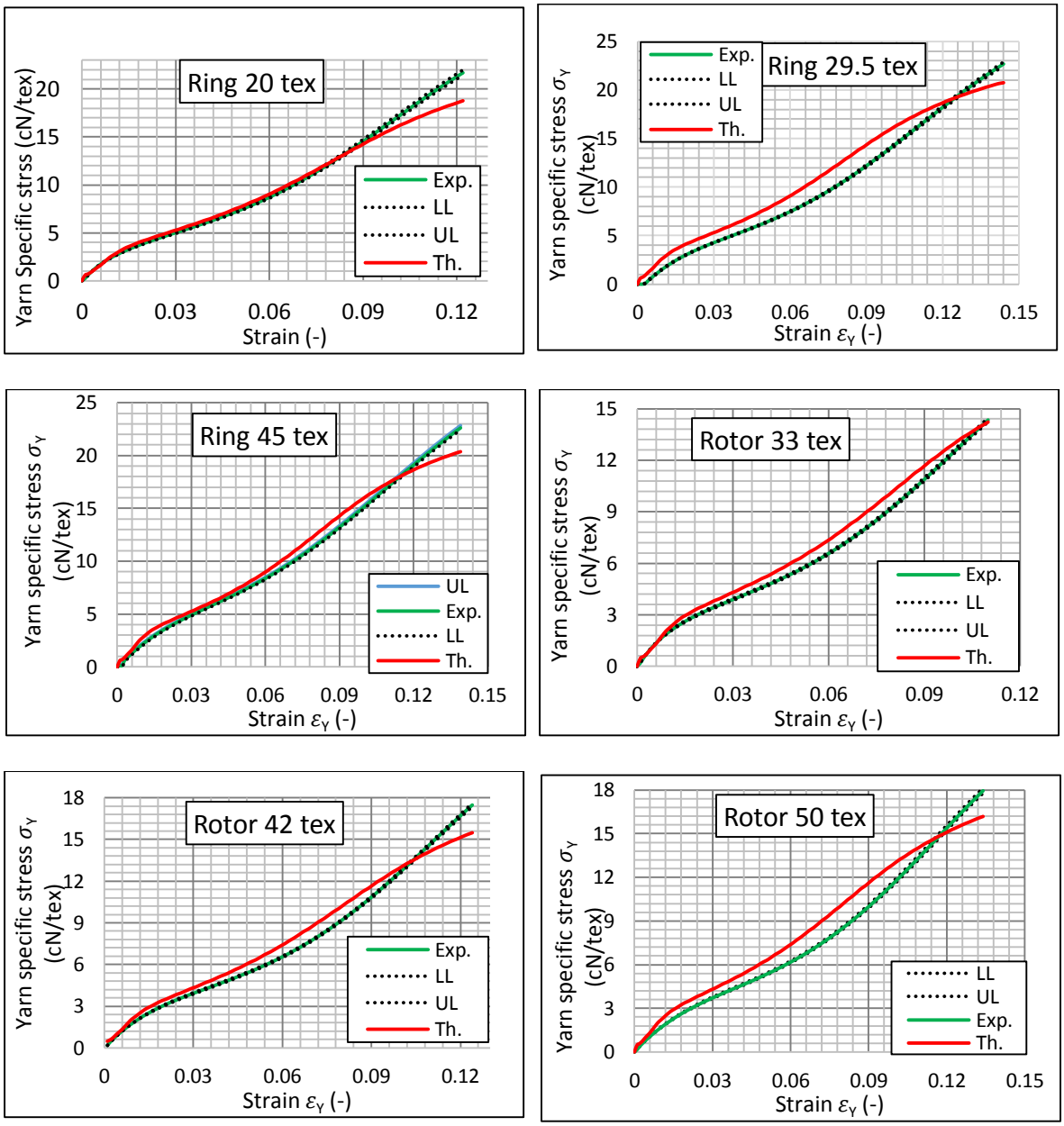

Figure 5.10 Predicted and experimental specific stress curves of polyester ring and rotor staple spun yarns

Polyester fibers consist of amorphous and crystalline regions and another amorphous region taking a phase called mesamorphous phase. During fiber stress-strain process, amorphous region initially align similar to mesamorphous phase. Subsequently, the load strains the bonds in both crystalline and amorphous phases and slippage occurs [80]. It may be attributed to the higher difference among the predicted and experimental yarn specific stress- strain curves at

higher strain values for polyester yarn. The slight difference in rotor polyester yarn might be attributed to the structure of rotor yarn.

5.9.3 Predicted and experimental specific stress-strain curves of carded cotton yarns

The experimental and theoretical specific stress-strain curves for cotton carded ring and rotor yarns are drawn in the figure 5.11. The predicted specific stress-strain curves have better agreement with the experimental specific stress-strain curves before break. The difference at higher strain for rotor yarns might be the result of variability in strength and fineness of cotton fibers and rotor yarn structure.

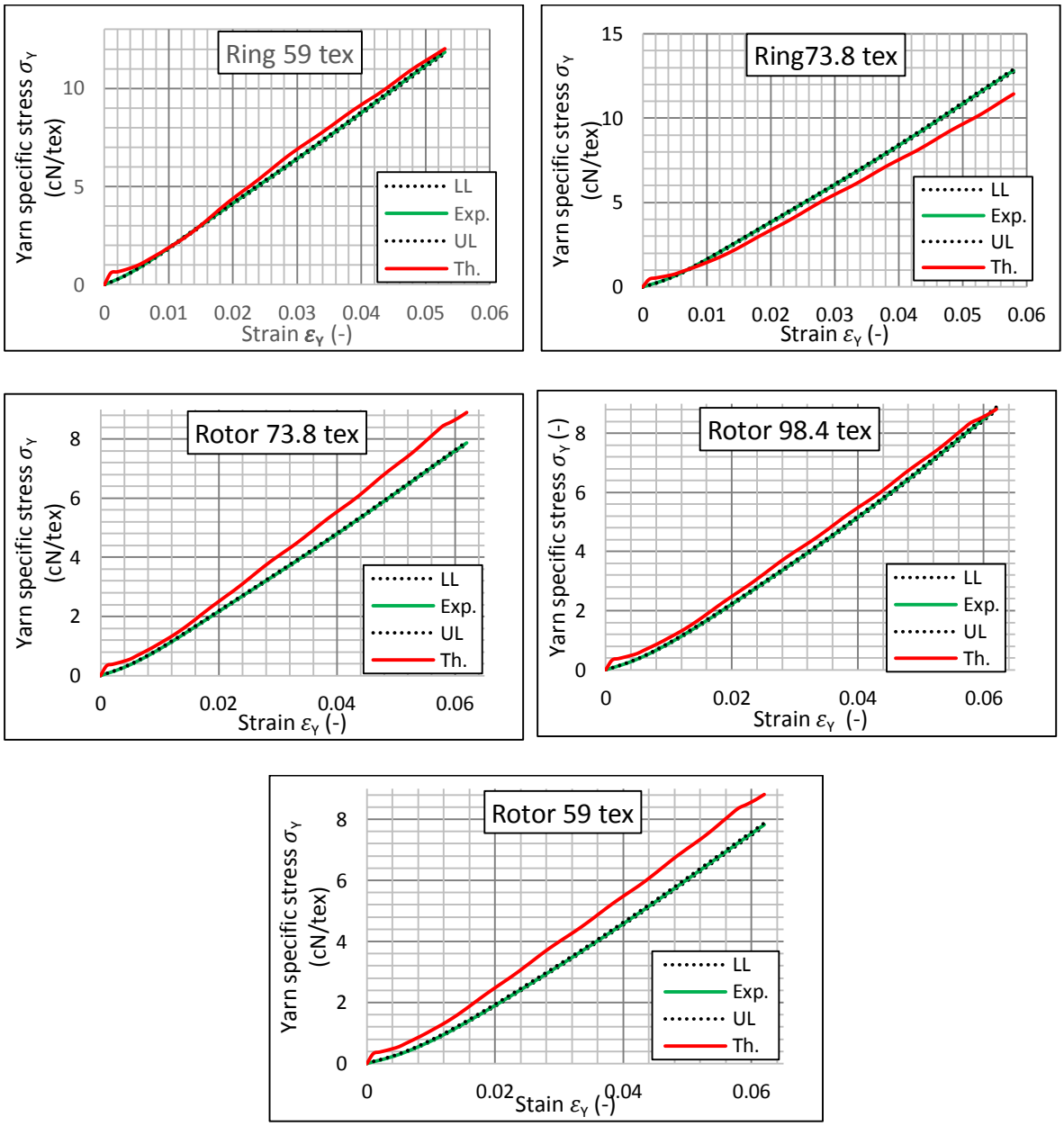

Figure 5.11 Predicted and experimental specific stress curves of carded cotton ring and rotor

The specific stress-strain curves are more linear as compared with viscose and polyester yarn curves due to the chemical nature of cotton fiber. The difference in specific stress-strain curves can again be explained similar to viscose rotor yarns.

5.9.4 Predicted and experimental specific stress-strain curves of combed cotton yarns

The experimental and theoretical specific stress-strain curves for combed cotton yarns are shown in the figure 5.12. The predicted yarn specific stress-strain curves captured well the experimental specific stress-strain curves before break of yarns. Again the specific stress-strain curves are more linear as compared with viscose and polyester yarn curves. The predicted and experimental curves exhibited less difference because of better orientation in combed cotton yarn. The shape of the experimental and predicted yarn specific stress-strain curves is similar to carded cotton yarns.

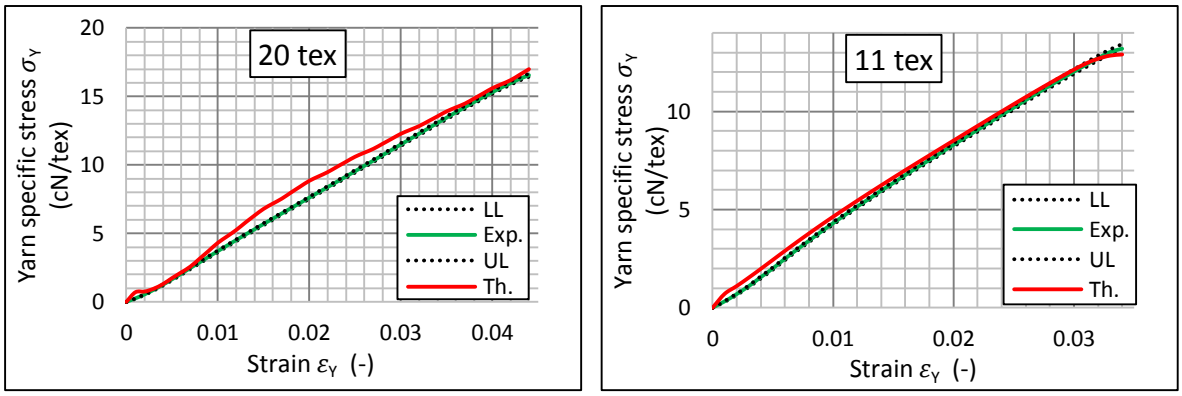

Figure 5.12 Predicted and experimental specific stress-strain curves of combed cotton staple spun yarns

5.9.5 Predicted and experimental specific stress-strain curves of linen yarns

The experimental and theoretical specific stress-strain curves for linen staple spun yarns are produced in the figure 5.13. The predicted yarn specific stress-strain curves have good agreement with the experimental curves before break of yarns. The yarn specific stress-strain curves for linen exhibit behavior in shape similar to cotton yarn because of cellulosic fiber. The relation is an empirical because the fibers are in the form of bundle and not easy to obtain elemental fiber so it is only estimation for linen yarns.

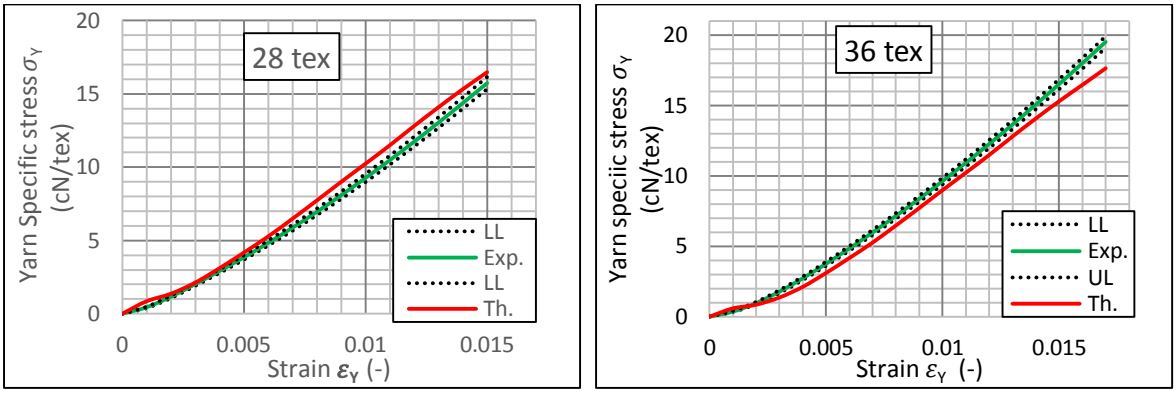

Figure 5.13 Predicted and experimental specific stress-strain curves of linen staple spun yarns

5.9.6 Predicted and experimental specific stress-strain curves of worsted yarns

The experimental and theoretical stress-strain curves for worsted yarns are presented in the figure 5.14. The predicted yarn specific stress-strain curves have good agreement with the experimental specific stress-strain curves before break of yarns. The difference for these yarns is also attributed to variability in the wool fiber fineness, strength and length.

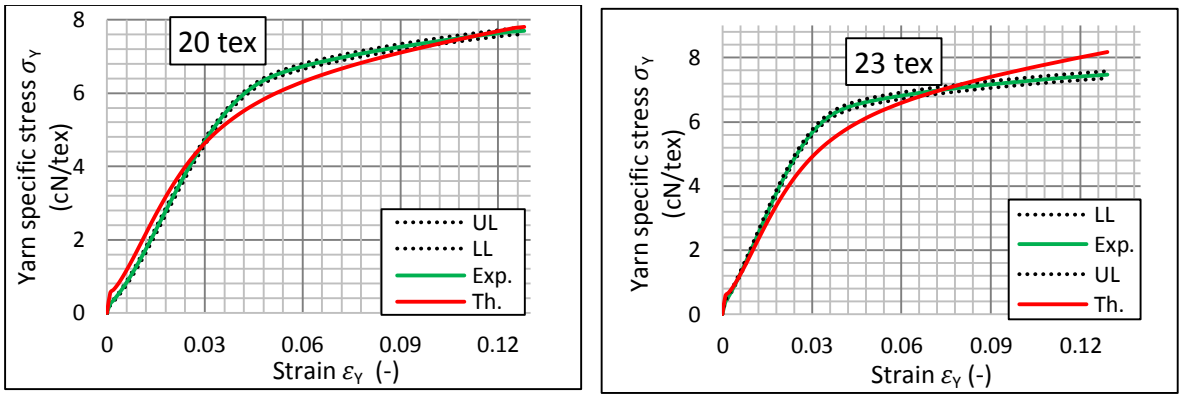

Figure 5.14 Predicted and experimental specific stress-strain curves of worsted staple spun yarns

5.9.7 Predicted and experimental specific stress-strain curves of acrylic staple spun yarns

The experimental and theoretical stress-strain curves for acrylic yarns are produced in the figure 5.15. The predicted yarn specific stress-strain curves also have good agreement with the experimental curves before break of yarns for all three types of yarn studied. The results of yarn specific stress are in better agreement near the point of break.

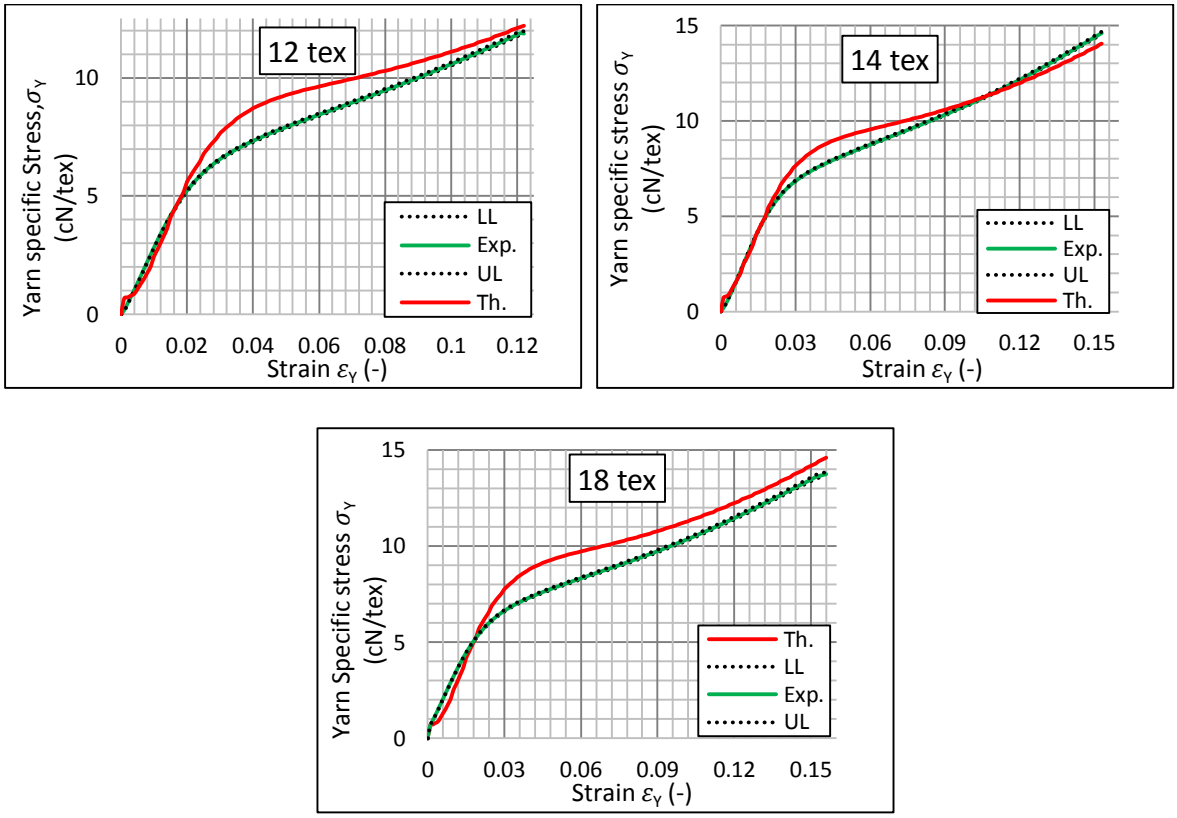

Figure 5.15 Predicted and experimental specific stress-strain curves of acrylic staple spun yarns

5.9.8 Comparison of yarn specific stress from mathematical models

The specific stress-strain curves for two viscose ring staple spun yarns were evaluated from our mathematical model and from other three Models like Gegauff, Pan and Frydrych. The predicted yarn specific stress-strain curves from all models before break of two viscose ring spun yarns are compared with the experimental yarn specific stress-strain curves. Our model exhibited good agreement with the experimental specific stress-strain curves as shown in the figure 5.16. The Gegauff's model overestimates and other two under estimates while our model predict the yarn specific stress-strain curves near the experimental curves before the yarn break.

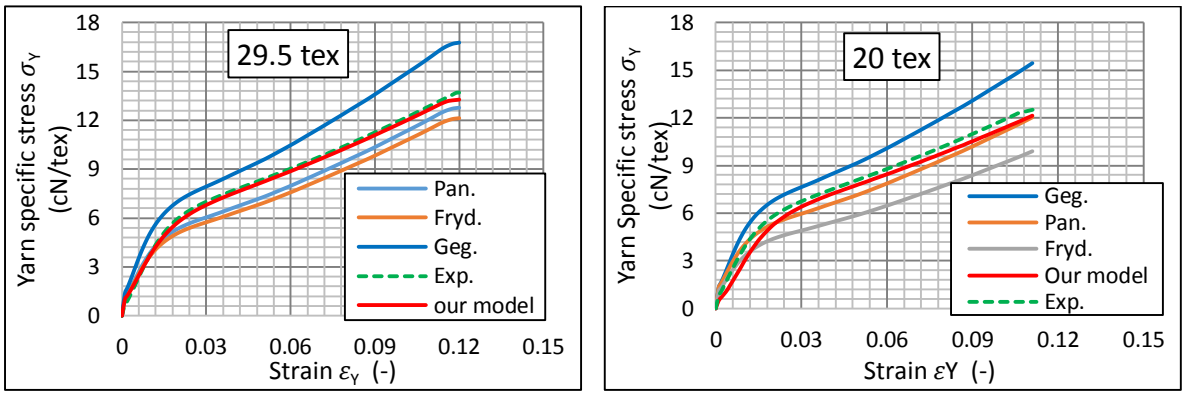

Figure 5.16 Comparison of mathematical models for yarn specific stress-strain in viscose ring staple yarns

The comparison between the experimental and predicted results from theoretical model in figure 5.1 through 5.7 shows a reasonable agreement between the predictions of coefficient of fiber stress utilization and its behavior. In general the theoretical prediction agrees well with the experimental results before break. The predicted coefficient of fiber stress utilization, general shape and trend of experimental data are well captured for all yarns under study with a slight difference due to some experimental measurement or due to specific fiber material.

The graph in figure 5.9 through 5.15 presents the yarn specific stress for all type of yarns. The predicted yarn specific stress for all yarns agreed well with the

experimental yarn specific stress-strain curves before the point of break. Comparison of our model for coefficient of fiber stress utilization and yarn specific stress-strain curves is found superior as compared with other three models of Gegauff, Pan and Frydrych for ring viscose yarns.

CHAPTER 6

SUMMARY OF THE RESULTS

This thesis presents a mathematical model that predicts fiber stress utilization along with its validation for staple spun yarns. The theoretical model considers fiber stress-strain curve, twist angle, yarn contraction ratio and fiber orientation. The four types of coefficient of fiber stress utilization from Gegauff's model, single integral model, double integral model and k times single integral model were predicted and compared with the experimental coefficient of fiber stress utilization. Further the specific stress-strain curves for different types of yarns were estimated from the knowledge of predicted coefficient of fiber stress utilization and the experimental fiber specific stress-strain curves.

6.1 Conclusion

From the experimental results it is clear that fiber type and technology have significant effect on the coefficient of fiber stress utilization of staple spun yarns. Viscose, worsted and acrylic yarns produced higher coefficient of fiber stress utilization as compared with cotton and polyester yarns. The low coefficient of fiber stress utilization in carded cotton yarns might be due to higher variability in length and strength of these fibers. The polyester fiber possess low coefficient of fiber stress utilization which might be attributed to higher slippage due to its chemical structure. The combed cotton yarn presented higher coefficient of fiber stress utilization due to better fiber orientation in these yarns. The rotor yarns exhibited low coefficient of fiber stress utilization due to the poor fiber orientation and small fiber portions due to rotor technology. The linen yarns displayed very low coefficient of fiber stress utilization which might be due to their higher modulus, less elongation and higher stiffness.

We can summarize the results of predicted and experimental coefficient of fiber stress utilization for viscose, cotton (carded and combed), polyester, linen, wool and acrylic yarns as shown through figure 5.1 to 5.7 in chapter 5.

- Coefficient of fiber stress utilizations from Gegauff's model φ_g are relatively far from experimental coefficient of fiber stress utilization curves φ_e on graph in term of their position as well as their shapes for all type of yarns.
- The predicted coefficient of fiber stress utilization curves φ_{c1} from single integral equation have a similar shape to the experimental coefficient of fiber stress utilization curves φ_e but these are lying too high in our graph near Gegauff's straight lines φ_g. Both

Gegauff's model and single integral model overestimate the coefficient of fiber stress utilization.

- When multiplying the empirical constant *k* by the coefficient of fiber stress utilization curves φ_{c1}, the results were so close to experimental coefficient of fiber stress utilization curve φ_e but it is without logical interpretation.
- An interesting phenomena is that one common value empirically determined parameter *k* = 0.79 satisfies to all viscose, wool, acrylic and cotton ring yarns while another common value *k* = 0.55 fulfils to all rotor yarns.
- One empirical value of *k* gives us an insight about the prediction of coefficient of fiber stress utilization curves φ_{c2} from our double integral model considering fiber orientation in yarn. That is why we are able to explain technically that the position of predicted coefficient of fiber stress utilization curves φ_{c2} lie in close contact with curves *k*. φ_{c1}in graphs.
- The suitable value of parameter *C* in double integral model (3.71) is also interesting which is synchronized with the fiber directional distribution in the yarn. The relatively high parameter of *C* = 4.9 was necessary to choose for viscose, cotton (carded), wool and acrylic ring yarns due to controlled drafting process which produced the fiber directions concentrated mostly round helical model angle β.
- In case of rotor yarns (viscose and cotton), we have to choose considerably smaller common value *C* = 1.6 which might be due to poor fiber orientation from higher short fiber portions in rotor yarns.
- We have to use a little less value of empirical constant *k* = 0.7 and higher value of parameter *C* = 5.5 for combed cotton yarns which concludes that fiber orientation in combed cotton yarns is enriched due to the combing process.
- In case of polyester yarns the considerable lower value of parameter *C* = 2.0 and *k* = 0.60 for ring yarns and *C* = 1.17 and k = 0.51 for rotor yarns enable us for evaluation of coefficient of fiber stress utilization which might be due to higher slippage among the fibers in these yarns.
- We have to choose very small value of *k* = 0.43 and *C* = 1.6 for linen yarns. It might be due to higher stiffness and low elongation of the linen fiber. It also might be attributed to poor directional distribution of fibers in linen yarns similar to rotor yarns. The results are semi empirical for this yarn due to absence of elemental fibers in linen.

It can also be concluded from figure 5.9 through 5.15 that predicted yarn specific stress-strain curves agreed well with the experimental yarn specific stress-strain curves for all type of

yarns before process of break. The higher difference in yarn specific stress for carded cotton and wool near the breaking point might be the result of variation in strength, staple length and fineness of these natural fiber materials. The slight difference between predicted and experimental curves in rotor yarns might be the result of the structure of rotor yarn due to difference in twist and migration between inner and outer yarn layers.

The comparison of coefficient of fiber stress utilization and yarn specific stress-strain curves among four types of models (Ours, Gegauff, Pan and Frydrych) represents that our model predicts the coefficient of fiber stress utilization as well as yarn specific stress-strain curves, which is in good agreement with the experimental results.

In graph 5.4, there are two new significant phenomena for polyester yarns.

I. **Angular preference *C***: The value C = 2 for ring yarns corresponds roughly to a common carded web value C = 1.17 represents practically isotropic orientation of fiber portions. Such high variability of fiber directional distribution is not imaginable going out of our experiences, might be investigated through yarn microscopy. It means that there must exists another significant influences other than fiber orientation which decreases positions of experimental coefficient of fiber stress utilization curves for polyester yarns..

II. **Higher breaking strain**: Beside above we can also observe that experimental coefficient of fiber stress utilization curves increases more rapidly by higher values of breaking strain about 0.07 or 0.08 in opposite to the trends of curves *k*. φ_{c1} and /or φ_{c2}.

The above mentioned phenomena might be the result of micro fibrils in polyester fiber and tri molecule which may result in variable crimp distribution on short fiber portions and slippage in fiber to fiber contacts at higher values of yarn strains.

We are unable to predict the coefficient of fiber stress utilization at lower strains 0.02 (2%) and higher values of strains (near break) because of catastrophic failure due to pre-tensioned yarn and higher friction near the point of break. All our results are valid for standard yarn twist.

6.2 Recommendations

- There is an important question of research regarding polyester fiber. The lower value for fiber orientation parameter C gives us an insight that there may be some reasons behind which can affect coefficient of fiber stress utilization of polyester fiber. The experimental coefficient of fiber stress utilization of polyester fiber is increased tremendously after

0.07 or 0.08 strain as compared with the predicted coefficient of fiber stress utilization. The reason may be studied up to a microscopic level.

- The prediction of coefficient of fiber stress utilization in the yarn and yarn specific stress-strain curves might be evaluated up to the point of break by modification of the mathematical model including the effect of coefficient of variation in fiber breaking strength and strain, variability of fiber crimp and the friction among the fibers (slippage effect).

REFERENCES

[1] B. C. Goswami, J. G. Martindale, and F. L. Scardino, *Textile yarns; Technology, stracture, and applications*. John Wiley and sons, 1977.

[2] C. M. Geaguff, "Strength and elasticity of cotton threads," *Bull. Soc. Ind. Mulhouse*, vol. 77, pp. 153–176, 1907.

[3] M. M. Platt, "Mechanics of Elastic Performance of Textile Materials: III. Some Aspects of Stress Analysis of Textile Structures-- Continuous-Filament Yarns," *Text. Res. J.*, vol. 20, no. 1, pp. 1–15, 1950.

[4] M. M. Platt, *Mechanics of elastic performance of textile materials: III. Some aspects of stress analysis of textile s tructures-- continuous-Filament Yarns*, vol. 20, no. 1. 1950.

[5] J. W. S. Hearle, "Theoretical Analysis of the Mechanics of Twisted Staple Fiber Yarns," *Text. Res. J.*, vol. 35, no. 12, pp. 1060–1071, 1965.

[6] F. T. Peirce, "Tensile tests for cotton yarns;V. the weakest link theorems on the strength of long composite specimen," *J. Text. Inst.*, vol. 17, pp. T355–T368, 1926.

[7] W. English, *The textile industry*. London: Longmans,Green, 1967.

[8] H. P. Gurney, "The distribution of stresses in cotton products," *J. Text. Inst.*, vol. 16, pp. T269–T289, 1925.

[9] F. T. Peirce, "Tensile tests for cotton yarns–'the weakest link' theorems on the strength of long and of composite specimens," *J. Text. Inst*, vol. 17, pp. T355–368, 1926.

[10] R. R. Sullivan, "A theoretical approach to the problem of yarn strength," *J. Appl. Phys.*, vol. 13, no. 3, pp. 157–167, 1942.

[11] M. M. Platt, "Mechanics of elastic performance of textile materials III. Some aspects of stress analysis of textile structures—continuous-filament yarns," *Text. Res. J.*, vol. 20, no. 1, pp. 1–15, 1950.

[12] M. M. Platt, "Mechanics of Elastic Performance of Textile Materials Part VI: Influence of Yarn Twist on Modulus of Elasticity," *Text. Res. J.*, vol. 20, no. 10, pp. 665–667, 1950.

[13] J. Gregory, "The strength of twisted yarn elements in relation to the properties of the constituent fibers," *J. Text. Inst.*, vol. 41, pp. T499–T512, 1953.

[14] J. Gregory, “The strength of artificial yarn elements in relation to bulk and twist,” *J. Text. Inst.*, vol. 41, pp. T30–T52, 1953.

[15] J. Gregory, “The relation between strength measurements made on fiber, fiber bundles, yarns and cloths,” *J. Text. Inst*, vol. 41, pp. T515–T515, 1953.

[16] J. W. S. Hearle, “29—The mechanics of twisted yarns: The influence of transverse forces on tensile behaviour,” *J. Text. Inst. Trans.*, vol. 49, no. 8, pp. T389–T408, 1958.

[17] J. W. S. Hearle, H. El-Behery, and V. M. Thakur, “The mechanics of twisted yarns: theoretical developments,” *J. Text. Inst. Proc.*, vol. 52, no. 5, pp. P203–P203, 1961.

[18] J. W. S. Hearle, “8—On the theory of the mechanics of Twisted Yarns,” *J. Text. Inst.*, vol. 60, no. 3, pp. 95–101, 1969.

[19] J. W. S. Hearle, P. Grosberg, and S. Backer, *Structural mechanics of fibers, yarns, and fabrics*. Wiley-Interscience, 1969.

[20] J. W. S. Hearle, “Theoretical analysis of the mechanics of twisted staple fiber yarns,” *Text. Res. J.*, vol. 35, no. 12, pp. 1060–1071, 1965.

[21] L. R. G. Treloar and G. Riding, “16—A theory of the Stress–Strain properties of continuous-filament yarns,” *J. Text. Inst. Trans.*, vol. 54, no. 4, pp. T156–T170, 1963.

[22] L. R. G. Treloar, “Rubber model of yarns and cords,” *J. Appl. Phys.*, vol. 13, p. 314, 1962.

[23] L. R. G. Treloar, “A migrating-filament theory of yarn properties,” *J. Text. Inst.*, vol. 56, pp. T359–T377, 1965.

[24] H. W. Holdaway, “Theoretical model for predicting the strength of single worsted yarns,” *J. Text. Inst.*, vol. 56, no. 11, pp. T121–T144, 1965.

[25] J. L. White, C. C. Cheng, and K. E. Duckett, “An Approach to Friction Effects in Twisted Yarns,” *Text. Res. J.*, vol. 46, no. 7, pp. 496–501, 1976.

[26] C. C. Cheng, J. L. White, and K. E. Duckett, “A Continuum Mechanics Approach to Twisted Yarns,” *Text. Res. J.*, vol. 44, no. 10, pp. 798–803, 1974.

[27] G. A. Carnaby and P. Grosberg, “Tensile behaviour of staple fibre yarns at small extensions,” *J. Text. Inst.*, vol. 67, pp. 299–308, 1967.

[28] J. J. Thwaites, "A continuum model for yarn mechanics," *NATO Adv. study Inst.*, vol. 87, 1979.

[29] N. Pan, T. Hua, and Y. Qiu, "Relationship between fiber and yarn strength," *Text. Res. J.*, vol. 71, no. 11, pp. 960–964, 2001.

[30] N. Pan, "Development of a constitutive theory for short fiber yarns: Mechanics of staple yarn without slippage effect," *Text. Res. J.*, vol. 62, no. 12, pp. 749–765, 1992.

[31] N. Pan, "Development of a Constitutive Theory for Short Fiber Yarns Part II: Mechanics of Staple Yarn With Slippage Effect," *Text. Res. J.*, vol. 63, no. 9, pp. 504–514, 1993.

[32] N. Pan, "Prediction of statistical strengths of twisted fibre structures," *J. Mater. Sci.*, vol. 28, no. 22, pp. 6107–6114, 1993.

[33] M. L. Realff, N. Pan, M. Seo, M. C. Boyce, and S. Backer, "A stochastic simulation of the failure process and ultimate strength of blended continuous yarns," *Text. Res. J.*, vol. 70, no. 5, pp. 415–430, 2000.

[34] E. Önder and G. Baser, "A comprehensive stress and breakage analysis of staple fiber yarns Part I: Stress analysis of a staple yarn based on a yarn geometry of conical helix fiber paths," *Text. Res. J.*, vol. 66, no. 9, pp. 562–575, 1996.

[35] E. Önder and G. Baser, "A Comprehensive Stress and Breakage Analysis of Staple Fiber Yams Part II: Breakage Analysis of Single Staple Fiber Yams," *Text. Res. J.*, vol. 66, no. 10, pp. 634–640, 1996.

[36] L. V. Langenhove, "Simulating the mechanical properties of yarn based on the properties and arrangement of its fibers,Part I:the finite element model," *Text. Res. J.*, vol. 67, pp. 263–268, 1997.

[37] L. V. Langenhove, "Simulating the mechanical properties of a yarn based on the properties and arrangement of its fibers, Part II: results of simulation," *Text. Res. J.*, vol. 67, pp. 342–347, 1997.

[38] L. V. Langenhove, "Simulating the mechanical properties of a yarn based on the properties and arrangement of its fibers," *Text. Res. J.*, vol. 67, pp. 406–412, 1997.

[39] P. J. Morris, J. H. Merkin, and R. W. Rennell, "Modelling of yarn properties from fibre properties," *J. Text. Institute. Part 1, Fibre Sci. Text. Technol.*, vol. 90, no. 3, pp. 322–335, 1999.

[40] A. N. Solovev, *The Prediction of Yarn Properties in Cotton Processing*. Moskva, 1958.

[41] Usenko, *The Use of Staple Fiber in Spinning*. Moskva, 1958.

[42] J. F. Bogdan, "The Prediction of Cotton Yarn Strengths1," *Text. Res. J.*, vol. 37, no. 6, pp. 536–537, 1967.

[43] J. F. Bogdan, "The Characterization of Spinning Quality," *Text. Res. J.*, vol. 26, no. 9, pp. 720–730, 1956.

[44] T. A. Subramanian, K. Ganesh, and S. Bandyopadhyay, "34—a Generalized Equation for Predicting the Lea Strength of Ring-Spun Cotton Yarns," *J. Text. Inst.*, vol. 65, no. 6, pp. 307–313, 1974.

[45] M. D. Ethridge, J. D. Towery, and J. F. Hembree, "Estimating Functional Relationships Between Fiber Properties and the Strength of Open-End Spun Yarns'," *Text. Res. J.*, vol. 52, no. 1, pp. 35–45, 1982.

[46] T. Swiech, "Influnence of fiber properties on the strength of rotor spun yarns," *melliandTextilber*, vol. 68, pp. 874–877, 1987.

[47] P. Neelakantan and T. A. Subramanian, "An Attempt to Quantify the Translation of Fiber Bundle Tenacity into Yarn Tenacity," *Text. Res. J.*, vol. 46, no. 11, pp. 822–827, 1976.

[48] R. L. N. Iyengar and A. K. Gupta, "Proportion of Fiber Strength Utilized in the Single Yarn," *Text. Res. J.*, vol. 44, no. 7, pp. 489–492, 1974.

[49] R. L. N. Iyengar and A. K. Gupta, "Some Functions Involving Fiber Properties for Estimating Yarn Tenacity," *Text. Res. J.*, vol. 44, no. 7, pp. 492–594, 1974.

[50] Y. E. El Mogahzy, *Selecting Cotton Fiber Properties for Fitting Reliable Equations to HVI Data*, vol. 58, no. 392. 1988.

[51] E. Hunter, L. and Gee, "Correlation between cotton fiber properties and ring and rotor yarn properties," *Melliand Textilber*, vol. 64, pp. 398–401, 1982.

[52] R. J. Chasmawala, S. M. Hansen, and S. Jayaraman, "Structure and properties of air-jet spun yarns," *Text. Res. J.*, vol. 60, no. 2, pp. 61–69, 1990.

[53] R. Rajamanickam, S. M. Hansen, and S. Jayaraman, "Analysis of the modeling

methodologies for predicting the strength of air-jet spun yarns," *Text. Res. J.*, vol. 67, no. 1, pp. 39–44, 1997.

[54] O. M. A. Hafez, "Yarn-strength prediction of American cottons," *Text. Res. J.*, vol. 48, no. 12, pp. 701–705, 1978.

[55] H. H. Ramey, R. Lawson, and S. Worley, "Relationship of cotton fiber properties to yarn tenacity," *Text. Res. J.*, vol. 47, no. 10, pp. 685–691, 1977.

[56] H. W. Krause and H. A. Soliman, "Theoretical study of the strength of single jet false twist spun yarns," *Text. Res. J.*, vol. 60, no. 6, pp. 309–318, 1990.

[57] I. Frydrych, "A new approach for predicting strength properties of yarn," *Text. Res. J.*, vol. 62, no. 6, pp. 340–348, 1992.

[58] W. Zurek, *The Structure of Yarn*. Poland: Warsaw, 1975.

[59] W. Zurek, I. Frydrych, and S. Zakrzewski, "A method of predicting the strength and breaking strain of cotton yarn," *Text. Res. J.*, vol. 57, no. 8, pp. 439–444, 1987.

[60] S. Das and A. Ghosh., "cotton fiber -to -yarn engineering; A simulated annealing approach," *FIBERS Text. East. Eur.*, vol. 23, no. 3, pp. 51–53, 2015.

[61] A. Ghosh, S. Ishtiaque, S. Rengasamy, P. Mal, and A. Patnaik, "Predictive models for strength of spun yarns: An overview," *AUTEX Res. J.*, vol. 5, no. 1, pp. 20–29, 2005.

[62] A. Ghosh, "A theoretical investigation on the generation of strength in staple yarns," *Fibers Polym.*, vol. 7, no. 3, pp. 310–316, 2006.

[63] B.A.Sami and H. Naima, "Prediction of the Mechanical behavior of Open-End and Ring SPUN Yarns," *J. Appl. Sci.*, vol. 9, no. 8, pp. 1466–2009, 2009.

[64] M. Dang, S. Wang, and G. Liu, "Theoretical prediction on tensile model of wool/spandex core-spun yarn," *J. Ind. Text.*, vol. 37, no. 4, pp. 301–313, 2008.

[65] A. Guha, R. Chattopadhyay, and Jayadeva, "Predicting yarn tenacity: a comparison of mechanistic, statistical, and neural network models," *J. Text. Inst.*, vol. 92, no. 2, pp. 139–145, 2001.

[66] M. Cybulska and B. C. Goswami, "Tensile behaviour of staple yarns," *J. Text. Inst.*, vol. 92, no. 3, pp. 26–37, 2001.

[67] X. Shao, Y. Qiu, and Y. Wang, “Theoretical modeling of the tensile behavior of low-twist staple yarns: part I - theoretical model,” *J. Text. Inst.*, vol. 96, no. 2, pp. 61–68, 2005.

[68] X. Shao, Y. Qiu, and Y. Wang, “Theoretical modeling of the tensile behavior of low-twist staple yarns: Part II–theoretical and experimental results,” *J. Text. Inst.*, vol. 96, no. 2, pp. 69–76, 2005.

[69] T. Liu, K. F. Choi, and Y. Li, “Mechanical Modeling of Singles Yarn,” *Text. Res. J.*, vol. 77, no. 3, pp. 123–130, 2007.

[70] K. Sriprateep and A. Pattiya, “Computer aided geometric modeling of twist fiber,” *J. Comput. Sci.*, vol. 5, no. 3, p. 221, 2009.

[71] K. Sriprateep and E. L. J. Bohez, “CAD/CAE for stress–strain properties of multifilament twisted yarns,” *Text. Res. J.*, p. 0040517516636000, 2016.

[72] B. Neckář and D. Das, “Tensile behavior of staple fiber yarns part I: theoretical models,” *J. Text. Inst.*, pp. 1–9, 2016.

[73] B. Neckář and D. Das, *Theory of structure and mechanics of fibrous assemblies*. Woodhead Publishing India, 2012.

[74] M. Zubair, B. Neckář, and D. Das, “Tensile behavior of staple fiber yarns part II: model validation,” *J. Text. Inst.*, pp. 1–4, 2016.

[75] B. Neckar, “Cross-dimensions and stress-strain curve of yarns,” Liberec, 1981.

[76] B. Neckar and D. Das, *Theory of Structure and Mechanics of Fibrous Assemblies*. New Dehli: Wood Head Publishing India, 2012.

[77] M. Zubair, M. Eldeeb, and B. Neckar, “Tensile behavior of staple fiber yarns part III: comparison of mathematical models,” *J. Text. Inst.*, pp. 1–4, 2016.

[78] M. Zubair, B. Neckar, M. Eldeeb, and G. A. Baig, “Tensile behavior of staple fiber yarns, part IV: experimental verification of predicted stress–strain curves,” *J. Text. Inst.*, pp. 1–6, 2016.

[79] P. R. Lord, “The structure of open-end spun yarn,” *Text. Res. J.*, vol. 41, no. 9, pp. 778–784, 1971.

[80] S. Basu, “Tensile deformation of fibers used in textile industry,” *Agil. Technol. Appl.*

Note, pp. 1–7, 2012.

LIST OF RESEARCH ARTICLES PUBLISHED

1 Publications in Journal

1. M. Zubair, B. Neckář, and D. Das, "Tensile behavior of staple fiber yarns part II: model validation," *J. Text. Inst.*, pp. 1–4, 2016.

***(Published on line*)**

2. M. Zubair, M. Eldeeb, and B. Neckar, "Tensile behavior of staple fiber yarns part III: comparison of mathematical models," *J. Text. Inst.*, pp. 1–4, 2016.

(Published on line)

3. M. Zubair, B. Neckar, M. Eldeeb, and G. A. Baig, "Tensile behavior of staple fiber yarns, part IV: experimental verification of predicted stress–strain curves," *J. Text. Inst.*, pp. 1–6, 2016.

(Published on line)

4. M. Zubair, B. Neckář, and Z. A. Malik, "Predicting Specific Stress of Cotton Staple Ring Spun Yarns: Experimental and Theoretical results," *FIBERS Text. East. Eur.*, vol. 2, 2017.

(Accepted)

5. M. Zubair, H. S. Maqsood, and B. Neckář, "Impact of Filling Yarns on Woven Fabric Performance," *Fibres Text. East. Eur.*, 2016.

(Published)

6. M. Zubair, T. Hussain, S. Hussain, and A. Mazari, "Development of polyester/cellulosic blend woven fabric for better comfort/Dezvoltarea tesaturilor din amestec poliester/celuloza pentru un confort mai bun," *Ind. Textila*, vol. 67, no. 6, p. 359, 2016.

(Published)

7. H. S. Maqsood, U. Bashir, M. Zubair, J. Wiener, and J. Militky, "Cationization of cellulose fibers for composites," *J. Text. Inst.*, pp. 1–6, 2016.

(Published on line)

2 Contribution in conference proceeding

1. M. Zubair and B. Neckář, "Stress strain curves for PES fiber and yarns," in *Strutex 2014*, 2014, pp. 49–52.

STRUTEX 2014

2. M. Zubair, B. Neckar, and H. S. Maqsood, "Experimental and predicted specific stresss strain curves of worsted yarns," in *Strutex*, 2016, pp. 125–130.

STRUTEX 2016

3. M. Zubair and B. Neckar, "Linen fiber and yarn stress strain curves," in *Workshop for PhD students of faculty of textile engineering and faculty of mechanical engineering TUL*, 2015, pp. 193–197.

Svetlanka Workshop 2015

4. M. Zubair and B. Neckář, "Specific stress strain curves of viscose yarn:experimental verification," in *Workshop for PhD students of faculty of textile engineering and mechanical engineering TUL*, 2016, pp. 149–152.

Bila Voda Workshop 2016

5. H. S. Maqsood, M. Zubair, J. Wiener, and J. Militky, "Reinforcement of cationized cellulose in anionic matrix," in *Workshop for PhD students of faculty of textile engineering and faculty of mechanical engineerin TUL*, 2016, pp. 91–97

Bila Voda Workshop 2016

APPENDIX A

TENSILE TEST CURVES FOR FIBERS

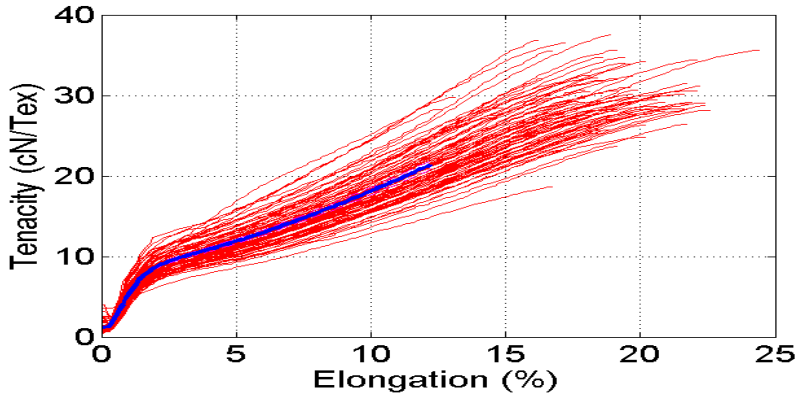

Figure A.1 Individual and mean specific stress-elongation curves for viscose fiber

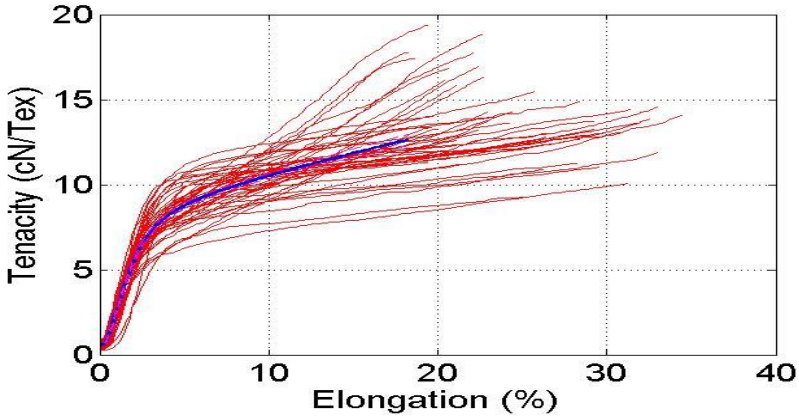

Figure A.2 Individual and mean specific stress-elongation curves for wool fiber

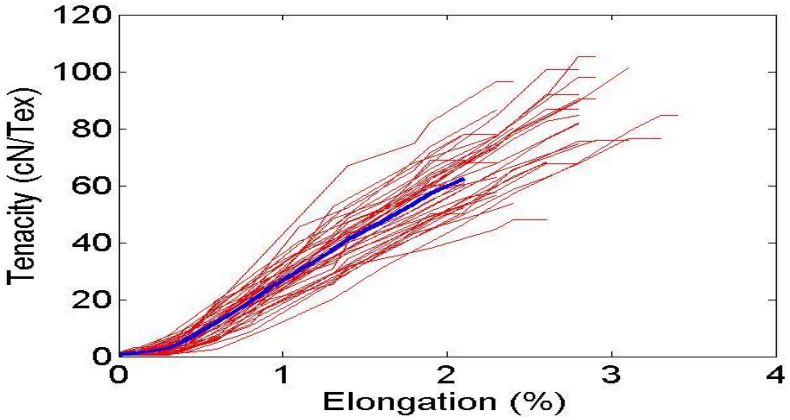

Figure A.3 Individual and mean specific stress-elongation curves for linin fiber

APPENDIX B: TENSILE TEST CURVES FOR YARNS

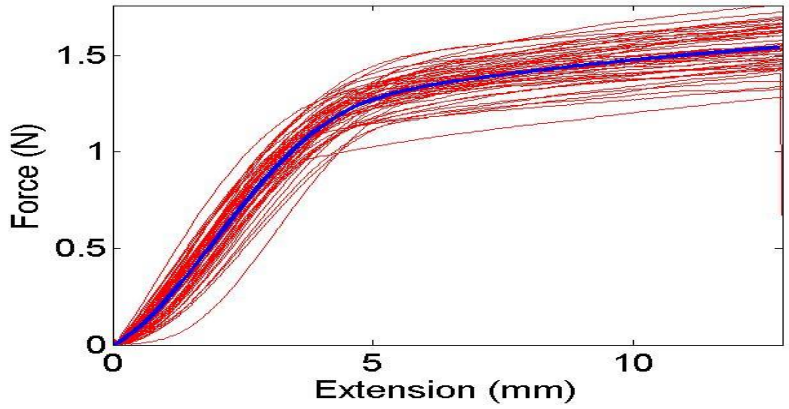

Figure B.1 Mean and individual force-elongation curves for worsted 20 tex yarn

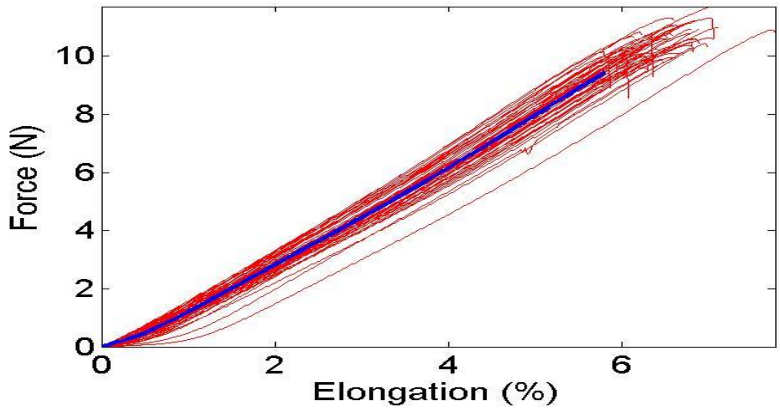

Figure B.2 Mean and individual force-elongation curves for cotton 73.8 tex ring yarn

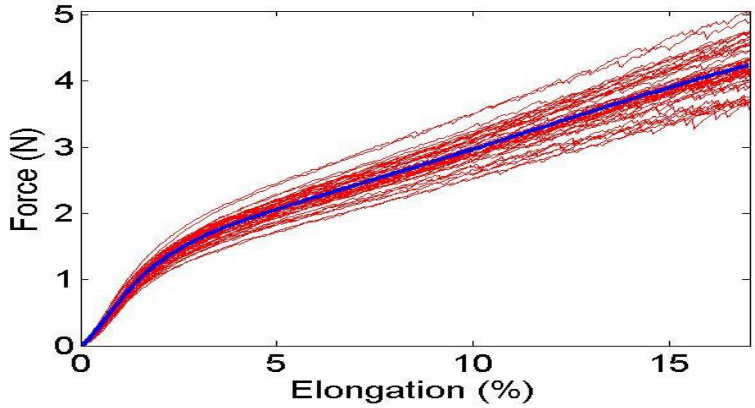

Figure B.3 Mean and individual force-elongation curves for viscose 29.5 tex ring yarn

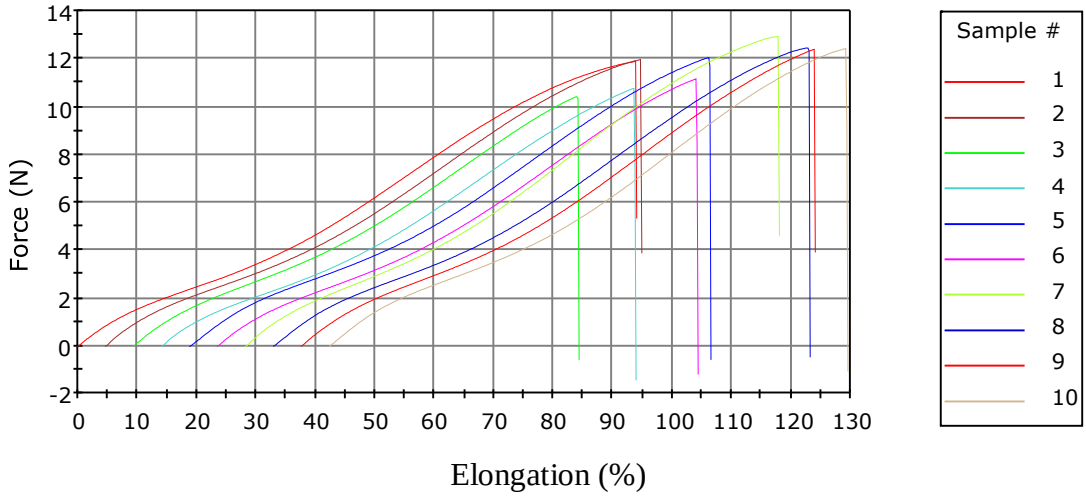

Figure B.4 Force elongation curves for Polyester 45 tex yarn

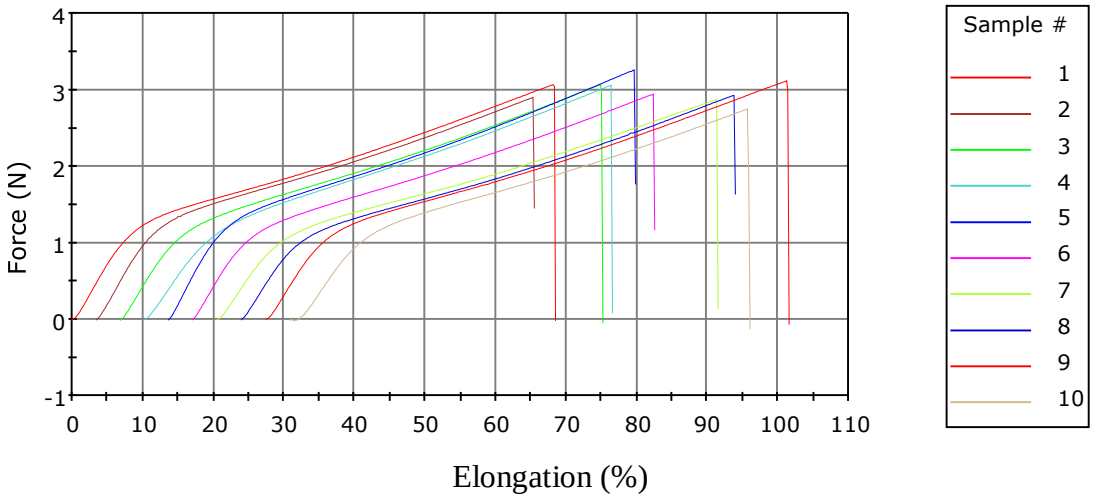

Figure B.5 Force and elongation curves for viscose 20 tex ring yarn

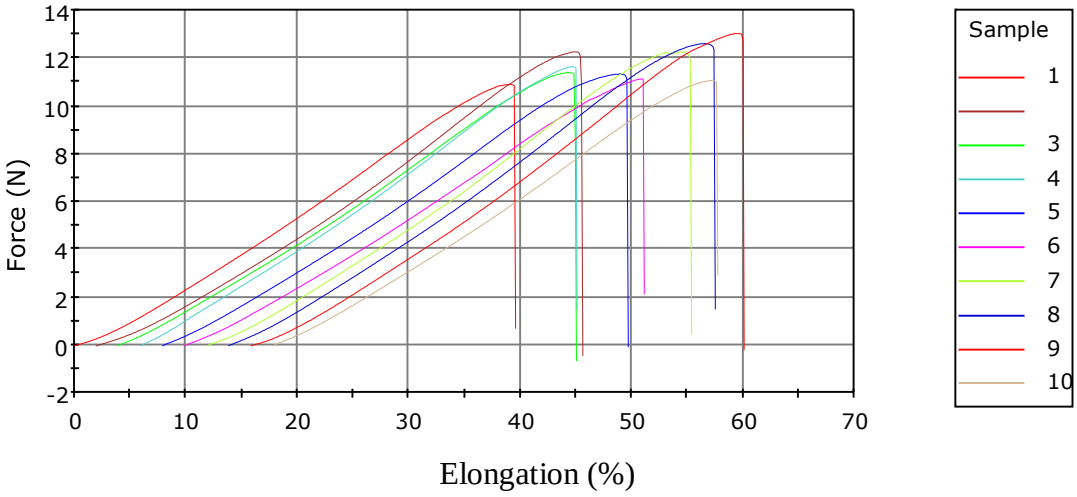

Figure B.6 Force and elongation curve for cotton 98 tex rotor yarn

APPENDIX C: RAW DATA OF EXPERIMENT

Table C.1 Breaking force and elongation data for 45-tex polyester ring yarn

Sample #	Max. Elongation (mm)	Max. Force (N)	Max. Energy (mJ)	Max. Young' s Modulus (gf/tex)	Time for Tensile Strength (sec)
1	94.03	11.87	568.78	192.066	24.500
2	90.18	11.96	536.40	196.344	23.500
3	74.85	10.40	371.43	193.992	19.450
4	79.84	10.75	410.59	192.385	20.750
5	87.71	12.03	516.43	198.480	22.800
6	80.79	11.15	430.87	195.425	21.000
7	89.79	12.92	582.08	216.349	23.350
8	90.19	12.43	553.44	202.340	23.400
9	86.34	12.39	519.08	205.631	22.500
10	87.14	12.40	529.25	211.073	22.650

Table C.2 Breaking force and elongation data for viscose 20 tex ring yarn

Sample #	Maximum Elongation (mm)	Max. Force (N)	Maximum Energy (mJ)	Young'modulus (gf/tex)	Time for max. tensile strength (sec)
1	68.47	3.07	130.65	405.896	18.600
2	62.06	2.90	114.52	408.991	16.900
3	68.30	3.07	129.04	385.368	18.550
4	66.28	3.06	123.98	334.719	18.050
5	66.10	3.26	134.47	453.193	18.000
6	65.38	2.94	119.90	397.509	17.800
7	70.87	2.88	125.28	348.783	19.300
8	69.94	2.93	125.08	369.244	19.050
9	74.16	3.12	140.62	374.100	20.150
10	65.17	2.75	109.14	334.027	17.700

Table C.3 Breaking force and elongation data for cotton 98 tex rotor yarn

Sample #	Max. Elongation (mm)	Max. Force (N)	Max. Energy (mJ)	Max. Young' Modulus (gf/tex)	Time for Tensile Strength (sec)
1	39.59	10.90	206.41	172.591	18.000
2	43.61	12.25	250.68	187.318	19.900
3	41.12	11.38	226.42	172.953	18.650
4	39.16	11.63	224.53	184.366	17.950
5	41.76	11.33	233.45	175.763	18.950
6	41.23	11.11	225.48	166.569	18.950
7	43.50	12.25	258.03	187.483	19.650

8	43.62	12.60	265.02	188.074	19.700
9	44.25	13.03	271.72	193.029	20.050
10	39.92	11.06	216.41	172.634	18.250

Table C.4 Yarn linear density for polyester yarn

Sample	Yarn linear density						
	1	2	3	4	5	Mean	S.D
Ring-20 tex	20.46	20.17	20.22	20.32	20.76	20.386	0.236
Ring 29.5 tex	30.22	30.14	30.28	29.98	30.34	30.192	0.139
Ring-45 tex	43.70	43.86	43.69	44.18	43.75	43.836	0.203
Rotor-42 tex	41.68	42.13	41.18	41.62	41.21	41.564	0.390
Rotr-50 tex	50.46	50.48	50.66	51.13	50.56	50.658	0.275
Rotor-33 tex	33.63	33.76	33.43	34.21	33.84	33.774	0.288

Table C.5 Yarn diameter for carded cotton yarn [mm]

Sample #	Ring 73.8 tex	Ring 59 tex	Rotor 59 tex	Rotor 73.8 tex
1	0.22	0.18	0.36	0.39
2	0.23	0.19	0.34	0.39
3	0.23	0.2	0.35	0.45
4	0.23	0.2	0.32	0.46
5	0.24	0.2	0.29	0.57
6	0.25	0.21	0.3	0.53
7	0.25	0.21	0.32	0.34
8	0.25	0.22	0.32	0.35
9	0.25	0.22	0.27	0.34
10	0.25	0.22	0.31	0.41
11	0.25	0.22	0.4	0.35
12	0.26	0.22	0.35	0.38
13	0.26	0.22	0.31	0.37
14	0.26	0.22	0.33	0.38
15	0.26	0.22	0.32	0.36
16	0.26	0.22	0.3	0.38
17	0.26	0.23	0.3	0.37
18	0.26	0.23	0.3	0.42
19	0.26	0.23	0.26	0.4
20	0.26	0.23	0.28	0.42
21	0.27	0.23	0.3	0.33
22	0.27	0.23	0.31	0.35
23	0.27	0.23	0.34	0.35
24	0.27	0.23	0.3	0.42
25	0.27	0.24	0.34	0.4
26	0.27	0.24	0.3	0.35
27	0.27	0.24	0.3	0.35
28	0.27	0.24	0.3	0.38
29	0.27	0.24	0.39	0.38
30	0.27	0.24	0.33	0.37
31	0.28	0.24	0.39	0.37

32	0.28	0.24	0.29	0.38
33	0.28	0.24	0.32	0.38
34	0.28	0.24	0.3	0.36
35	0.28	0.25	0.3	0.41
36	0.28	0.25	0.35	0.36
37	0.28	0.25	0.34	0.42
38	0.28	0.25	0.31	0.41
39	0.28	0.25	0.33	0.41
40	0.28	0.25	0.31	0.38
41	0.28	0.25	0.28	0.38
42	0.28	0.25	0.29	0.38
43	0.28	0.25	0.37	0.39
44	0.28	0.25	0.37	0.35
45	0.28	0.25	0.36	0.36
46	0.28	0.25	0.35	0.35
47	0.28	0.25	0.32	0.34
48	0.29	0.25	0.38	0.29
49	0.29	0.25	0.33	0.3
50	0.29	0.25	0.32	0.33
51	0.29	0.25	0.36	0.32
52	0.29	0.25	0.38	0.42
53	0.29	0.25	0.3	0.4
54	0.29	0.25	0.29	0.37
55	0.29	0.25	0.32	0.45
56	0.29	0.26	0.34	0.43
57	0.29	0.26	0.34	0.39
58	0.29	0.26	0.33	0.38
59	0.29	0.26	0.33	0.39
60	0.29	0.26	0.33	0.39
61	0.3	0.26	0.3	0.37
62	0.3	0.26	0.02	0.35
63	0.3	0.26	0.32	0.38
64	0.3	0.26	0.3	0.37
65	0.3	0.26	0.33	0.39
66	0.3	0.26	0.34	0.38
67	0.3	0.26	0.34	0.36
68	0.31	0.26	0.31	0.33
69	0.31	0.26	0.33	0.34
70	0.31	0.26	0.31	0.35
71	0.31	0.26	0.31	0.35
72	0.31	0.26	0.32	0.35
73	0.31	0.26	0.34	0.35
74	0.31	0.26	0.33	0.36
75	0.31	0.27	0.35	0.37
76	0.31	0.27	0.38	0.39
77	0.31	0.27	0.37	0.34
78	0.31	0.27	0.37	0.38
79	0.31	0.27	0.35	0.4
80	0.31	0.27	0.29	0.39

81	0.31	0.27	0.3	0.39
82	0.31	0.27	0.31	0.4
83	0.32	0.27	0.29	0.39
84	0.32	0.27	0.33	0.39
85	0.32	0.27	0.3	0.38
86	0.32	0.27	0.43	0.38
87	0.32	0.27	0.41	0.39
88	0.32	0.27	0.35	0.38
89	0.32	0.28	0.34	0.38
90	0.32	0.28	0.33	0.39
91	0.32	0.28	0.33	0.43
92	0.32	0.28	0.37	0.43
93	0.32	0.28	0.42	0.41
94	0.32	0.28	0.45	0.43
95	0.32	0.28	0.42	0.42
96	0.32	0.28	0.43	0.45
97	0.32	0.28	0.39	0.43
98	0.32	0.28	0.42	0.36
99	0.33	0.28	0.43	0.35
100	0.33	0.28	0.34	0.35
101	0.33	0.28	0.32	0.33
102	0.33	0.28	0.37	0.33
103	0.33	0.28	0.35	0.4
104	0.34	0.28	0.33	0.39
105	0.34	0.28	0.33	0.39
106	0.34	0.28	0.36	0.36
107	0.34	0.28	0.34	0.36
108	0.34	0.29	0.33	0.32
109	0.34	0.29	0.31	0.32
110	0.35	0.29	0.39	0.39
111	0.35	0.3	0.33	0.37
112	0.35	0.3	0.35	0.36
113	0.35	0.3	0.35	0.4
114	0.36	0.3	0.38	0.38
115	0.36	0.3	0.37	0.39
116	0.36	0.31	0.36	0.38
117	0.37	0.31	0.36	0.39
118	0.37	0.31	0.36	0.4
119	0.37	0.31	0.38	0.37
120	0.38	0.31	0.36	0.44
Mean	0.297917	0.256833	0.335	0.381083
S.D	0.033629	0.026851	0.047297	0.038801

Table C.6 Yarn twist for carded cotton yarns [tpm]

Sample #	Ring 59 tex	Ring 73.8 tex	Rotor 59 tex	Rotor 73.8 tex
1	524	512	523	450
2	505	478	522	460
3	530	507	535	454
4	553	496	545	452
5	505	529	537	451
6	551	509	524	459
7	510	515	521	459
8	533	488	523	447
9	516	504	535	463
10	553	487	523	448
11	516	455	538	448
12	553	470	543	443
13	502	475	538	453
14	530	515	527	453
15	565	506	521	446
16	522	479	544	458
17	553	474	531	442
18	520	475	523	463
19	521	488	527	457
20	541	495	532	457
21	533	480	532	454
22	502	495	530	465
23	541	495	521	442
24	561	501	520	455
25	549	498	526	456
26	538	502	535	446
27	536	494	523	453
28	542	517	531	467
29	541	482	521	447
30	540	477	532	462
Mean	532.8667	493.266667	529.433333	453.6666667
S.D	18.07405	16.7824484	7.54153251	6.889939359

APPENDIX D: Polyester Fiber Tensile Data

Vibroskop / Vibrodyn

LENZING INSTRUMENTS

Serial number : 000 / 000

Measurenumber: :155 Program version : V1.75 20.2.2015 10:11:33

Sample ID :	PES 150	Operator :	sara
Ballen ID :		Nominal Titer :	1,5 dtex
Product :	Produkt2	Stapel length :	38 mm
Type :		Gauge length :	10 mm
Article :	z prize	Test speed :	10 mm/min
Material :	PES	Tension weight :	150 mg
Comment :			

No.	Titer dtex	Force cN	Elong. %	Ten. cN/tex	Ten/10% cN/tex	YM1% cN/tex	YM1% cN/dtex	YM1% g/den
1	1,26	5,26	19,40	41,75	33,61	521,16	52,12	59,03
2	1,39	6,99	21,90	50,29	43,60	561,15	56,12	63,56
3	1,39	6,36	15,40	45,76	41,65	563,55	56,35	63,83
4	1,25	6,44	13,40	51,52	49,04	562,67	56,27	63,73
5	1,41	6,38	12,40	45,25	42,46	535,46	53,55	60,65
6	1,45	6,26	13,40	43,17	40,34	558,62	55,86	63,27
7	1,54	6,59	15,10	42,79	36,95	522,73	52,27	59,21
8	1,33	6,04	22,20	45,41	37,14	552,63	55,26	62,59
9	1,30	5,58	14,70	42,92	39,44	557,69	55,77	63,17
10	1,26	6,25	20,40	49,60	43,13	642,86	64,29	72,81
11	1,56	6,37	28,70	40,83	30,83	474,36	47,44	53,73
12	1,41	5,92	16,20	41,99	35,99	556,74	55,67	63,06
13	1,38	6,32	15,20	45,80	41,88	554,35	55,43	62,79
14	1,52	5,68	15,90	37,37	31,54	503,29	50,33	57,00
15	1,47	5,26	10,10	35,78	35,78	505,67	50,57	57,27
16	1,37	5,83	15,20	42,55	38,43	565,69	56,57	64,07
17	1,48	6,76	15,60	45,68	41,49	506,76	50,68	57,40
18	1,60	6,53	24,90	40,81	32,12	528,12	52,81	59,82
19	1,41	5,68	29,90	40,28	28,65	546,10	54,61	61,85
20	1,56	6,75	22,90	43,27	30,26	467,95	46,79	53,00
21	1,52	7,07	16,40	46,51	40,10	497,81	49,78	56,38
22	1,56	6,07	13,10	38,91	32,50	509,62	50,96	57,72
23	1,60	4,88	11,40	30,50	29,19	484,37	48,44	54,86
24	1,44	6,02	22,10	41,81	34,44	538,19	53,82	60,96
25	1,41	6,03	17,70	42,77	34,75	496,45	49,65	56,23
26	1,48	5,16	14,90	34,86	28,65	537,16	53,72	60,84
27	1,45	4,52	11,90	31,17	26,07	489,66	48,97	55,46
28	1,32	6,34	12,20	48,03	44,05	564,39	56,44	63,93
29	1,42	6,41	20,70	45,14	39,27	545,77	54,58	61,82
30	1,45	5,28	10,40	36,41	35,59	548,28	54,83	62,10
31	1,33	5,81	20,60	43,68	34,85	518,80	51,88	58,76
32	1,54	6,75	16,60	43,83	32,37	493,51	49,35	55,90
33	1,45	7,07	18,20	48,76	31,97	537,93	53,79	60,93
34	1,39	6,53	27,70	46,98	30,32	492,81	49,28	55,82
35	1,26	6,54	19,20	51,90	31,61	547,62	54,76	62,03
36	1,45	6,71	24,20	46,28	38,38	541,38	54,14	61,32
37	1,40	6,83	21,20	48,79	40,05	575,00	57,50	65,13
38	1,37	6,31	14,90	46,06	37,08	532,85	53,28	60,35
39	1,52	5,78	12,70	38,03	34,37	491,23	49,12	55,64
40	1,50	6,59	24,90	43,93	34,33	553,33	55,33	62,67
41	1,35	5,84	15,10	43,26	26,79	451,85	45,19	51,18
42	1,64	7,21	37,90	43,96	27,53	467,48	46,75	52,95
43	1,41	6,14	23,90	43,55	33,33	508,87	50,89	57,64
44	1,40	4,69	11,20	33,50	29,29	457,14	45,71	51,78
45	1,33	6,31	21,70	47,44	37,29	537,59	53,76	60,89

Vibroskop / Vibrodyn

Serial number : 000 / 000

Measurenumber: :155 Program version : V1.75

LENZING INSTRUMENTS

20.2.2015 10:11:33

No.	Titer dtex	Force cN	Elong. %	Ten. cN/tex	Ten/10% cN/tex	YM1% cN/tex	YM1% cN/dtex	YM1% g/den
46	1,46	6,15	24,90	42,12	29,68	534,25	53,42	60,51
47	1,32	6,55	14,20	49,62	46,57	581,44	58,14	65,86
48	1,44	6,01	13,70	41,74	33,91	503,47	50,35	57,02
49	1,38	6,03	28,00	43,70	32,79	514,49	51,45	58,27
50	1,44	4,72	12,90	32,78	29,58	472,22	47,22	53,49
Average :	**1,43**	**6,11**	**18,35**	**42,98**	**35,42**	**526,25**	**52,63**	**59,61**
Std.dev. :	0,09	0,64	5,94	5,04	5,40	37,10	3,71	4,20
CV% :	6,59	10,42	32,38	11,72	15,25	7,05	7,05	7,05
Maximum :	1,64	7,21	37,90	51,90	49,04	642,86	64,29	72,81
Minimum :	1,25	4,52	10,10	30,50	26,07	451,85	45,19	51,18
Span width :	0,39	2,69	27,80	21,40	22,97	191,01	19,10	21,63
Confid- :	1,40	5,93	16,63	41,52	33,86	515,55	51,55	58,39
Intervall :	1,45	6,30	20,06	44,43	36,98	536,95	53,70	60,82

T / E Line

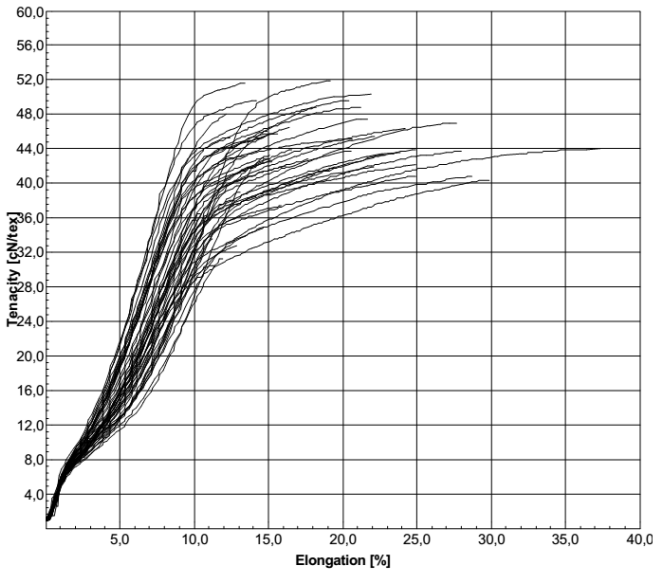

Vibroskop / Vibrodyn

Serial number : 000 / 000

Measurenumber: :155 Program version : V1.75

20.2.2015 10:11:33

Mean T / E Line

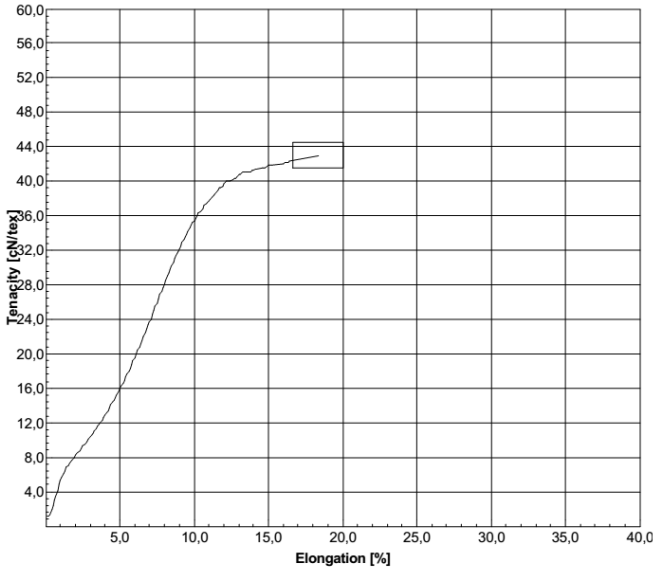

APPENDIX E: Published Paper

THE JOURNAL OF THE TEXTILE INSTITUTE, 2016
http://dx.doi.org/10.1080/00405000.2016.1204898

Taylor & Francis
Taylor & Francis Group

Tensile behavior of staple fiber yarns part II: model validation

Muhammad Zubair[a], Bohuslav Neckář[a] and Dipayan Das[b]

[a]Faculty of Textiles, Department of Textile Technology, Technical University of Liberec, Liberec, Czech Republic; [b]Department of Textile Technology, Indian Institute of Technology Delhi, New Delhi, India

ABSTRACT

The theoretical models of tensile behavior of staple fiber yarns derived in Part I of this work are compared and validated with experimental results. It is observed that the stress–strain curve of yarn always lies under the stress–strain curve of fiber. The well-known Gégauff's theory is found to overestimate fiber stress utilization in yarn. The partial generalization of helical model by taking fiber orientation into account results in satisfactory agreement with the experimental results. Clearly, fiber orientation plays an important role in deciding the fiber stress utilization in yarns. The lower is the variability of fiber direction in relation to the corresponding helical direction of fibers, the higher is the fiber stress utilization in yarn.

ARTICLE HISTORY
Received 4 March 2016
Accepted 20 June 2016

KEYWORDS
Staple fiber yarn; fiber stress utilization in yarn; fiber orientation; experimental results; model validation

1. Introduction

In Part I of this work, we mathematically modeled the initial but most dominant part of yarn stress–strain curve, where yarn structure remains relatively stable and fiber breakage is not significant, but practically all fibers are mechanically stressed. Our theoretical results showed that fiber stress utilization in yarn depends on yarn axial strain which contradicted the well-known Gégauff's theory (Gégauff, 1907). Of the models derived in Part I, the most general one showed that the coefficient of fiber stress utilization in yarn depends on stress–strain function of fiber, radial function of packing density, and radial function of contraction ratio, besides yarn twist and yarn diameter. Nevertheless, this model is very difficult to calculate as the radial function of packing density and the radial function of contraction ratio are generally unknown. The other model, based on the assumptions of small deformation and constant packing density and contraction ratio, is calculable using numerical integration. This model showed that the coefficient of fiber stress utilization in yarn depends on stress–strain function of fiber, fiber packing density in yarn, yarn twist, yarn diameter, and yarn lateral contraction. Another model was developed assuming random character of fiber direction in yarn. This model is also calculable using numerical integration. It showed that the coefficient of fiber stress utilization in yarn depends on fiber stress–strain function, fiber orientation in yarn, fiber packing density in yarn, yarn twist, yarn diameter, and yarn lateral contraction. It is of interest to know which of these models corresponds to reality. An attempt is made here to compare and validate the theoretical models discussed in Part 1 of this work in light of experimental results.

2. Materials and methods

In this work, viscose fibers of 1.3 dtex linear density and 38 mm cut length were used to prepare a set of ring yarns of three different (nominal) counts (20, 29.5, and 45 tex) and a set of rotor yarns of three different (nominal) counts (20, 29.5, and 50 tex).

The fiber was tested for stress–strain behavior using Lenzing Vibrodyne-400 instrument in accordance with CSN-ENISO 1973 standard test method. A total of 100 fibers were tested at a gage length of 10 mm and a test speed of 10 mm/min. The raw data were used and recalculated to obtain the average specific stress–strain curve $\sigma_f\left(\varepsilon_f\right)$ of fiber. Subsequently, using linear interpolation method, the specific stresses were calculated for the given strains with a step of 0.1% fiber strain.

The ring and rotor yarns were tested for stress–strain behavior using Instron-4411 tensile tester in accordance with CSN-ENISO 2060 standard test method. A gage length of 500 mm and a test speed of 110 mm/min were maintained during the tensile testing of yarns. A total of 100 tests were performed on each yarn. The tensile force and elongation data were obtained directly from the instrument and converted into average specific stress–strain function $\sigma_Y\left(\varepsilon_Y\right)$ with a step of 0.1% yarn strain.

The count of each yarn was measured in the form of a lea of 100 m length. The diameter of each yarn was determined using image analysis technique. Three hundred observations were taken for determination of mean diameter of each yarn. The twist of each yarn was measured using a twist tester. Fifty samples from each yarn were tested for twist measurements. The measured values of yarn diameter and yarn twist were used to determine the twist angle β_D of surface fibers using the well-known relationship $\tan\beta_D = \pi DZ$, where D stands for yarn diameter and Z refers to

CONTACT Dipayan Das dipayan@textile.iitd.ac.in

Table 1. Yarn characteristics.

Technology	Nominal yarn count T[tex]	Actual yarn count T[tex]	Yarn twist $Z\,[m^{-1}]$	Yarn diameter D[mm]	Twist angle of surface fibers β_D[deg]
Ring	45	46.78	515	0.263	22
	29.5	32.45	650	0.210	21
	20	20.07	840	0.169	23
Rotor	50	52.15	550	0.294	27
(Type BD)	29.5	30.71	680	0.222	23
	20	20.03	900	0.177	27

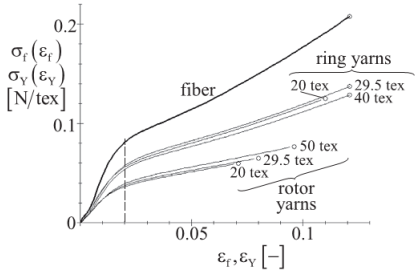

Figure 1. Experimental stress–strain diagrams of fiber and yarns.

yarn twist. Table 1 reports on the physical characteristics of the ring and rotor yarns used in this study.

3. Results and discussion

3.1. Stress–strain diagrams of fiber and yarns

Figure 1 displays the experimental stress–strain diagrams of fiber and yarns. It can be noticed that the shape of the fiber stress–strain curve is very similar to that of the yarn stress–strain curve, but, as expected, the former is lying above the latter. Using these curves the coefficient of fiber stress utilization in yarn was calculated from the following formula

$$\varphi(\varepsilon_Y) = \sigma_Y(\varepsilon_Y) \Big/ \sigma_f(\varepsilon_f = \varepsilon_Y) = \sigma_Y(\varepsilon_Y) \Big/ \sigma_f(\varepsilon_Y), \quad (1)$$

where φ denotes coefficient of fiber stress utilization in yarn, σ_f indicates specific fiber stress, ε_f refers to fiber strain, σ_Y represents specific yarn stress, and ε_Y expresses yarn strain. This calculation was performed for a range of strains started from $\varepsilon_f = \varepsilon_Y = 0.02$ and ended to the breaking strain of yarn. Based on our experience, a very small value of strain was not chosen mainly as a consequence of relative uncertainty of measurement and/or fiber crimp. Recently, Liu, Choi, and Li (2007) reported a similar conclusion for measurement of fiber and yarn strains and they studied the stress–strain relationship beyond a strain of 2%. We, therefore, decided to analyze the mutual stress–strain relation between fiber and yarn for a strain value ε_Y and/or ε_f of 0.02 (2%) and beyond. The fiber stress and yarn stresses for a given strain were found out from the corresponding stress–strain curves and then the coefficient of fiber stress utilization in yarn was determined using Equation (1). Such experimentally obtained values of $\varphi(\varepsilon_Y)$ is expressed by symbol φ_E for brevity.

3.2. Comparison between models and experiment

The experimentally obtained numerical values for the coefficient of fiber stress utilization in yarns were compared with those obtained from the theoretical models presented in Part I of this work. The simplest of all models is Gégauff's model. According to this model, the coefficient of fiber stress utilization in yarn φ_G (Gégauff's model) is expressed as follows

$$\varphi_G = (1+\eta)\cos^2\beta_D + \eta\frac{\ln\cos^2\beta_D}{\tan^2\beta_D}. \quad (2)$$

This corresponds to Equation (37) in Part I of this work. Here, η denotes yarn lateral contraction ratio and β_D indicates twist angle of surface fibers in yarn. The other model, considering real fiber stress–strain relation, expressed the coefficient of fiber stress utilization in yarn φ_{C1} (single integral formula) as follows

$$\varphi_{C1} = \frac{2}{\sigma_f(\varepsilon_Y)\tan^2\beta_D}\int_0^{\beta_D}\sigma_f(\varepsilon_f)\tan\beta\,d\beta. \quad (3)$$

This corresponds to Equation (32) in Part I of this work. Here, $\sigma_f(\cdot)$ refers to fiber stress–strain function, ε_f represents fiber axial strain according to Equations (26) and (27) stated in Part I, ε_Y shows yarn axial strain, and β is general twist angle of fiber. Another model, considering real fiber stress–strain relation and fiber orientation distribution in yarn, expressed the coefficient of fiber stress utilization in yarn φ_{C2} (double integral formula) as follows

$$\varphi_{C2} = \frac{2}{\sigma_f(\varepsilon_Y)\tan^2\beta_D}\int_0^{\beta_D}\left[\int_0^{\vartheta_u}\sigma_f(\varepsilon_f)\cos^2\vartheta\,u(\vartheta)\,d\vartheta\right]\frac{\sin\beta}{\cos^3\beta}d\beta. \quad (4)$$

This corresponds to Equation (50) in Part I of this work. Here, $u(\vartheta)$ denotes probability density function of fiber inclination angle ϑ and ϑ_u indicates upper limit of fiber inclination angle. Further, the following expressions are required for calculations.

$$\tan\beta_D = \pi DZ, \quad (5)$$

$$u(\vartheta) = \frac{1}{\pi}\frac{C}{C^2-(C^2-1)\cos^2(\vartheta+\beta)} + \frac{1}{\pi}\frac{C}{C^2-(C^2-1)\cos^2(\vartheta-\beta)}, \quad (6)$$

$$\varepsilon_f \doteq \varepsilon_Y\left(\cos^2\vartheta - \eta\sin^2\vartheta\right), \quad (7)$$

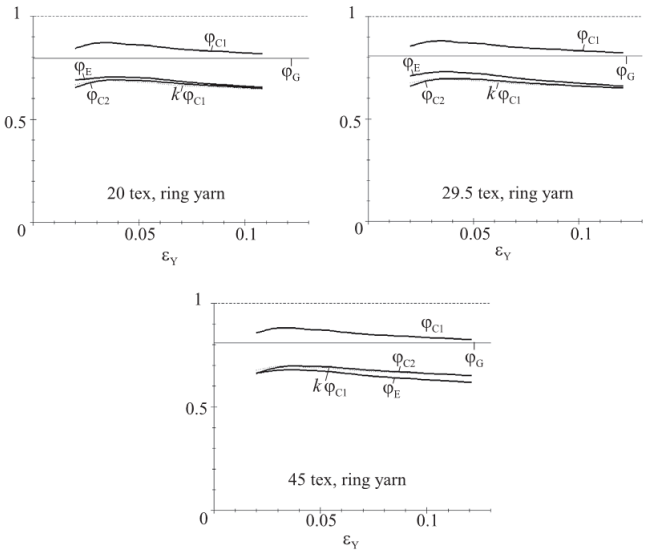

Figure 2. Coefficient of fiber stress utilization in ring yarns. Parameters used: See Table 1 and $\eta = 0.5$, $C = 4.9$, $k = 0.79$.

$$\vartheta_u = \arcsin\left(1 \Big/ \sqrt{1+\eta}\right), \tag{8}$$

where Z is yarn twist, D is yarn diameter, and C is a measure of angular preference.

The coefficients of fiber stress utilization in yarns $\varphi_G, \varphi_{C1}, \varphi_{C2}$ were calculated according to Equations (2–4), respectively, using Equations (5–8). The calculated values of these coefficients are plotted against axial strain of ring yarns of three different counts in Figure 2. Also, the experimentally obtained coefficient of fiber stress utilization in yarns φ_E, using Equation (1) and Figure 1, is plotted for different axial strain of these yarns in Figure 2. Further, the calculated values of φ_{C1} are multiplied by an empirical parameter k, and the resulting values $k\varphi_{C1}$ are also plotted in Figure 2. It can be observed that all three graphs show very similar results. The experimental curves φ_E are relatively flat and lie a little under 0.7 for all three yarns. The coefficient of fiber stress utilization φ_G according to Gégauff's model is independent to yarn strain as expected and its value is around 0.8, which is higher than those obtained experimentally. Further, it can be seen that all three curves of φ_{C1} (single integral formula) lie over Gégauff's model φ_G, but the shape of the three curves is very similar to the experimental ones so that after multiplication by a common empirical constant $k = 0.79$ the curves $k\varphi_{C1}$ (thin doted lines) lie very near to the experimental curve φ_E. The curves of φ_{C2} (double integral formula) are also very near to the experimental curve φ_E with a common 'measure' of angular preference $C = 4.9$. Such a value of C is relatively high and it shows pronounced orientation of fibers (fiber portions) to the corresponding 'helical' direction. On the other hand, this fiber orientation is not 'absolutely perfect' as with φ_{C1} (ideal helical model) and therefore φ_{C2} lies markedly under φ_{C1}. It shows that the phenomenon of fiber orientation probably plays an important role in deciding the fiber stress utilization in yarns.

Figure 3 shows a graphical display of φ_G, φ_{C1}, $k\varphi_{C1}$, φ_{C2}, *and* φ_E against ε_Y for rotor yarns of three different counts. The basic character of these graphs is generally similar to that of the corresponding graphs for ring yarns. Here, also the experimental curves φ_E are relatively flat and lie a little under 0.5 for all three yarns. Evidently, the rotor yarns exhibit lower fiber stress utilization than the ring yarns. Gegauff's model φ_G, independent to yarn strain, shows practically 75% fiber stress utilization, which is a little lower than that (80%) of ring yarns. The smaller fiber stress utilization in rotor yarns is evidently the effect of higher level of twisting used to produce them. (Compare twist of ring and rotor yarns as reported in Table 1.) All three curves of φ_{C1} (single integral formula) lie again over Gégauff's model and their shapes are similar to the experimental ones so that after multiplication by a common empirical constant $k = 0.55$ the curves $k\varphi_{C1}$ (thin doted lines) lie very near to the experimental curve φ_E. Note that the smaller value of k in case of rotor yarns as compared to ring yarns corresponds to less fiber stress utilization by the rotor yarns. The curves of φ_{C2} (double integral formula) are also very near to the experimental curve φ_E, nevertheless using of another suitable value of common 'measure' of angular preference $C = 1.6$. Such a value of C is relatively small now and it indicates 'bad' orientation, i.e. higher variability of directions of fibers (fiber portions) in relation to the corresponding 'helical' direction of fibers. Such a value of C reminds us of a carded web which is described by a C-value of 1.8 (Neckář & Das, 2012). Let us remind that in rotor spinning the fibers, after getting opened by opening roller, 'fly' free, without any control, before they are deposited onto rotor surface. It is therefore well imaginable that such fibers (fiber portions) create something like 'web' on the collecting surface of rotor. It is acknowledged that the phenomenon of fiber orientation probably plays a dominant role in deciding the fiber stress utilization in rotor yarns too.

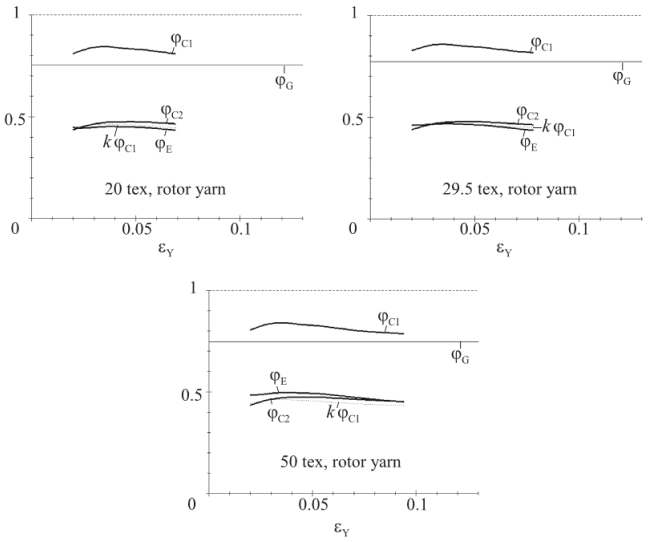

Figure 3. Coefficient of fiber stress utilization in rotor yarns. Parameters used: See Table 1 and $\eta = 0.5$, $C = 1.6$, $k = 0.55$.

4. Conclusion

The differences between stress–strain curves of fiber and yarn can be expressed as follows. The stress–strain curve of yarn lies always under the stress–strain curve of fiber. The experimental fiber stress utilization in ring as well as rotor yarn is markedly smaller than that obtained from the well-known Gégauff's model as well as from the single integral model considering real fiber stress–strain relation. Further, the experimental fiber stress utilization decreases markedly with the higher variability of fiber directions in relation to the corresponding 'helical' direction of fibers. The model of fiber stress utilization, considering fiber orientation and fiber stress–stress relation, exhibits satisfactory agreement with experimental results.

Disclosure statement

No potential conflict of interest was reported by the authors.

References

Gégauff, M. C. (1907). Strength and elasticity of cotton threads. *Bulletin de la Société Industrielle de Mulhouse, 77*, 153–176.

Liu, T., Choi, K. F., & Li, Y. (2007). Mechanical modeling of single yarns. *Textile Research Journal, 77*, 123–130.

Neckář, B., & Das, D. (2012). *Theory of structure and mechanics of fibrous assemblies*. New Delhi: Woodhead Publishing India.